Molecular Qubits based on Photogenerated Spin-Correlated Radical Pairs for Quantum Sensing

Tomoyasu Mani[1,2,3,a]

[1]Department of Chemistry, University of Connecticut, Storrs CT 06033, United States

[2]Chemistry Division, Brookhaven National Laboratory, Upton NY 11973, United States

[3]Japan Science and Technology Agency, PRESTO, 4-1-8 Honcho, Kawaguchi, Saitama 332-0012, Japan

[a]Author to whom correspondence should be addressed: tomoyasu.mani@uconn.edu; tmani@bnl.gov

Abstract

Photogenerated spin-correlated radical pairs (SCRPs) in electron donor-bridge-acceptor (D-B-A) molecules can act as molecular qubits and inherently spin qubit pairs. SCRPs can take singlet and triplet spin states, comprising the quantum superposition state. Their synthetic accessibility and well-defined structures, together with their ability to be prepared in an initially pure, entangled spin state and optical addressability, make them one of the promising avenues for advancing quantum information science (QIS). Coherence between two spin states and spin selective electron transfer reactions form the foundation of using SCRPs as qubits for sensing. We can exploit the unique sensitivity of the spin dynamics of SCRPs to external magnetic fields for sensing applications including resolution-enhanced imaging, magnetometers, and magnetic switch. Molecular quantum sensors, if realized, can provide new technological developments beyond what is possible with classical counterparts. While the community of spin chemistry has actively investigated magnetic field effects on chemical reactions via SCRPs for several decades, we have not yet fully exploited the synthetic tunability of molecular systems to our advantage. This review offers an introduction to the

photogenerated SCRPs-based molecular qubits for quantum sensing, aiming to lay the foundation for researchers new to the field and provide a basic reference for researchers active in the field. We focus on the basic principles necessary to construct molecular qubits based on SCRPs and the examples in quantum sensing explored to date from the perspective of the experimentalist.

Table of Contents

I. INTRODUCTION

Quantum sensing is an emerging field of research in quantum information science (QIS). Along with quantum computing and communication, it is a promising real-world application of quantum mechanics that exploits counterintuitive and sometimes "spooky" behavior of quantum system.[1] QIS uses quantum bits (qubits) that can be placed into a quantum superposition of their two constituent states (i.e., $|\psi\rangle = c_0|0\rangle + c_1|1\rangle$ where c_1 and c_2 are coefficients), by which we can access multiple states simultaneously unlike classical bits. DiVincenzo formalized a widely used set of requirements for a viable qubit.[2] Desirable characteristics of a qubit, specific to quantum computing,[3] include (i) a long coherence time, which is the lifetime of the superposition state, (ii) the ability to initialize a qubit in a well-defined initial state, (iii) the system should be well-defined and scalable, (iv) a qubit should be individually measurable, (v) the system must provide a set of universal quantum logic gates that operate on one or two entangled qubits. Degen et al.[1] formulated another criterion for quantum sensing: systems interact with a relevant physical quantity of the environment such as electric, magnetic field, temperature, and pressure. The challenge is to make a qubit that simultaneously satisfies these strict and somewhat arbitrary criteria for computing or sensing.

Following the classifications introduced by Degen et al.,[1] quantum sensing describes the system's 1) use of a quantum object to measure a classical or quantum physical quantity; 2) use of quantum coherence to measure a physical quantity; 3) use of quantum entanglement to improve the sensitivity or precision of measurement beyond classical limits. While the third definition is considered a true quantum (Type-III) sensor, most current systems satisfy the first two definitions (Type-I and Type-II). A widely studied class of systems based on electron spin qubits has electronic spins located at defect sites in solid-state materials.[4] Examples include nitrogen-vacancy centers in diamond (NVC)[5-7] and double-vacancy sites in silicon carbide (SiC).[8-10] Here, qubits are provided by a superposition of spin up and down states. The popularity of these defect-based systems lies in the fact that they can exhibit long coherence times over a wide temperature range because the spin site is well protected from the environment. These defects-based systems are also optically addressable qubits with spin-dependent fluorescence, which permits an optical readout of their spin dynamics. Recent studies showed that metal-centered molecular qubits such as vanadyl complexes,[11, 12] chromium complexes,[13, 14] and metal-organic framework (MOF)[15, 16] can compete with solid-state defects by removing the decoherence sources from their environment. Molecular qubits have distinct advantage of a wider control of spin properties by chemical synthesis and assembly.[17] Molecular counterparts, as well as defect-based qubits, are simple qubit, two-level quantum system, and scaling to multiqubit systems is one of the current challenges in the field;

some recent developments of these molecular qubits are summarized in Refs,[18, 19]and their application in quantum sensing are also summarized in Ref.[20]

Another type of molecular qubits, and the focus of this review, is based on spin-correlated radical pairs (SCRPs) in electron donor-bridge-acceptor (D-B-A) molecules.[17, 21] SCRPs are created by a transfer of an electron (or hole) from an donor (D) to an excited acceptor (A*) to form a radical pair ($D^{\bullet+}$ and $A^{\bullet-}$) that inherits the spin state of the A*; e.g., usually singlet for optical excitation. An electron transfer step can occur from an excited donor (D*) depending on the energetics of the system. Singlet and triplet spin states of SCRPs, produced in either form, can undergo coherent evolution in time (^{1}RP ↔ ^{3}RP, **Fig. 1**).[22]

Fig. 1. Spin selective chemical reactions and coherent spin evolution between singlet and triplet RPs are the foundation of SCRPs as optically addressable qubits for quantum sensing-related applications. We can have optical signatures from singlet and triplet channels that can be spin-selective response/readout.

In the presence of external magnetic fields (high-field limit), two stationary mixed states of RPs are the superpositions of singlet $|S\rangle$ and triplet $|T_0\rangle$ states. Spin coherence between these two states is called zero quantum coherence (ZQC). Differences in electron−nuclear hyperfine couplings and *g*-factors of spins primarily drive ZQC in SCRPs, and ZQC can occur with oscillation periods on the time scale of nanoseconds or longer.[23, 24] These interactions are weakly coupled to the thermal bath so that coherence can last for 10's-100's of nanoseconds even at room temperature.[25, 26] Therefore, SCRPs hold promise for use in quantum computing, communication, and sensing by overcoming the tyranny of low temperature[27] that is typically required to suppress decoherence in many inorganic materials. SCRPs based on organic molecules are also inherently a pair of qubits, or spin qubit pairs (SQPs),[21] offering an alternative and unique approach in terms of scaling as well. The Wasielewski group pioneered their usage as qubits in quantum computing and communication, successfully demonstrating a gate operation[28] and quantum teleportation.[29]

Spin dynamics of SCRPs is strongly tied with the studies of magnetic field effects (MFEs) on chemical and biochemical reactions. When magnetically susceptible spin species are involved in their reaction pathways, external magnetic fields can affect the fates of chemical reactions. The required magnetic field strengths are orders of magnitude smaller than thermal energy (k_BT ~ 25 meV at room temperature). Early developments of this field, collectively known as Spin Chemistry, on both the experimental and theoretical aspects were described in the thorough review paper by Steiner and Ulrich,[30] and in the textbook by Hayashi.[31] Among the

possible spin species, SCRPs is arguably the most well-studied one along with triplet-triplet (TT) exciton pairs.[32-34] As we can more easily modify the properties of radicals such as energies, we usually have a more expansive chemical and synthetic control over the spin dynamics of RPs compared to TT annihilation. A prominent example of SCRP-based MFEs is the RP mechanism hypothesis of magnetoreception in birds, other animals, and insects. Proof-of-principle experiments have demonstrated the sensitivity of a model artificial RP system to the direction of an Earth-strength magnetic field (around 50 μT),[35] and the magnetic sensitivity of key suspect proteins cryptochromes such as CRY1 and CRY4.[36, 37] Yet, this hypothesis, including the signal transduction pathway and cellular responses, has not yet been confirmed while there are ongoing efforts, including monitoring MFEs at a cellular level by microscopy.[38-40] A couple of review papers summarized this field's history and recent developments.[41-43] The early efforts on understanding spin dynamics of the photogenerated SCRPs primarily come from the interest in photosynthetic energy transduction.[22, 44-46] Recently, Harvey and Wasilewski reviewed the research development of SCRPs in the areas from light-to-charge transduction chemistry of the photosynthetic reaction center and their artificial mimicry to the recent attempts of using them in quantum computation and communication.[21] SCRPs can also be an excellent platform for quantum sensing by exploiting the coherence nature and spin-selective chemical reactions of SCRPs. While magnetoreception in animals has recently been discussed in the context of quantum biology,[47] we can consider our efforts of using SCRPs in quantum sensing to mimic mother nature and develop new technologies. Their sensitivity to external magnetic fields enables us to design molecules whose properties can be magnetically controlled. Spin-selective recombination products of both singlet and triplet channels can act as a response or optical readout of the spin state of SCRPs that form the basis of quantum sensing technologies such as resolution-enhanced imaging and magnetometer (**Fig. 1**).

Despite unique quantum features and opportunities for synthetic tunability of magnetic sensitivity and spectral properties, this area is still largely underexplored to date. The motivation behind this review is to offer an introduction to students and researchers new to the field of spin chemistry in general and summarize some recent findings relevant to this area that act as a reference for researchers in closely related fields. This review will focus on using SCRPS in quantum sensing, particularly the application of MFEs on molecular emission, while we will draw key findings from the studies of fundamental spin chemistry, magnetoreception, and quantum computation. The remainder of the paper is organized as follows. A brief sketch of the basic spin chemistry of SCRPs is given in section II so as to provide a focused context of their usability as qubits for quantum sensing. Section III presents several MFEs on chemical reactions with focus on molecular emission, followed by a set of illustrative applications in quantum sensing. Conclusions and outlook are summarized in section IV.

II. SPIN CHEMISTRY AND QUBITS

A. Basics

A.1. SCRPs as Qubits

In a typical organic donor-acceptor (D-A) molecule, photoexcitation produces a local singlet excited state with typical energy of ~2-4 eV (~1.6 - 3.2 x 10^4 cm^{-1} corresponds to 300 – 600 nm excitation wavelength). Electron transfer reactions within D-A create an RP ($D^{\bullet+}$-$A^{\bullet-}$) that can function as two entangled spin qubits, giving rise to an entangled two-spin singlet or triplet state ($|S\rangle$ and $|T_0\rangle$, see **Section II.A.2**), therefore acting as an SQP. Because of the spin selection rule, electron transfer from the photogenerated singlet excited state results in an SCRP having an initial pure singlet spin configuration; spin initialization (**Fig. 2a**).

Fig. 2. (a) Energy level diagram of photogenerated singlet-born RPs: fl = fluorescence, IC_S = internal conversion; CS = charge separation; bCR = back charge recombination; CR_S = singlet charge recombination; CR_T = triplet charge recombination; ISC_T = intersystem crossing between local triplet excited and ground states. (b) Zeeman splitting of RP energy levels (J < 0). a_{eff} represents an effective hyperfine coupling. The energy scale is arbitrary. (c) Spin configurations (vector representations) for each sublevel and a mixed state. A mixing of $|S\rangle$ and $|T_0\rangle$ to yield stationary population of Φ_A and Φ_B.

Alternatively, one can produce an SCRP as an initial pure triplet spin configuration from the triplet excited state. In the absence of a perturbation (i.e., strong spin-orbit couplings), recombination of RPs also conserves spin: singlet RPs recombine to form singlets while triplet formation is forbidden (Wigner-Witmer rules[48, 49]). Spin states of singlet or triplet RPs can undergo coherent spin evolution in time and interconvert before decoherence, random phase pick up during the evolution of the spins,[3] and spin relaxation cause random transitions between states. As the rates of spin-selective RPs recombination are usually different for singlet and triplet RPs, applied magnetic fields and/or microwave pulses can alter the relative population of singlet and triplet RPs and the lifetime of RPs (τ_{RP}). This modification leads to changes in the relative contributions of the respective recombination to the overall kinetics and product yields. This spin selective electron transfer reaction, coupled with coherence within RPs, forms the foundation of using SCRPs as qubits. It is worth noting that the S-T interconversion can indeed exhibit quantum oscillations that can be transmitted to the chemical reaction kinetics, considered as a hallmark of coherence. Such quantum beats[50] on recombination products are routinely observed in radiolytically generated SCRPs,[23, 51] but are rare in photogenerated SCRPs because of relatively slow recombination processes.[52] Steiner,

Lambert, and co-workers recently showed pump-push spectroscopy could detect quantum beats.[53] Their demonstration clearly illustrates that the process is a genuine quantum phenomenon.

A.2. Spin Dynamics of SCRPs

We will now describe the spin dynamics of SCRPs in some detail. We limit ourselves to the basics necessary to understand 1) the coherent nature of SCRPs and 2) spin selectivity and accompanying MFEs. More thorough treatments of spin dynamics of SCRPs can be found somewhere else.[30, 31, 54]

The terminology of SCRPs as qubits is used in conjunction with an applied magnetic field, either manipulating by microwave pulse for computing and communication or using a varying magnetic field for sensing. Application of a magnetic field, B_0, results in the Zeeman splitting of the RP triplet sublevels (**Fig. 2b**). The splitting provides $|T_{+1}\rangle$, $|T_0\rangle$, and $|T_{-1}\rangle$ eigenstates that are quantized along the external magnetic field, B_0 while the energies of $|S\rangle$ and $|T_0\rangle$ are field-insensitive. Vector representations[55] of each spin state are shown in **Fig. 2c**. Under this condition, the total spin Hamiltonian for SCRPs is given by

$$\mathcal{H} = \sum_{i=1,2} \frac{\mu_B B_0 g_i}{\hbar} S_{zi} + \sum_m a_m S_1 \cdot I_m + \sum_n a_n S_2 \cdot I_n - 2J\left(\frac{1}{2} + \cdot S_1 \cdot S_2\right) + \frac{1}{2}(D(3\cos^2\zeta - 1))[S_z^2 - \frac{1}{3}S^2] \quad (1)$$

where μ_B and g_i are the Bohr magneton (5.788 x 10^{-5} eV/Tesla) and g-factors for each radical. S_1 and S_2 are electron spin operators for the two radicals within RPs; S_{zi} is a spin operator in the z direction (along the field B_0). I_m and I_n are nuclear spin operators, a_m and a_n are the isotropic hyperfine coupling constants of nucleus m with radical 1 and nucleus n with radical 2. $2J$ and D are the exchange coupling and the spin-spin dipolar coupling between the two electrons where ζ is the angle between the principal axis of dipolar interaction and external magnetic field. The fourth and fifth terms describe an energy difference for any two radicals interacting at a given distance. J stems from the electron exchange of the two spins and defines the relative energies of the singlet and triplet states of RPs; $2J = E_S - E_{T_0}$ (J can be negative or positive – it is negative in **Fig. 2b**). The above equation also assumes that the nuclei associated with a given radical couple only with the electron spin within that radical. In the molecular systems in solutions, the anisotropies usually do not affect the spin dynamics. However, such rotational modulations can induce incoherent spin relaxations for individual radicals, which may, in turn, affect the spin dynamics through a relaxation term.[56]

For an SCRP in an applied external magnetic field in the rotating frame, the states $|S\rangle$ and $|T_0\rangle$ are not eigenstates of the Hamiltonian, $\mathcal{H}$. We, therefore, use mixed states $|\Phi_A\rangle$ and $|\Phi_B\rangle$ such that,

$$|\Phi_A\rangle = cos\phi|S\rangle + sin\phi|T_0\rangle \quad (2a)$$

$$|\Phi_B\rangle = cos\phi|T_0\rangle - sin\phi|S\rangle \quad (2b)$$

meaning that they are the superposition of $|S\rangle$ and $|T_0\rangle$. An angle ϕ rotates $|S\rangle$ and $|T_0\rangle$ into the mixed basis, taking the following form:

$$\phi = \frac{1}{2} arctan\left(\frac{B_0 \Delta g \mu_B + \Delta A}{2J + \frac{1}{3}D(3cos^2\zeta - 1)}\right) \quad (3a)$$

The numerator is the contribution from Δ*g*, the difference *g*-factors of the two electron spins (Δ*g* = g_1 - g_2), and Δ*A,* the differences in hyperfine couplings *a*, and the denominator is *J* and *D*. In the high-field limit, Δ*A* can be expressed as

$$\Delta A = \frac{1}{2}\sum_m a_m I_{m,z} - \sum_n a_n I_{n,z} \quad (3b)$$

where $I_{m,z}$ and $I_{n,z}$ are the spin quantum numbers.[57, 58] As most of the spin systems described here are in solutions, for simplicity, we can ignore the dipolar term since the angular function $(3cos^2\zeta - 1)$ averages to zero. While a transition between $|S\rangle$ and $|T_0\rangle$ is possible (ZQC), the microwave-induced transition between the mixed states of the ZQC is itself spin-forbidden (Δm_s = 0, zero-quantum transition).[59] However, the mixed states can be manipulated and probed by external electromagnetic fields as there is a finite transition probability from these mixed states to $|T_{+1}\rangle$ and $|T_{-1}\rangle$, enabling the gate operations.[28] Thus, the ZQC formed by SCRPs placed in a magnetic field enables manipulation and probing, satisfying a requirement for qubits. While quantum computing and communication use microwave pulse for active spin manipulation, the current examples relevant to quantum sensing mostly rely on the SCRPs' sensitivity to external magnetic fields. However, further manipulation of their spin dynamics by microwave pulse is possible at the expense of additional experimental setups in the form of reaction yield detected magnetic resonance (RYDMR)[60] where we apply resonant microwave pulses to investigate the spin dynamics of SCRPs in a time-resolved manner.[60] Magnetic response of SCRPs' spin dynamics and associated chemical reactions are often measured by magnetically affected reaction yield (MARY) spectroscopy,[61] where the yields of reactions are recorded while scanning the external magnetic fields. The MARY spectrum characterizes the sensitivity of the SCRPs to an external magnetic field. The parameters of the interactions, described in eqs. 1 and 3, play important roles for the performance of such systems as qubits. Below, we shall describe them in the context of spectral parameters for MARY spectra.

B. Parameters for MARY spectra

B.1. MARY Spectra and Classification

Long lifetimes of RPs and efficient spin mixing are necessary to use coherence for QIS. Ways to elongate RPs' lifetimes are actively explored in the field of photo-generated electron transfer reactions, mainly in the context of photon energy conversion and storage. Important parameters are reviewed elsewhere,[44, 45] and we will not cover them under the current topic directly while we will touch upon some when necessary. Here, we shall confine our attention to parameters primarily important for spin dynamics and resulting MARY spectra. The basic assumptions are that 1) lifetimes of RPs are long enough for spin mixing and 2) charge recombination occurs spin selectively. Indeed, when these assumptions fail, we do not observe MFEs. Lifetime (τ_{RP}) can be a significant limiting factor and impact the shape of MARY spectra, as described below (e.g., **II.B.4.c**). As a rough estimate, the oscillator frequency of S-T mixing induced by hyperfine coupling (ω_{hfc}) is usually on the order of 10^7-10^8 s^{-1},[23, 24] and coherence can last for 10's-100's of ns at room temperature.[25, 26] Therefore, RPs' lifetimes must be longer than those time windows for efficient mixing and using coherence to advantage. Spin-orbit coupling, which can induce spin-forbidden transition, is typically negligible and usually ignored in pure organic molecules.[62] One notable exception is when ^{1}RP directly recombines onto local triplet excited state ($^1RP \rightarrow {}^3A^*$), so-called spin-orbit charge-transfer ISC (SOCT-ISC).[63-65] When this process is operative and faster than RP-ISC, we do not observe MFEs on RPs and spin recombination products.[66]

The MARY spectrum is usually represented by plotting the difference between the intensities of either recombination product (such as exciplex emission intensity and triplet excited states absorption) or those of radicals' absorption in the presence and absence of external magnetic fields. The photophysical pathway discussed in this section largely follows the general energy diagram presented in **Fig. 2a** (i.e., singlet-born RPs).

We can broadly classify the spin systems into two, depending on the magnitude of exchange interaction $2J$ with respect to the effective hyperfine interactions of the individual radical ions in the RPs (a_{eff}); $|2J| < a_{eff}$ (or ~0) and $|2J| > a_{eff}$ (or ≠ 0). The parentheses indicate relative magnitude compared to the applied magnetic field of our interest (see **Fig. 2b** for a qualitative picture). Describing a_{eff}, Weller and co-workers[67] showed

$$a_{eff} = 2\left(\frac{a_{eff,1}^2+a_{eff,2}^2}{a_{eff,1}+a_{eff,2}}\right) \quad (4a)$$

where

$$a_{eff,i}(i = 1,2) = \sqrt{\sum_k a_k^2 I_k(I_k+1)} \quad (4b)$$

where a_k is the isotropic hyperfine coupling constants for the nuclear spin I_k on radical i. RPs of typical organic D/A molecules have a_{eff} on 1-10 millii-Tesla (mT) order while B_0 of our specific interest is usually up to 1000 mT. In energy scale (using conversion with Bohr magneton), a_{eff} ~ 1 – 10 x 10^{-3} cm^{-1} and B_0 up to 1 cm^{-1}. When the unpaired electron spins are localized on both radicals, a_{eff} of an RP is a constant that is independent of the distance between two electron spins (r_{DA}).[55]

MARY spectra exhibit different features for these two cases. Representative curves are shown in **Fig. 3a**: blue line for $|2J| > a_{eff}$ and red line for $|2J| < a_{eff}$. The schematic diagrams of spin dynamics at three different B_0 regions are presented in **Fig. 3b**. While the applications on quantum computation usually require $2J \sim 0$ to achieve ZQC at any given field, it is one parameter we can control, and one may like to tune for quantum sensing applications. Please note that as the superposition consists of singlet $|S\rangle$ and triplet $|T_0\rangle$ states, strictly speaking, we may call SCRPs as qubits only when they achieve ZQC ($2J \sim 0$). Nevertheless, as we can achieve coherent spin S-T evolution even when $2J \neq 0$ at a specific field, they can act like qubits, and therefore, we call SCRPs as qubits for both cases in this review.

Fig. 3. (a) Schematic MARY spectra for $|2J| < a_{eff}$ (red line) and $|2J| > a_{eff}$ (blue line). LFE = low field effect; FWHM = full-width at half-maximum. (b) Diagrams of spin dynamics and spin selective charge recombination kinetics for the case of $|2J| < a_{eff}$ (upper panel), and for the case of $|2J| > a_{eff}$ (lower panel) at zero magnetic field (left column), resonance (middle), and very high magnetic fields (right). $2J$ is depicted as negative. Relaxation within triplet manifolds and charge recombination processes are omitted for clarity. The photophysical pathway follows that of **Fig. 2a**. A singlet RP can recombine to the local singlet excited state (bCR) or the ground state (CR_S), while each triplet sublevel can recombine to local triplets only (CR_{TT}). The size of red dots indicates a relative population of the singlet character among the three conditions. ω_{hfc} and k_{rlx} are the oscillatory frequency of S-T mixing induced hyperfine coupling and relaxation rate. ω_{hfc} is field-independent while k_{rlx} is field-dependent.

B.2. $|2J| < a_{eff}$

We first consider the case of $|2J| < a_{eff}$ (**Fig. 3a**, red line). Examples of this case include freely diffusing (or unlinked) D/A systems or D-A systems connected by a long flexible linker: some molecular structures are shown in **Fig. 4**.

A general scenario of this case is the following. The application of an external magnetic field results in the Zeeman splitting of the triplet sublevels, two of the three triplet levels (T_{+1} and T_{-1}) become progressively decoupled, resulting in singlet-triplet mixing being restricted to the S-T_0 transition only. If the RP is generated in a singlet state, this decrease in S-T mixing at high

fields leads to an increase in the yield of the singlet recombination product; i.e., we observe a positive MFE. At a very high field, we expect to observe the saturation of the mixing when the spin mixing by Δg is negligible (see below).

Fig. 4. Chemical structures of selected molecular systems whose exchange interactions 2*J* are measured experimentally. Reported 2*J* and linewidth are listed in **Table 1**.

At low field ($|B_0|$ ~ or < a_{eff}), the electron spin precesses around a total field (i.e., the sum of external and hyperfine vector fields) and does not align with the external field. Therefore, the projection of the electron spin onto the external field direction changes over time, and the mixing of S-$T_{\pm1}$ becomes possible. In this regime, we could observe the opposite MFE, i.e., for a singlet-born RP, we observe a decrease in the yield of the singlet recombination product. This opposite MFE[68] is commonly known as the low field effect (LFE). Timmel et al. established the origin of the LFE[69] theoretically. It arises from superpositions of the electron-nuclear spin states in SCRPs at zero fields. Applying a small magnetic field may lift some or all the energy level degeneracies associated with these coherences, leading to an alteration in the efficiency of S-T interconversion. Consequently, the formation rate of singlet recombination products is modified. The reviews of LFE are provided by Timmel et al.[70] and more recently by Miura.[71] LFE is the strong contender for magnetoreception of Earth's magnetic fields; B_0 ~ 50 μT < a_{eff}. While it can similarly play a critical role for quantum sensing applications where we either detect such small fields or use them to manipulate chemical reactions, we do not cover LFE in detail in this review.

We now take a closer look at the situation at the high field (B_0 > a_{eff}). When *J* and *D* are relatively small (i.e., on the same order of magnitude or less) compared to $\Delta g \times B_0$ *and* ΔA (eq. 3b), mixing of $|S\rangle$ and $|T_0\rangle$ occurs through *g*-factor difference and/or hyperfine coupling terms. The S-T_0 oscillation through the *g*-factor term, the first term in eq.1, occurs at the frequency

$$\Delta\omega = \frac{\Delta g \mu_B B_0}{\hbar} \qquad (5)$$

This spin mixing is called the Δg mechanism. Obviously, this mechanism cannot contribute to the S-T_0 mixing at zero fields (B_0 = 0). The Zeeman interaction induces field-dependent energy splitting between the S-T_0 mixed states and the $T_{\pm1}$ states. As the strength of the magnetic field increases, contributions from this term will come into play. When *J* ~ 0 (< a_{eff}), for organic radicals, the small differences in *g*-factors contribute to the S-T_0 mixing only at high field. For example, a sufficiently large $\Delta g = 10^{-3}$ gives only $\Delta\omega = 8.8 \times 10^7$ s^{-1}/T. Δg of typical organic RPs is smaller than that, and $\Delta\omega$ is not fast enough to contribute to the S-T mixing at B_0 < 1

Tesla. At this low magnetic field regime, the primary driver for the S-T mixing is, therefore, the hyperfine coupling (the second and third terms in eq. 1). This contribution can be defined as a difference in Gaussian distributions of the total isotropic hyperfine coupling constants to account for the hyperfine interaction distributions (ΔA),[25] and typical ΔA values are translated to the frequency of ω_{hfc} = 10^7-10^8 s^{-1}. Of course, the Δg mechanism could contribute significantly even at B_0 < 1 T under specific circumstances (e.g., ΔA is very small), and prominent examples are quantum beats observed in recombination fluorescence of radiolytically generated SCRPs.[72, 73]

B.3. $|2J| > a_{eff}$

The other type of MARY spectral shape appears where $2J$ is large enough compared to a_{eff} (**Fig. 3a**, blue line). Examples of this case include D-A systems connected by a short flexible linker and rigidly linked D-A systems: some molecular structures are shown in **Fig. 4**. In this case, in the absence of an external magnetic field, S-T mixing is not efficient and is governed by incoherent spin relaxation (k_{rlx}).[56] Here, spin relaxations encompass both spin-lattice relaxation T_1 and spin-spin relaxation T_2. Largely, they are T_1[74] while T_2 is critical for incoherent S-T_0 mixing.[75] k_{rlx} is usually on the order of 10^4-10^6 s^{-1} and slower than ω_{hfc} while k_{rlx} is field-dependent and decreases at high field.[56, 74, 76] The application of an external magnetic field results in the Zeeman splitting of the triplet sublevels, and either T_{+1} or T_{-1} become progressively coupled with S, resulting in a coherent mixing *via* hyperfine coupling. This coherent mixing becomes most efficient at the resonance field ($B_0 = 2J$), and this level-crossing feature is called *J*-resonance.[74] If the RP is singlet-born, this increase in S-T mixing leads to a decrease in the yield of the singlet recombination product, a negative MFE. At high field $B_0 >> 2J$, we can neglect the coherent mixing by the hyperfine interaction, and only incoherent spin relaxations can mediate the S-T mixing. At further higher field (B_0 > 1 Tesla), we expect to observe the effect of Δg (see above).

B.4. Magnitude, field-response range ($2J$), linewidth.

MARY spectra are characterized by the three parameters: magnitude of MFE, linewidth, and resonance field $2J$ (**Fig. 3a**). Here, we neglect the LFE for the case of $|2J| < a_{eff}$. These parameters describe the responsiveness of the spin system to external magnetic fields, and therefore define the performance of SCRPs as quantum sensors.

B.4.a. Magnitude

The magnitude of the MFE represents the degree to which a signal of interest responds to applied external magnetic fields. The MFE can be expressed as

$$\mathrm{MFE} = \frac{F_B - F_0}{F_0} \times 100\ (\%) \qquad (6)$$

where F_0 and F_B are the signals in the absence (B_0 = 0) and the presence of an external magnetic field ($B_0 \neq 0$). F can be intensity (I) or rate ($k = 1/\tau$ where τ is lifetime). For simplicity, the maximum effect is defined as the magnitude (**Fig. 3a**). One can also express the field-effect simply as the ratio of the two quantities (i.e., $\frac{I_B}{I_0}$); i.e., when the ratio is two, we can say the intensity increases two-fold in the presence of the magnetic field. From the perspective of applications, it is usually desirable to maximize the magnitude, and an ideal situation is a complete turn-on/off. The magnitude of MFEs greatly depends on the molecular system and environment; experiments measured from < 1-2 % to > 100 %. In freely diffusing systems or D-A systems connected by a flexible linker, steady-state MFEs on intensity-based measurements are typically in the range of 0 – 50%,[77, 78] and as much as 80% MFEs on chemical reactions rates were reported for unlinked systems.[79] We can achieve a much higher effect in the rigidly linked D-B-A molecules. Measuring the MFEs on the yield of the triplet excited state, the Wasilewski group measured up to a 700% increase of triplet yield.[80] When τ_{RP} is sufficiently long, a clear switching between fast coherent and relatively slow incoherent mixing will result in a larger magnitude (**Fig. 3b**). In other words, we need to suppress decoherence sources to achieve larger effects. In principle, we can have a complete turn-on/off by either shutting down the singlet or triplet pathway at a given magnetic field. However, realizing such an ideal condition is still experimentally tricky.

B.4.b. 2*J*

As we used it to classify the spin system, the singlet-triplet splitting of a two-spin system, 2J, is a critical parameter. Note MARY spectroscopy alone does not provide the sign of 2J. We can use 2J as a field-response range of the SCRPs.[81] Anderson[82] used a perturbational approach to relate 2J to the magnitude of the electron transfer superexchange coupling, $V_{RP\text{-}n}$, between the RP states and surrounding states n

$$2J = E_S - E_T = \sum_{n,S} \frac{|V_{RP-n,S}|^2}{\Delta E_{RP-n,S}} - \sum_{n,T} \frac{|V_{RP-n,T}|^2}{\Delta E_{RP-n,T}} \quad (7)$$

where ΔE_{RP-n} is the vertical energy gap provided by $\Delta E_{RP-n} = E_{RP} - E_n - \lambda_T$ at a fixed reaction coordinate of the RP.[83] E_{RP}, E_n, and λ_T are the energies of the RP state, the close-by local states, and the total reorganization energies. $V_{RP\text{-}n,S}$ and $V_{RP\text{-}n,T}$ are the electronic couplings between the singlet RP and the neighboring singlet states and between the triplet RP and the neighboring triplet states. Eq. 7 is simply the summation over all perturbations of local triplet states/^{3}RP and local singlet states (both ground and excited states)/^{1}RP, each given by the square of the electronic coupling divided by the vertical energy gap. One can often restrict summation to only a single term with the interaction of the smallest ΔE_{RP-n}. In a typical situation where RPs energetically lie closer to the lowest local triplet excited state than

any local singlet (ground or excited) state (**Fig. 2a**), this single term is $\Delta E_{\mathrm{RP-T}}$ with T the first triplet excited state.[84] Under this assumption, eq. 7 becomes

$$2J = -\frac{|V_{\mathrm{RP-T}}|^2}{E_{\mathrm{RP}} - E_{\mathrm{T_1}} - \lambda_{\mathrm{T}}} \quad (8)$$

This framework connects electron transfer reactions and spin chemistry,[84] and eq. 7 directly correlates *V* and 2*J*. While we can adopt a simple version like eq. 8, it turns out that rigorously testing Anderson's approach is challenging because of the difficulty of assessing all the parameters experimentally if more than a few states contribute significantly. While the extensive studies by the Wasielewski group could correlate V^2 and 2*J*, as suggested by perturbation schemes using eq. 8, in weakly coupled systems,[65, 83, 85, 86] it is still an open question, as noted by Verhoeven,[84] that whether such a proportionality between V^2 and 2*J* can hold in general. Only the molecular system consisting of a 1,4-dimethoxynaphthalene donor (D) and a 1,1-dicyanoethylene acceptor (A) interconnected by rigid, norbornylogous bridges (DMN[n]DCV) is the series for which this relation has been tested (for n = 8, 10, 12), and their distance dependencies are different by 50%.[87] The discussion of distance dependence is provided below. As the Wasielewski group pointed out two decades ago[88] and reaffirmed more lately by Steiner and Lambert,[89] for a small S-T splitting such as those measured by MFE, we can measure 2*J* much more accurately than we can account for by theory. Yet, Anderson's equation presents an opportunity and guideline for designing the molecules with 2*J* of interest. Eq. 7 shows that we can change the sign and the magnitude of 2*J* by adjusting *V* and $\Delta E_{\mathrm{RP\text{-}n}}$. Concerning magnetic control of the chemical reaction, this framework points to the possibility of tuning a magnetic field-response range by chemical or environmental means (see below). Indeed, the study by Kobori and co-workers, by time-resolved EPR spectroscopy, showed that one could vary the sign of 2*J* by changing $\Delta E_{\mathrm{RP\text{-}n}}$.[83] While the sign of 2*J* is usually not important for sensing applications, their demonstration clearly supports the Anderson framework.

One easy way to adjust the magnitude of 2*J* is changing distance within the homologous bridge series. As the electronic coupling depends on the RP distance r_{DA} exponentially, the exchange interaction decreases approximately exponentially with r_{DA}

$$2J(r) = 2J_0 \exp\left(-\beta r_{\mathrm{DA}}\right) \quad (9)$$

where J_0 and β are the preexponential factor and decay constant, respectively. Please note that one could define J_0 either at $r_{\mathrm{DA}} = 0$ or the van der Waals contact distance.[90] Weiss et al. reported distance dependence of |2*J*| for a series of rigidly linked fixed-distance D-B-A molecules based on phenothiazine (PTZ) donor and perylenediimide (PDI) acceptor with *p*-oligophenylene bridge (PTZ-Ph_n-PDI, n = 1-5). They demonstrated that eq. 9 holds with a

decay constant β = 0.37 Å^{-1}.[88] A similar value was observed for the series consisting of dimethyl 3,5-dimethyl-4-(9-anthracenyl)-julolidine (DMJAn) donor, Ph_n bridge, and naphthalene-1,8:4,5-bis(dicarboximide) (NI) acceptor (DMJAn-Ph_n-NI, n = 1-5).[91] Weller reported a significantly larger β = 2.1 Å^{-1} for saturated oligoethylene linkers in the study of pyrene and dimethylaniline (DMA) connected by a methylene linker (Pyr-$(CH_2)_n$-DMA): this is one example of D-A systems connected with a flexible linker.[92] As a methylene chain can take different conformations, the reported r_{DA} values are the distance of "equilibrium" structures. A similarly large β = 1.6 Å^{-1} was reported by Tanimoto and co-workers, where they used phenanthrene as an electron acceptor (Phen-$(CH2)_n$-O-$(CH2)_2$-DMA).[93] While most of the 2*J* measurements were performed below 1 Tesla, one of the rare examples at high field (> 1 Tesla) came from Wegner et al., [87] in which they determined 2*J* of several members (n = 8, 10, 12) of the DMN[n]DCV series.[94, 95] They made the measurements in nonpolar solvents using magnetic field dependent chemically induced dynamic polarization (CIDNP); CIDNP measures polarization of nuclear spins that result from spin-selective charge recombination.[96-98] Measuring *J* by CIDNP exploits the magnetic field dependence of the CIDNP intensity. Measuring the field dependence requires a special procedure, whereby the photoreaction in a variable field is conducted outside the NMR magnet and rapid sample transfer to the NMR field after product generation. They reported β = 1.06 Å^{-1}. Paddon-Row and Shephard later examined the shorter DMN[n]DCV series (n = 4-7) computationally, and estimated they could reach up to 400 Tesla.[99] Representative 2*J* values as well as β values of D-A and D-B-A molecules measured to date are plotted in **Fig. 5** and tabulated in **Table 1**. Even a brief survey of these distance dependence studies illustrates the importance of the "bridge" segment: Conjugated bridges such as Ph_n and *p*-phenylethynylene (PE_nP) exhibit a significantly smaller β value than nonconjugated bridges like $(CH_2)_n$. More in-depth analysis of β and their importance on the rate constants of electron transfer reactions were covered by many previous reviews.[100-102]

Fig. 5. Distance dependence of the experimentally determined 2*J* (mT). The light red box highlights a significant change in 2*J* at a fixed distance. The data points represent the following molecular series: Gray □ for Pyr-$(CH_2)_n$-DMA;[92] Blue △ for ANI-*m*eta-Ph-NI;[90] Red ○ for DMN[n]DCV;[87] Green ▽ for PTZ–Ph_n –PDI;[88] Purple ◊ for DMJ-An-$(PE)_n$P-NI;[103] orange ◀ for C-P-C_{60};[104] sky blue ▶ for BD_H-FL-iFL-TA_RA.[81]

While the exponential dependence is one crucial factor in the long-range electron transfer reactions, and traditionally a topic of intense investigation, this data set (**Fig. 5** and **Table 1**) delineates that there is a great degree of *tunability of 2J at a fixed distance* and their

importance in the design of molecular qubits, especially for quantum sensing (see **Section III.D.1**). For example, Carbonera and co-workers measured $|2J|$ of only 0.09 mT (0.9 Gauss)[104] for the D-B-A molecule consisting of tetrathiafulvalene (TTF) donor, C_{60} acceptor, and porphyrin antenna (TTF-P-C_{60}) with r_{DA} = 28 Å in 2-methyltetrahydrofuran (2MeTHF). Similarly, very small values were measured for r_{DA} > 20 Å (entry 11 and 12 in **Table 1**).[105, 106]

Table 1. Selected Examples of Molecular D-B-A systems and their Spin Characteristics.[a]

Entry	Donor	Bridge	n	Acceptor	Solvent (Temperature)	Method	r_{DA} (Å)	2*J* (mT)	FWHM (mT)	References
1	DMA	-$(CH_2)_n$-	6	Pyr	MeCN (Room Temp)	MFE	6.9[b]	7600[c]	ND	77, 92, 107
			7				7.45	165[d]	127	
			8				7.98	75	51	
			9				8.43	28.5	23	
			10				8.87	11.1	9	
			11				9.35	4	ND[e]	
			12				9.75	--	18.7 ($B_{1/2}$)	
			16				11.3[f]	--	13.5 ($B_{1/2}$)	
2	DMA	-$(CH_2)_n$-O-$(CH_2)_2$-	4	Phen	DMF (300 K)	MFE	7.88[g]	180	120[h]	93
			6				8.97	30.2	30[h]	
			7				9.66	11.1	ND[e]	
			8				9.88	7.7	ND[e]	
			10				11.9	-- (0.31)[i]	20 ($B_{1/2}$)	
			12				11.6	-- (0.49)[i]	20 ($B_{1/2}$)	
3	DMA	-$(CH_2)_n$-O-$(CH_2)_2$-	6	DMeAnt	BN (295 K)	MFE	9[j]	10	16[h]	108
			8				10	--	18 ($B_{1/2}$)	
			10				12	--	9.5 ($B_{1/2}$)	
			16				12	--	5.6 ($B_{1/2}$)	
4	PTZ	-$(Ph)_n$-	1	PDI	Toluene (Room Temp)	MFE	12.8	ND[e]	ND[e]	88
			2				17.1	170	84[h]	
			3				21.4	31	24[h]	
			4				25.7	6.4	3[h]	
			5				30	1.5	1[h]	
5	DMJ-An	-$(Ph)_n$-	1	NI	Toluene (295 K)	MFE	16.5	170	94[h]	91
			2				20.9	30	18[h]	
			3				25.5	5.7	4.3[h]	
			4				29.9	0.9	ND[e]	

			5				34.3	0.4	ND[e]	
6	PTZ	-(FL)$_n$-	1 2 3 4	PDI	Toluene (Room Temp)	MFE	16.3 24.2 31.7 38.9	>1000 28.7[k] 3.1[k] 0.50[k]	ND[e] 27 2[h] ND[e]	109, 110
7	DMJ-An	-(FN)$_n$-	1 2 3	NI	Toluene (295 K)	MFE	20.7 29.3 37.6	40 3 0.2	21[h] ND[e] ND[e]	103
8	DMJ-An	-(PE)$_n$P-	1 2 3	NI	Toluene (295 K)	MFE	23.7 30.3 37.7	13.5 3 0.3	9.5[h] ND[e] ND[e]	103
9	DMN	[n]	8 10 12 13	DCV	Dioxane (298 K)	MF dependent CIDNP	11.5 13 14.9 15.9	10800[i] 2260 500 320[l]	ND[e] 1670 390 ND[e]	84, 87
10	TFF	Porphyrin (antenna)		C_{60}	2MeTHF (10 K)	TREPR	28	0.09	ND[e]	104
11	Carotenoid	Porphyrin (antenna)		C_{60}	2MeTHF (20 K)	TREPR	>20[m]	0.24	ND[e]	105
12	ZnP	1,3 benzene-HP’		PIM	THF (297 K)	MFE	22.4	0.4	0.39	106
13	$TA_{OMe}A$	DEB (X = OMe)		NDI	Toluene ([n])	MFE	18.9	30.5	18[h]	74
14	TA_RA (R = OMe, Me, H)	FL-iFL		BD_H	Anisole (298 K)	MFE	27	108	96	81

[a] Only the absolute value of 2*J* are shown. FWHM of the *J*-resonance are reported unless otherwise noted. [b] r_{DA} for this series is an effective distance as defined in ref [92]. [c] Estimate. [d] Taken from ref [107]. [e] ND = not determined. [f] Estimated from eq. 8 of ref [92]. [g] r_{DA} for this series is the mean distance calculated by the molecular dynamics/stochastic calculation. [h] Vales are estimated from MARY spectra in the references. [i] Estimate from the trend. [j] r_{DA} was not reported for this series. The values are simple estimates from the series with the same linker.[93] [k] Values shown here are taken from figures of ref [110]. [l] Taken from ref [84]. [m] Distance is not reported, and the value is an estimate. [n] Not reported.

On the other hand, we measured |2*J*| ~100 mT for a series of D-B-A molecules that consist of triarylamine (TAA) donor, boron dipyrromethene (BD_H) acceptor, connected by a rigid bridge (FL and iFL, where FL and iFL are fluorene and indenofluorene, respectively) with r_{DA} = 27 Å (BD_H-FL-iFL-TA_RA).[81] Over four orders of magnitude difference of |2*J*| at a comparable distance shows the instrumental and sizable role of *V* and Δ*E*. Here, we identify and briefly summarize a couple of synthetically controllable approaches/factors to modulate |2*J*|, following the Anderson framework. They are broadly classified to the factors through their influences on *V* or Δ*E*: distance, conformational changes, changes in bridge segment, and control of RP energy (**Fig. 6a**). They are illustrated in **Fig. 6**.

Fig. 6. Chemical modulation of exchange coupling 2*J*. (a) Examples of the factors that control 2*J*. (b) Well-defined MARY spectra with distinct 2*J*. Dashed curves illustrate contributions from inhomogeneous broadening to a single MARY spectrum. (c) Structural factors that change 2*J* primarily through electronic couplings. (d) Schematic potential energy surface. We can control the vertical energy gap by changing the energy of RPs by tuning the reduction potentials of acceptor and/or donor cation and solvent polarity.

We have discussed the distance dependence above. We will discuss conformational changes in the context of linewidth (**Section II.B.4.c**). Among ways of modulating electronic coupling,[111] using different bridge molecules is likely the most straightforward way to tune 2*J*. Keeping the other variables fixed (i.e., the same D/A pair of PTZ/PDI and comparable r_{DA}) and assuming the bridge state (energetically) does not significantly contribute to Eq. 7, the Wasielwski group reported about four times larger 2*J* value for fluorenone dimer (FN_2) bridge than Ph_4 bridge (29 mT vs 6.4 mT).[88, 110] An interesting case is given by Steiner and co-workers performed for a series of rigidly linked D-B-A systems consisting of triarylamine (TAA) donor and naphthalenediimide (NDI) acceptor, connected by a *meta*-conjugated diethynylbenzene bridge (**Fig. 7a**), which exhibit a pronounced *J*-resonance MARY spectrum.[89] They observed some 2*J* variations when modifying the bridge segment (functional group X in **Fig. 7a**).[89] While the detailed contributions are not clear, the result implies that relatively minor modifications on the bridge segment could make nonnegligible contributions to *V* (or possibly Δ*E*), which may be an intriguing factor for further investigations in tuning 2*J*.

Fig. 7. (a) Molecular structure of $TA_{OMe}A$-DEB-NDI. (b) Detailed analysis of the MARY peak from quantum calculations (X = OMe). Black curve: without isotropic hyperfine coupling. Red solid curve: full isotropic hyperfine coupling without S-T dephasing. Adapted with permission from J. Phys. Chem. C 122, 11701 (2018). Copyright 2018 American Chemical Society.

Regarding another factor, control of RP energy, (**Fig. 6d**), we used the series of rigidly linked BD_H-FL-iFL-TA_RA to demonstrate that we could systematically tune the magnitude of 2*J* (from ~100 to 200 mT) through chemically changing Δ*E* at a fixed distance (see **Section III.D.1** for more details).[81] This step-wise tuning of 2*J* experimentally further verifies Anderson's equation. While it is still unclear to what extent we can exploit it over a wider range, the study shows one concrete way to control a critical parameter, |2*J*|.

B.4.c. Linewidth

The spectral linewidth of the MARY spectra represents the resolution of magnetic sensitivity: a narrow linewidth of the MARY spectra means the SCRPs are responsive to external magnetic fields only within a smaller window of strengths. The linewidth of MARY spectra is usually measured either as magnetic field value at half-saturation ($B_{1/2}$) for $|2J| < a_{eff}$ or the full-width-at-half-maxima (FWHM) of the *J*-resonance for $|2J| > a_{eff}$ (**Fig. 2a**). They can be expressed by a_{eff} when we only consider coherent spin mixing by hyperfine interactions.

In the case of $|2J| < a_{eff}$, Weller and co-workers[67] showed that $B_{1/2}$ due to hyperfine couplings can be approximated by a_{eff} (eq. 4a)

$$B_{1/2} = a_{eff} \tag{10}$$

Following the pioneering works by Michel-Beyerle[112] and by Schulten,[113] Weller and co-workers[67] experimentally measured $B_{1/2}$ on the SCRPs generated by quenching reactions of pyrene singlet excited state with amines ($Pyr^{\bullet-}$/$Amine^{\bullet+}$). They found that the measured $B_{1/2}$ values are well correlated with the calculated $B_{1/2}$ values based on eqs. 4a and 10: the plot of the measured $B_{1/2}$ against the calculated $B_{1/2}$ value gives a straight line going through the origin with a slope of unity. Furthermore, Werner et al. showed that deuterating both components in the pair of Pyr/DMA result in the reduction of $B_{1/2}$ by nearly a factor of two compared to regular Pyr/DMA,[114] confirming the general validity of eq. 10 for SCRPs of $|2J| < a_{eff}$ (especially freely diffusing RPs). Note that deuteration lowers a_{eff}. However, additional factors could contribute to $B_{1/2}$, particularly the RP's lifetime (τ_{RP}). Michel-Beyerle et al. first observed the lifetime effect on $B_{1/2}$ in the study of anthracene (Ant) singlet excited state quenching by DMA. They observed $B_{1/2}$ increases as the

probing laser pulse's delay time decreases.[115] Generally, we can write $B_{1/2}$ as a function of the lifetime[116, 117]

$$B_{1/2} = B_{1/2}(\tau_{\mathrm{RP}} \to \infty) + \frac{\hbar}{\mu_B g}\frac{1}{\tau_{\mathrm{RP}}} \qquad (11a)$$

For freely diffusing RPs, one factor affecting τ_{RP} is electron self-exchange between a neutral molecule and its charged radical.[118, 119 120] In this case, τ_{RP} is expressed as

$$\frac{1}{\tau_{\mathrm{RP}}} = k_{ex}[\mathrm{Q}] \qquad (11b)$$

where k_{ex} is the rate of self-exchange and [Q] is the quencher concentration. In the pair of Ant/DMA, the quencher is an electron donor DMA. An increasing self-exchange rate with a higher concentration of the neutral quencher molecule results in shorter τ_{RP}, leading to line broadening. Further increase in concentration results in subsequent narrowing and saturation of the spectrum.[121] Eq. 11 is usually applicable in the initial broadening (so-called the limit of slow exchange). It can be explained by the energy broadening of the spin levels due to Heisenberg's uncertainty principle.[116] The latter narrowing is due to the effect of weakening the hyperfine couplings of the radical undergoing the exchange, and the saturation occurs eventually as only the non-exchanging radical contributes to $B_{1/2}$ in the very fast exchange regime.[121] This effect on the linewidth is similar to those observed in EPR spectroscopy.[122]

Another factor affecting $B_{1/2}$ is the solvation of the radical ions.[123, 124] The Grampp group experimentally demonstrated that $B_{1/2}$ decreases with increasing solvent polarity (larger solvent dielectric constant ε_S) in "heterogeneous" solvents (e.g., toluene and dimethylsulfoxide (DMSO) mixtures) for the pair of DMA donor and 9,10-dimethylanthracene (DMeAnt) acceptor.[123] A similar trend was observed for the pair of DMA donor and pyrene acceptor by Nath and co-workers.[125] On the other hand, $B_{1/2}$ stayed relatively constant in "homogeneous" solvents. Here, homogenous solvent means solvent mixtures in which macroscopic solvent parameters are similar to a pure/individual solvent.[117, 123] They were propyl acetate (PA) and butyronitrile (BN) solvent mixtures in the Grampp's work.[123] Studies of the magnetic isotope effect revealed no contributions to $B_{1/2}$ from solvent molecules, and therefore the observed effects were attributed to the RP properties.[123] These effects were explained by preferential solvation. In general, the lifetime of freely diffusing RPs is reduced in heterogeneous solvents due to an enhanced cage-effect that facilitates the recombination of SCRPs (i.e., shorter lifetime τ_{RP}). As the concentration of polar solvents increases, the solvation shell with the polar solvent component diminishes the cage effect, and the lifetime of RPs increases due to a smaller

depth of the dielectric trap and RPs escaping from the trap. The solvation model based on the Onsager theory can qualitatively explain this effect[126] and a more quantitative picture can be obtained by the continuum solvation model.[127] Time-resolved MFE (TR-MFE) studies provided further details of the reaction mechanism including the dynamics of exciplex and direct formation of SCRPs.[128, 129]

In the case of $|2J| > a_{\mathrm{eff}}$, coherent spin mixing by isotropic hyperfine coupling (a_{eff}), spin relaxation based on rotational modulation of anisotropic hyperfine interactions, and dephasing contribute to the MARY line shape. Miura, Scott, and Wasielewski showed that FWHM of the *J*-resonance can be described by (single nucleus approximation)

$$\mathrm{FWHM} = \sqrt{2}a_{eff} \qquad (12)$$

when spin mixing is governed only coherently by the hyperfine interaction.[110] However, the studies found that, for many D-B-A systems, FWHM is much bigger than predicted by eq. 12. Some linewidth values are tabulated in **Table 1**: The authors specifically reported them, or we estimated from Figures.

In the case of D-A connected with short flexible linkers, the resonance peaks are relatively broad, reflecting the distribution of *J*-values scanned by the chain dynamics of the linker, i.e., inhomogeneous broadening through distance-dependent *J* (eq. 9, see **Fig. 6c** for a cartoon picture).[92, 130] This inhomogeneous broadening of the *J*-resonance is illustrated in **Fig. 6b** (dotted curves). Generally, FWHM decreases with increasing chain length.[107] For the series of Pyr-$(CH_2)_n$-DMA, FWHM = 127, 51, 23, and 9 mT are reported with n = 7, 8, 9, and 10 in acetonitrile (MeCN), respectively (**Table 1**). They are significantly wider than the a_{eff}-based estimate (FWHM = 8.2 mT with a_{eff} = 5.8 mT[92]). Bittl and Schulten showed that the experimental *J*-resonance could be satisfactorily modeled by assuming through-space exchange interactions modulated by the stochastic folding motion of the linker, but also noted that they can be dynamically narrowed in comparison to the true *J*-distribution.[131, 132]

Interestingly, even for the rigidly linked D-B-A molecules where we do not expect to have distance fluctuations, FWHM can be much bigger than an estimate of eq. 12. For example, for PTZ–FL_n–PDI (n = 2) investigated by the Wasielewski group, FWHM is 27 mT,[109, 110] which is again larger than the theoretical estimate of eq. 12 (2.5 mT). Miura[71] attributed this broadening to S-T dephasing, which enhances S-T mixing at out-of-resonance magnetic fields, where mixing by the hyperfine interaction is inefficient (see **Fig. 3b**).[71, 133] If spin dephasing works on this mixing process, it alters the degree of mixing and eventually induces an incoherent population transfer

between the S and T states.[134] S-T dephasing is the consequence of the randomization of the S-T coherences by a varying J as caused by the molecular motion.[133] S-T dephasing was also invoked in the case of motion-constrained (caged) RPs such as those in micellar systems.[135, 136] Such a variation of $2J$ is due to diffusional fluctuations of r_{DA} similar to those with flexible linkers mentioned above. On the other hand, for the rigidly linked D-B-A molecules with fixed r_{DA}, Miura[110] proposed that fluctuations of $2J$ result from a torsional dynamics of bridge segments: it is well documented that electronic couplings V depend on torsional angles, and therefore modulate $2J$ as well as superexchange-mediated electron transfer reactions (non-Condon effect).[137-139] They ruled out the contribution of spin relaxation due to the stochastic modulation of anisotropic hyperfine interactions. One extreme case of structural/conformational effects on $2J$ is reported for another D-B-A molecule consisting of a *p*-methoxyaniline (MeOAn) donor, a 4-(Npiperidinyl)naphthalene-1,8-dicarboximide (6ANI) chromophore, and 1,8:4,5-naphthalenediimide (NI) acceptor by the Wasilewski group (MeOAn-6ANI-NI). They observed at least two conformations (likely chair/boat interconversion of piperazine linker, **Fig. 6b**) contribute to the resonance peak at room temperature, and their contributions can be resolved when the temperature is decreased.[80, 140] While effects may be subtle, these conformational changes could be exploited for synthetic control of $2J$. More discussions on these conformational effects can be found in the review by Miura.[71]

Steiner and co-workers performed a detailed investigation[74] of a series of rigidly linked D-B-A systems (**Fig. 7a**).[89] In this case, they identified that a spin relaxation (T_1-spin relaxation) caused by anisotropic hyperfine interaction essentially determines the width of the basic MARY line shape, which is superimposed by a narrow hyperfine peak broadened by a dephasing mechanism.[74] The interplay among all the contributions is illustrated in **Fig. 7b**.

While decoherence by T_1-spin relaxation and S-T dephasing can be a dominant factor broadening MARY spectra, one could nonetheless achieve a smaller linewidth. As shown in **Table 1**, the linewidth decreases with increasing r_{DA} in the homologous series, and some can be comparable to the theoretical estimate based on a_{eff}. In the extreme case, Werner et al. observed very narrow linewidths in their study of porphyrin-based D-B-A molecules; FWHM is only ~0.4 mT for ZnP-1,3-benzene-HP'-PIM (with $|2J| = 0.4$ mT).[106] Measurements were conducted in THF at 297 K. This is even smaller than $B_{1/2} = 1.1$ mT of a structurally similar ZnP-1,4 benzene-HP-PIM ($2J \sim 0$ mT – no clear resonance peak was observed), which agreed quite well with the theoretical estimate of $B_{1/2} = 1.1$ mT. The authors of this study speculated that a narrow FWHM might stem from the spin-charge delocalization of positive charges over two porphyrin units, which can reduce

hyperfine coupling interactions. Indeed, reduction of hyperfine couplings of individual charges by increasing delocalization has been observed in multiple oligomeric systems.[141-144] While it is not clear if and to what extent decoherence sources (spin relaxation and S-T dephasing) were suppressed in these narrow linewidth cases, these examples suggest that appropriate chemical design could suppress incoherent spin evolution to achieve a very narrow linewidth, possibly smaller than the theoretical estimates by a_{eff}, even for the $|2J| > a_{\text{eff}}$ case.

We would like to note that we need the quantum dynamical treatment of SCRPs in order to separate all the contributions mentioned above,[74, 145] which may well be challenging. Steiner and co-workers demonstrated that the classical treatment, based on a simple relaxation mechanism introduced by Hayashi and Nagakura,[56] could quantitatively explain the MFEs[76] and reproduce the MARY spectra if both coherent and incoherent spin transitions are included within the classical simulation.[74, 145] The observed tow-step magnetic field effect on the effective relaxation rate constant clearly exhibits the regimes of dominant coherent or incoherent spin conversion processes.[76] We expect this classical simulation to facilitate analyzing MARY spectra of future D-B-A molecules, helping uncover the strategies to maximize the contribution of coherent mixing.

III. MFE AND QUANTUM SENSING

A. General Idea

This section will draw connections between MFEs/MARY spectra and quantum sensing. A generic scheme of quantum sensing consists of five steps:[1] the initialization of the quantum sensor, transformation to the superposition state, the interaction with the signal of interest, and transformation back to the measurable state, the readout of the final state. Initialization and readout can pose a challenge for spin qubits.[2] Optical initialization and readout[19] are especially well-suited in sensing because of the relative ease of implementation, and molecular qubits based on SCRPs have natural advantages. We can achieve spin initialization by spin-selectively generating RPs. RPs and excited states can also have distinct spectroscopic signatures for optical output.

Exploiting the magnetic sensitivity of SCRPs and optical addressability, one promising area of quantum sensors is emission-based magneto-optical probes for imaging, magnetometers, and others. Incorporation of SCRPs in the photophysical pathway leading to emissive states that “address” only one spin state of RPs makes it possible to design magneto-optical probes whose emission properties (e.g., intensity, lifetime, wavelength) respond to external magnetic fields. One can improve the spatial resolution of optical imaging by magnetically imposing a spatial constraint on emissive species by using a magnetic field gradient,[146, 147] and in principle, such improvement

can go beyond the diffraction limit[147] because the spatial resolution depends only on the sensitivity of magneto-optical probes and strengths of field gradients. Such probes can also act as magnetometers. (**Section III.E.1**). In a similar manner to imaging, spatial localization of photochemically generated triplet excited states and subsequent generation of singlet oxygen may prove helpful in photodynamic therapy (PDT) (**Section III.E.2)**.[148] We can also use this magnetic sensitivity as a general switch mechanism to control chemical and biochemical reactions in real-time nondestructively, triggering different chemical reaction pathways to obtain the desired outcome at will. Applications to molecular logic gates are explored (**Section III.E.3**).

Magnetic control of emissivity/reactivity can be performed in the defects-based system, and the integrations of NVC to scanning probes[149] and optical microscopy[150] were demonstrated to help improve the spatial resolution of respective imaging techniques. Such sensors were also applied to living systems for particle tracking[151]and temperature sensing.[152] Admittedly, developments of molecular qubits based on SCRPs for quantum sensing are behind compared to these defects-based qubits, yet again, molecular systems have a clear advantage of synthetic tunability in terms of their basic qubits properties and scaling to multiple qubits beyond simple qubits. While SCRPs are SQPs, the usage for quantum sensing discussed below follows that of single qubits,[1] meaning that we consider the superposition $|\psi\rangle = c_0|S\rangle + c_1|T\rangle$. As mentioned above, this is not technically correct, but it simplifies our arguments and we can broadly classify the following examples as Type-I/II quantum sensors.

The following sections will first survey various MFEs on molecular emission in the relevant molecular systems **(Sections III.B-D**). We will then discuss a series of applications of MFEs in quantum sensors (**Section III.E**). We aim to explain how the parameters discussed in Section II affect spin dynamics and MFEs on emission by showing concrete examples and their implications for designing quantum sensors. While our primary focus is on emission, we will cover some essential examples of nonemissive readouts in **Section III.E**. We do not discuss the examples of MFEs on emission through SCRPs generated by radiolysis,[23, 51], and electric current (electroluminescence) and their implications and applications in molecular electronics[153, 154] and spintronics.[155, 156] For interested readers, the overlap and difference between the latter and traditional spin chemistry were previously reviewed.[157]

B. Freely diffusing D/A System

B.1. Energy Diagram

The majority of RPs-based MFEs on molecular emission in the solution phase uses either unlinked D/A dyads or D−A dyads connected by flexible linkers. The most well-studied type of

emissions is exciplex emission from partial charge-transfer (CT) species or exciplex ($D^{\delta+}/A^{\delta-}$) transiently formed by the electron donor and acceptor, separately from a fully CS state (SCRP), which diffusively separates and possibly reencounter.[30, 54, 158, 159] SCRPs can be formed directly from $^1A^*$, too. Exciplexes can have a variable charge-transfer character due to mixing the pure RP state with locally excited states.[160-162] Due to this mixing, exciplex can emit photons. While MFEs on exciplexes formed from triplet precursors are reported,[163] they are typically formed from singlet precursors and a typical energy diagram is shown in **Fig. 8**.[164]

Fig. 8. Energy diagram and species involved in the formation of the MFE on the exciplex and local singlet excited state. The exciplex energy is depicted as lower than SCRPs because of stabilization by the Coulomb interaction. bCR = back charge recombination. Please see **Fig. 2** legend for other acronyms.

Please note that we do not include different types of SCRPs (e.g., solvent-separated ion pairs and solvent-shared ion pairs)[165] for clarity. The observation of MFEs on exciplex emission dated back to 1980, using Pyr/dialkylaniline systems where Pyr and dialklyaniline serve as an electron acceptor and donor, respectively.[124, 166, 167] In these systems, $|2J|$ is usually < a_{eff}, and a typical MARY spectrum of exciplex resembles the red line in **Fig. 3a**. The key to observing the MFEs on exciplex is the reversibility (thermal equilibrium) of SCRPs and exciplex.[168] As r_{DA} for the exciplex is usually 3-4 Å (contact distance), their exchange interaction $2J_{exc}$ is too large so that the spin interconversion within the exciplex is usually not affected by a weak magnetic field (< 1 Tesla). On the other hand, r_{DA} for SCRPs is larger; while it depends on solvent polarity,[126] usual estimates are 7-8 Å in a polar solvent such as MeCN.[160] Only the spin interconversion within SCRPs can be magnetically sensitive in this range of magnetic fields. In the scheme presented in **Fig. 8**, exciplex is a singlet recombination product, and MFEs on exciplex can be observable only when spin information is transferred to exciplex through the reversible process. In other words, MFEs on exciplex emission are time-dependent. Treichel et al. performed the MARY spectroscopy on the local triplet excited state to show the sign of the MFE on triplet excited state is opposite to the sign of the MFEs on exciplex, validating the RP mechanism.[169]

B.2. Exciplex and Delayed Fluorescence

Kattnig, Grampp, and co-workers conducted the most systematic studies on MFE on emission using unlinked D/A systems. In the study of the unlinked pair of DMeAnt and DMA, they observed the MFE on delayed fluorescence from the local singlet excited state, in addition to the commonly

observed MFEs on exciplex (**Fig. 9a**).[164] They could spectrally resolve their contributions (**Fig. 9b**). MFEs on the local excited fluorophore were previously observed in TT annihilation[170] or in pulse radiolysis,[51, 171] and electrochemiluminescence studies.[172]

Fig. 9. MFEs on exciplex and delayed fluorescence of the pair of DMeAnt/DMA. (a) Difference in fluorescence intensity, $\Delta I = I(B_0 = B_{sat}) - I(B_0 = 0)$ in a BN/PA mixture at ε_s = 12.4. B_{sat} = 150 mT. The dashed lines correspond to the emitting species (the emitting fluorophore and the exciplex), while the solid black line denotes their sum. The gray line is the difference of the experimental spectra at B_{sat} and zero fields. (b) Wavelength dependence of the MFE, X of the same solution. X_E and X_F for MFEs of exciplex and delayed fluorescence, respectively. MFE is defined as in eq. 6. Reproduced with permission from Angew. Chem. Int. Edit. 47, 960-962 (2008). Copyright 2008 Wiley. (c) Time-resolved exciplex emission in a toluene/DMSO mixture at ε_s = 7.3 and the time evolution of the MFE $\Delta I(t)$ at B_0 = 62 mT. Van Thi Bich Pham, Hao Minh Hoang, Günter Grampp, Daniel R. Kattnig, J J. Phys. Chem. B, 121, 2677, 10.1021/acs.jpcb.7b00510, 2017; licensed under a Creative Commons Attribution (CC BY) license.

This observation was enabled by the reversibility of interconversion between the local excited state, exciplex, and SCRPs.[164] Following this initial observation, they further revealed that this effect is not peculiar to the particular system and can be observed in other unlinked D/A pairs.[78] Using a total of 17 exciplex-forming D/A systems, their study delineated how energetic factors such as a Gibbs energy change associated with the initial charge separation and recombination affect the MFEs on exciplex and delayed fluorescence. Kattnig and coworkers employed the three-state model of the exciplex (singlet excited state, RPs, and ground state), refining the model initially developed by Murata and Tachiya,[159] to analyze the experimental exciplex emission band shapes to determine the energetics. They showed that the Gibbs energy change for the exciplex formation plays a large role in determining the reversibility and, therefore, the existence of the MFEs on delayed fluorescence. Of note was a pair of 9-methylanthracene (MeAnt) acceptor and 1,3-benzendicarbonitrile donor. In this pair, the estimated Gibbs energy change between the local singlet excited state and RPs is as large as -0.36 eV, which is assumed to be too large to be reversible. It turns out that the Gibbs energy change between the local singlet excited state and the exciplex is only -0.21 eV, enabling reversibility and, therefore, the observation of the MFEs on the delayed fluorescence.

The reversibility of SCRPs and exciplex (and singlet excited states) is a prerequisite and unique aspect of the MFEs on exciplex (and delayed fluorescence). In general, they concluded that the MFE on the exciplex emission increases with the Gibbs energy of charge separation, as electron transfer results in SCRPs of a larger r_{DA} which are *a priori* more susceptible to spin conversion. Larger MFEs were also observed in systems where the charge recombination occurs in the Marcus inverted region that elongates the RP lifetime. Their model also predicts indirect contributions to 2*J* become negligible; RPs of nonzero 2*J* values contribute negatively to the magnitude of MFE, and 2*J* is closer to 0 in this region. Combined with a general consideration of exciplex emission,[160, 162] these work provide a firm starting point for searching new pairs of donor and acceptor molecules that could exhibit MFEs on exciplex and delayed fluorescence. As briefly mentioned in **Section II.B.4.c**, Kattnig and co-workers took advantage of this unique reversibility and performed TR-MFE measurements on emission. They showed that the magnitude of MFEs is indeed time-dependent (**Fig. 9c**), reflecting the interplay among spin mixing, electron transfer reactions, and diffusion. They illuminated the details of photo-generated exciplex and SCRPs; e.g., direct production of RPs from singlet excited state.[128, 129, 173]

The magnitude of the MFEs on exciplex and delayed fluorescence in unlinked systems are usually < 10-20%.[78] While a_{eff} are constant over the range of r_{DA}, the other parameters that depend on the distance (e.g., *V* and 2*J*) affect the entire spin dynamics and response to magnetic fields. One key issue is diffusion-dependent distance between the radicals, and indeed diffusive nature and wide distribution of r_{DA} diminish the overall MFEs.

C. D-A System with Flexible Linker

We now consider D-A systems connected with a flexible linker. Linking D and A with a flexible chain molecule generally increases the magnitude of MFEs. Staerk et al.[174] studied a series of polymethylene-linked D-A systems, Pyr-$(CH2)_n$-DMA (n = 8-16), that they had previously characterized for their MFEs on triplet excited state formation.[92] They observed up to ~50 % MFE with the longest linker n = 16 at B = 100 mT in MeCN (**Fig. 10a**). The exciplex emission intensities also increased as the chain length increased (**Fig. 10b**).

Fig. 10. Magnetic field effects on exciplex emission of Pyr-$(CH_2)_n$-DMA (n = 8-16) in MeCN. (a) Emission spectra (n = 16) with external magnetic field on (B_0 = 350 Gauss = 35 mT) and off. Pyr was excited at 337 nm. Exciplex emission increased in the presence of the magnetic field. (b) MARY spectra of exciplex emission detected at 595 nm at room temperature. Reproduced with permission from Chem. Phys. Lett. 118, 19 (1985). Copyright 1985 Elsevier B.V.

Tanimoto and co-workers observed a similar trend in another polymethylene-linked D-A system where they used phenanthrene as an electron acceptor instead of pyrene (Phen-$(CH_2)_n$-DMA n = 3 –10). [175] They observed a larger MFE on exciplex emission than a pyrene derivative of the same length; for example, at n =10, MFE is only ~20% for a Pyr system while it is ~50% for a Phen system. They attributed this difference to a faster nonradiative deactivation process from the Pyr-$(CH_2)_n$-DMA because of a large Franck-Condon factor; the lowest singlet excited state of Phen is higher than that of Pyr. Using a similar series of polymethylene-linked systems (Phen-$(CH_2)_n$-O-2-DMA, n = 4 – 12),[175] they also reported that the longest n= 12 exhibited the largest modulation in the exciplex emission in the presence of an external magnetic field (B_0 < 1 Tesla): up to 140% increase in the intensity and 200% increase in the lifetime at 620 mT.[93] They later performed MFEs at high field (B_0 up to 13 T) and showed a clear Δg contribution to MFEs on exciplex emission as well: decrease in the intensity and exciplex lifetime.[176] A more recent study on linked D-A systems by the Kattnig group closely looked at the effect of flexible linker on the spin dynamics using an analogous series using 9-methylanthracene as an electron acceptor and photon absorber (9-MeAnt-$(CH_2)_n$-O-2-DMA, n = 6, 8, 10, and 16).[108] For n = 8, 10, 6, the MARY spectra reveal that the average exchange interaction is negligible during the coherent lifetime of the SCRPs ($2J \sim 0$ – no clear resonance peak was observed). They observed as large as 38 % increase in exciplex emission at $B_0 = B_{sat}$ = 75 mT for the longest n = 16. They could also distinguish the MFEs on local excited emission from 9-MeAnt; 2.2 % increase at B_0 = 75 mT. These systematic studies of the D-A molecules with a flexible linker showed that 1) $2J$ is usually < a_{eff} for larger r_{DA} (> 10Å) and 2) the magnitude of MFE becomes bigger for larger r_{DA} because of larger spin mixing likely due to extended RP lifetime. Extended lifetime also provides a benefit in terms of linewidth (**Section II.B.4.c**).

D. Ordered System

D.1. Rigidly Linked D-B-A System

While they are motionally restricted compared to a freely diffusing system, the electron transfer reactions are still influenced by the stochastic conformational changes in a flexible linker system. Chain dynamics and spin dynamics are intimately coupled through the exchange interaction throughout the lifetime of the RPs, which can negatively affect MFEs and possible applications. Arranging D and A molecules in an ordered manner provides a more well-defined r_{DA}. With fixed r_{DA}, these molecular systems usually have non-zero J values (**Fig. 5**). While linking D/A with a

rigid bridge is a logical step forward, compared to flexible linker systems, only a handful of examples of MFEs on emission have been reported for a rigidly linked D-B-A system.

The majority of the rigidly linked D-B-A molecules measured MFEs on non-emissive triplet excited states and/or RPs, and did not observe MFEs emission. This is because many of the systems were designed to have a large Gibbs energy change for the initial charge separation to efficiently produce SCRPs, and therefore no reversibility between the local excited state, exciplex (if any), and SCRPs. We have recently demonstrated the magnetic modulation of recombination fluorescence produced by back charge recombination of photogenerated SCRPs in a series of rigidly linked D-B-A molecules (**Fig. 11**).[81]

Fig. 11. MFEs on recombination fluorescence of BD_H-FL-iFL-TA_RA. (a) MFEs on steady-state emission with an applied magnetic field switched between 0 and 140 mT (R = OMe). (b) The MFE on the total steady-state emission (left axis) and recombination fluorescence (right axis) as a function of the applied magnetic field. (c) Dependence of 2*J* on the energy changes. The gray and purple solid lines indicate B_{2J} for the largest and smallest $|\Delta E_{\mathrm{RP-n,S}}|$ examined. The smaller |Δ*E*| results in larger 2*J*, following Anderson's eq. 7. Adapted with permission from J. Am. Chem. Soc. 142, 20691 (2020). Copyright 2020 American Chemical Society.

To do so, we designed and constructed molecular systems that consist of boron dipyrromethene triarylamine (BD_H-FL-iFL-TA_RA , **Fig. 5**). They follow the photophysical pathway depicted in **Fig. 2a,** except we have an efficient back charge recombination process from ^{1}RP to singlet excited state ($^1A^*$). The emission occurs from $^1A^*$ exclusively produced by the spin-selective recombination of ^{1}RP ($BD_H^{\bullet-}$-Bridge-$TA_RA^{\bullet+}$), allowing us to "address" only one spin state optically. The emission responded to applying an external magnetic field, and the change was completely reversible (**Fig. 11a**). We also observed the MFE on the triplet excited state but opposite in sign to the recombination fluorescence, thereby validating the RP mechanism. This is a rare example where MFEs were observed on both singlet and triplet channels.[53] As mentioned in **Section II.B.4.b**, 2*J* is much larger than a_{eff} despite r_{DA} = 27 Å, likely because of the strong electronic couplings provided by the conjugated bridges and smaller $\Delta E_{\mathrm{RP}-n}$ (eq. 7). This results in a *J*-resonance spectrum (**Fig. 11b**), following the general picture presented in **Fig. 3a**. The magnitudes of MFEs on steady-state emission are small ~ 2-3% at most because a larger fraction of fluorescence

emission comes from nonmagnetic responsive prompt fluorescence. Yet, larger MFEs of up to ~50% were observed in a time-resolved fashion.

We further demonstrated the tunability of the field response range, expressed in terms of 2*J*, by changing the energy levels of RPs (**Fig. 11c**). We modulated the energy of RPs and thereby Δ*E* of Eq. 7 either by changing R groups of TA_RA or slightly changing solvent polarity: the bridge segment was unchanged. Thus this study demonstrated a rational design of emission-based rigidly linked D-B-A molecules that operate on SCRPs, and we can use the Anderson framework[82] to chemically tune *J*, which can be advantageous for sensing applications. One could design magnetometers or switch responsive to a specific range of magnetic field strengths (**Fig. 6b**). For example, we can activate only one probe with a specific field, even with multiple probes present. This tuning capability of field-response range is one of the unique properties of SCRPs-based quantum sensors. We also identified that incoherent spin relaxation significantly diminish the overall magnitude and broaden the linewidth employing the classical treatment.[56, 76] Therefore, we must overcome decoherence to realize the full potential of SCRPs in these emission-based qubits similar to quantum computing.[21] In this respect, we could use the insights laid out in **Sections II.B.4.b-c** to develop a better probe/sensor in the future.

We would like to note that the series of DMN[n]DCV molecules, one of the most well-studied rigidly linked D-B-A molecules, do exhibit SCRPs-associated emission in the form of long-range radiative charge recombination (i.e., CT emission).[177, 178] However, no MFEs on CT emission were reported likely because of large 2*J* values (> 1 Tesla).[87] In this respect, our recent demonstration of rational design of rigidly linked D-B-A molecules with long-range CT emission[179] by using the intensity borrowing mechanism,[180] may help us clarify if we can realize MFEs on CT emission within easily accessible magnetic field strengths, and possible use in quantum sensing.

D.2. Ordered Arrangement in Scaffold

We can achieve on ordered system through noncovalent interactions (i.e., without linking D and A directly). One excellent example is provided by Lee and co-workers. They developed exciplex-forming peptoid conjugates, linking phenyl phenanthrene and phenyl DMA on single oligomeric peptoid conjugates (PhD-PCs, **Fig. 12a**, **b**).[181] This relatively rigid structure provides conformational stability, making it possible to exhibit MFEs on exciplex emission (up to 18%) in various polarities from nonpolar diethyl ether (ε_S = 4.3) to mixtures of MeCN and water (ε_S up to 67.1) (**Fig. 12c**).

Fig. 12. (a) Molecular structures of the peptoid conjugates developed by Lee and co-workers. Phen and DMA act as electron acceptor and donor, respectively. All of the peptoid conjugates are nonamers except for (*i*, *i* + 6), which is a 12-mer. (b) The cartoons for (*i*, *i* + 2)-Ac, (*i*, *i* + 3)-Ac, and (*i*, *i* + 6) show the approximate relative orientations and distances between D and A on the peptoid structures. (c) Emission spectra of the helical PhD-PCs in the presence (solid line) and absence (dashed line) of an external magnetic field (B = 180 mT) in diethyl ether (ε_S = 4.3) and (d) at a mixture of MeCN and water (ε_S = 67.1). Adapted with permission from J. Phys. Chem. Lett. 11, 4668 (2020). Copyright 2020 American Chemical Society.

The observation of MFEs on exciplex over this wide range of solvent polarity is rare. SCRPs-associated emissions generally inherit the properties of SCRPs. As the energy of the SCRPs usually depends on solvent polarity or, more generally, electric field, the emissions can also exhibit solvent dependence.[182] For example, in the series of Phen-$(CH_2)_n$-O-2-DMA studied by the Tanimoto group, the reversibility between exciplex and SCRPs collapse at low and high polarity solvents.[93] In a nonpolar solvent, the energy of SCRPs becomes too high and energetically inaccessible. Because of the favorable Gibbs energy change for forming SCRPs, emissive exciplex formation lacked in a polar solvent.[160] Therefore, the MFEs are usually observed in the narrow range of solvent polarity.[117, 123] One can use such sensitivity for developing polarity sensors based on SCRPs' spin dynamics. We also partly took advantage of this property to tune the field-response range in the above example of BD_H-FL-iFL-TA_RA.[81] Nonetheless, for a general-purpose application, one may want spin dynamics that are relatively insensitive to solvent environments, and using a peptide-scaffold is one appealing solution.

D.3. Photosynthetic Reaction Center

The above examples show the output of the singlet channel. While still underexplored, the triplet channel can also have emission output as phosphorescence. One example comes from mother nature. Boxer and co-workers[183] have extensively studied spin dynamics of the photosynthetic reaction center. In the carotenoidless, quinone (Q)-depleted *Rhodobacter* (*Rb.*) *sphaeroides* and *Rhodopseudomonas* (*Rps.*) *viridis* reaction centers, the photophysical dynamics follows the one depicted in **Fig. 2a**. Here, D is the primary electron donor, consisting of two bacteriochlorophylls (special pair, usually represented by P), and A is the initial electron acceptor, bacteriopheophytin (usually represented by I). In Q-depleted reaction centers, they observed phosphorescence from ^{3}P at cryogenic temperature (the emission is in the NIR region, **Fig. 13a**). On this ^{3}P, they measured the MFEs on the phosphorescence yield of ^{3}P (**Fig. 13b**). The measurements were

made in polyvinyl alcohol (PVA) films at 80 K. Up to 40% reduction was observed at a relatively low field (< 50 mT), and the observed effect on phosphorescence agreed very well with the absorption measurements.[183] This is consistent with the estimated 2*J* value of the system (1.4 mT).[184] While the quantum yield of phosphorescence in this system was extremely low (2 x 10^{-8}), their demonstration was the first to show that we could detect spin dynamics of SCRPs by emission from the low-lying triplet excited states. The sign of MFE suggests an equilibrium between RP and ^{3}P. In the subsequent study, they also observed the MFEs on the delayed fluorescence (recombination fluorescence of ^{1}P) at high fields (100 mT – 15 T); the lifetimes and the yield decreased at high fields, and the saturation of the MFE was observed at 15 T.[185] At this high field, the decrease was attributed to the Δ*g* mechanism while the exact Δ*g* value was not resolved due to the absence of quantum beats.[185, 186]

Fig. 13. MFE on phosphorescence. (a) Luminescence spectrum of quinone (Q)-depleted *Rb. Sphaeroides* reaction centers in a PVA film at 20K. The peak at 1318 nm was assigned as phosphorescence. (b) MFE on phosphorescence intensity and that on the triplet yield measured by transient absorption spectroscopy. Both measurements were performed on Q-depleted *Rb. Sphaeroides* reaction centers in a PVA film at 80K. Reproduced with permission from Biochimica Et Biophysica Acta 932, 325 (1988). Copyright 1988 Elsevier B.V. (c) Photophysical energy diagram for PtP-$(Ph)_n$-$RosB^+Cl^-$ (n = 1 and 2, inset shows the structure). Please note that an electron acceptor is positively charged in its ground state. MFE is considered to originate from triplet-born RPs. (d) Emission intensity decreased in the presence of an external magnetic field (B_0 = 200 mT). Adapted with permission from J. Phys. Chem. Lett. 3, 3115 (2012). Copyright 2012 American Chemical Society.

D.4. Triplet-born RPs

We now turn our attention to one special case. Vinogradov et al. explored the possibility of measuring MFEs on phosphorescence in artificial D-B-A molecules. (**Fig. 13c**).[187] Using a series of D-B-A molecules based on Pt porphyrin and Rosamine derivative, they observed a decrease in phosphorescence emission when a magnetic field was applied. In this particular example, the initial charge separation occurs from the triplet excited state to produce ^{3}RP. Because of a strong spin-orbit coupling within Pt porphyrin, photoexcitation of PtP creates the triplet excited state

within a couple of ps.[188] Unlike the reaction centers mentioned above, the MFEs on phosphorescence in this system were realized via the reversibility between the triplet excited state and RPs (**Fig. 13d**). They only observed a simple and small decrease in emission intensity (~1 %) with increasing magnetic field; no resonance peak was observed within the test field strengths, suggesting $2J > 1$ Tesla. TR-EPR and transient absorption spectroscopies identified the existence of long-lived RPs (tens of μs at room temperature), created from the long-lived triplet excited state of Pt porphyrin, confirming that the MFEs originate from triplet-born SCRPs. While MFEs from triplet-born RPs are not uncommon,[189-192] their manifestation on photogenerated phosphorescence has still been rare.

E. Applications

E.1. Imaging

E.1.a. MFI and Magnetometers

Emission-based measurements are usually preferred to "address" spin state optically over absorption-based measurements because of their relative background-free condition and associated high sensitivity. The Cohen group explored the use of MFEs on emission to improve optical imaging. Using an unlinked pyrene/DMA system, they demonstrated the application of MFEs to optical imaging, which they called magnetofluorescence imaging (MFI).[147] Their apparatus is shown in **Fig. 14a**. As the emission intensity is a function of an external magnetic field, the magnetic field gradients lead to a spatially varying emission intensity. With the responsivity of the magneto-optical probes (MARY curve) and the gradient field, we can have *a priori* knowledge of the source of emissive species. In other words, we can perform spatial selection of emissive species by magnetic field gradient (i.e., optical sectioning).[193] The spatial resolution (δx in one direction) of such imaging techniques is defined by $\delta x = \frac{\sigma}{\nabla B_{2J}}$ where σ is the linewidth of the MARY spectra ($2 \times B_{1/2}$ or FWHM, expressed in mT) and ∇B_{2J} is the gradient in the field strength at the peak (in mT/mm).[147] As you see, the resolution is only dependent on σ and ∇B_{2J}, in principle going beyond the diffraction limit. In the example of pyrene/DMA system examined by the Cohen group, they experimentally obtained δx = 0.9 mm with σ = 18 mT and ∇B_{2J} = 26 mT/mm while a theoretical δx = 0.7 mm (**Fig. 14b**).

Fig. 14. (a) Apparatus for magnetofluorescence imaging described in [147]. The sample is immersed in a solution of pyrene/DMA (yellow disk) and placed in an octupole magnet. UV illumination impinges from above, and fluorescence is sent via 10 mm acrylic light guide to a photomultiplier

(PMT). (b) Direct optical imaging of the point spread function. A CCD camera replaced the light guide and PMT. The sample chamber was filled with pyrene/DMA, and the exciplex fluorescence was imaged onto the camera. The dark spots correspond to the locations of the null in the magnetic field. The point spread function has an FWHM of 0.94 mm. Reproduced from Opt. Express 18, 25461 (2010). Copyright 2010 Optica Publishing Group. (c) Apparatus for mapping magnetic fields described in [146]. A sample contains planar iron nanostructures and a solution of Phen-$(CH2)_n$-O-$(CH2)_2$-DMA in degassed DMF. A pair of NdFeB permanent magnets mounted below the sample generated an in-plane magnetic field that could be rotated about the optical axis. DM = dichroic mirror; TL = tube lens; F = emission filter. (d) Maps of magnetic field strength around nano- and microstructures (white light images). Scale bars are 20 μm. Adapted with permission from Nano Lett 11, 5367 (2011). Copyright 2011 American Chemical Society.

Another unique property of MFI is the insensitivity to the light paths because the magnetic field only determines the detection volume; this property makes it possible to acquire images even in the presence of arbitrary strong optical scattering (e.g., biological tissues).[147] However, relatively small MFEs on unlinked systems hampered their ability.

The Cohen group subsequently used Phen-$(CH_2)_{12}$-O-2-DMA, exhibiting higher MFE on exciplex emission (80% increase in exciplex emission), which could increase the signal-to-noise ratio. With this probe of better sensitivity, they quantified magnetic field distributions of iron nanostructures (**Fig. 14c, d**).[146] This, in turn, shows that one can use these probes as a magnetometer. While Phen-$(CH_2)_{12}$-O-2-DMA exhibits an excellent magnitude of MFEs, one of the drawbacks is that the excitation wavelength is limited to UV (up to 350 nm) and associated poor photo-stability that significantly limit the applicability. One way to circumvent this UV problem is to use multi-photon excitation, as demonstrated by Lee and Cohen.[194] In the ensuing work, Lee and co-workers used another D-A linked system based on pyrene instead of phenanthrene (Pyr-$(CH_2)_{12}$-O-2-DMA). While the magnitude of MFE itself is slightly lower (~50% increase, see **Section III.B.2**), Pyr-$(CH_2)_{12}$-O-2-DMA can be excited with a slightly longer wavelength (up to 380nm), and the system is also ~25 times brighter than Phen-$(CH_2)_{12}$-O-2-DMA. The combined improvements allowed them to perform MFI with a better signal-to-noise ratio and perform 3D magnetic field distribution imaging by two-photon fluorescence microscopy.[195] Another way to increase the signal-to-noise ratio is to suppress the magnetically unresponsive emission. This can be achieved by performing measurements in a time-resolved fashion. As prompt fluorescence (innate emission that occurs before charge separation and subsequent recombination) is not field-dependent and short-lived,

measuring only magnetically responsive emission (exciplex and/or delayed fluorescence) can increase the MFEs[81] and the signal-to-noise ratio of imaging. On the other hand, emission intensities at a later time are usually low, and the necessity of a pulsed light source could complicate the implementation of MFI.[147]

E.1.b. Challenges

While these imaging results are promising, the achieved spatial resolution was far from the diffraction limit. Practical implementations in living systems are also still difficult to achieve. We identify a couple of challenges, many of which are associated with molecular design. One is excitation wavelengths and associated photostability. The molecular systems so far explored for imaging are based on exciplex and delayed fluorescence in freely diffusing and flexible linker systems whose excitation wavelength is limited to blue to UV lights (< 400 nm)[108, 113, 164] except for two-photon excitation mentioned above.[194] Such high-energy photoexcitation is unsuitable for many intended applications, especially in living systems. Furthermore, Ikeya and Woodward recently showed that cellular autofluorescence is sensitive to an external magnetic field: $B_{1/2}$ value of 18 mT with a magnitude of 3.7%.[196] Their study suggests that the observed autofluorescence comes from flavins (λ_{em} ~ 520 nm), and the MFE data is consistent with the triplet-born SCRPs. Such MFEs on autofluorescence could affect the analysis when excitation and emission wavelengths are overlapped with spectral properties of magneto-optical probes, while time-resolved measurements could overcome this issue. Another problem is the use of a flexible linker. As chain dynamics and spin dynamics are intimately coupled when a flexible linker is used, any disturbance of chain dynamics (e.g., interactions with other molecules) can undermine the MFEs. Therefore, rigidly linked D-B-A molecules or D/A pairs arranged in scaffolds with visible-NIR absorption/emission bands are preferred as emission-based magneto-optical probes; such examples are still rare.[81, 187] These requirements put additional constraints on the molecular design. Most rigidly-linked D-B-A molecular systems studied to date (see **Fig. 4** for examples) are photoinitiated with UV-blue lights, resulting in the initial high-energy singlet excited states (~3-4 eV) that create ample energy window to perform subsequent electron transfer reactions. Moving into the visible-NIR range (~2-3 eV) limits energy windows available for all the intermediate states. It becomes more difficult but not impossible to regulate electron and energy flow in a controllable fashion to achieve necessary reversibility between emissive states and SCRPs and at the same time realize large magnitudes of MFEs on emission.

We can learn from mother nature. Acknowledging it is still the hypothesis, magnetoreception in animals based on the RP mechanism[42] is a quantum magnetometer targeted explicitly at the

strength and orientation of Earth's weak magnetic fields. Within the RP mechanism hypothesis, τ_{RP} and coherence lifetimes should be longer than 1 μs for them to be sensitive to the field and orientation of ~50 μT.[43] Cryptochrome-based systems can satisfy this threshold.[36, 37] Their artificial mimicries were also developed using an artificial D-B-A molecule[35] and model proteins[197, 198] known as maquette developed by Dutton and co-workers.[199, 200] Hore and co-workers showed an artificial D-B-A molecule of a carotenoid-porphyrin-fullerene model system (analogous to C-P-C_{60}) could work as a compass. In this example, the lifetime of the photogenerated RP responds to both the strength and direction of the magnetic field below 50 μT[35]; orientation dependence stems from the anisotropic hyperfine coupling.[201] While effects may be small, using LFE could be another venue for exploration.

Another challenge is to improve resolution. A narrower linewidth or steeper field gradients will improve spatial resolution. As mentioned in **Section II.B.4.c**, one can achieve a narrow linewidth of MARY spectra by limiting the spin relaxation and S-T dephasing mechanism. When the linewidth is limited only by isotropic hyperfine coupling, smaller a_{eff} leads to a narrower linewidth. Promising strategies of decreasing a_{eff} include largely spin-*inactive* isotopes such as deuterium (e.g., Pyr/DMA)[70, 114] and delocalization of charges.[141-144] However, these effects are largely underexplored in both flexible linker and rigidly linked D-B-A molecules, and it is an area of future exploration. Regarding the field gradient, as Yang and Cohen mentioned,[147] we can obtain a steeper gradient by decreasing their size and separation, and the group expects that their system in principle can be miniaturized by at least four orders of magnitude (sub-micron scale). While not a micron scale, a high field gradient (on the order of 60-70 mT/mm) is already used in magnetic resonance microscopy.[202, 203]

One unique problem of using magneto-optical probes in the solution phase is their relative susceptibility to unwanted disturbance such as molecular oxygen that can react with the triplet states (both RPs and local excited states). These interactions quench RPs, shortening their lifetimes to diminish or sometimes completely kill MFEs. Most experiments have been performed either in deoxygenated solutions or at low temperatures (e.g., film and frozen glass) where oxygen diffusion is limited, and this problem was not well addressed. In this regard, the body of work on magnetoreception and their mimicries, mentioned above, provide possible solutions. They could achieve long τ_{RP} and coherence time (> 1 μs) by placing a spin system in an ordered protein scaffold (e.g., cryptochromes[36, 37] and maquette-based magnetosensors[197, 198]). We could adopt a similar approach of using natural or artificial proteins or synthetic polymers like dendrimers[204]

that can adequately regulate oxygen permeability to protect spin systems from molecular oxygen and other unwanted disturbances.

E.2. Photodynamic Therapy

On the flip side, one can take advantage of sensitivity to oxygen. Following the works of Boxer[183, 205] and Mathis,[206] the Hore and Gast groups examined MFEs on singlet oxygen ($^1O_2$) in the carotenoidless *Rb. sphaeroides*.[207]

Fig. 15. (a) MARY spectrum of relative $^1O_2$ yield in Q-depleted reaction centers from the R-26 mutant from *Rb. sphaeroides*. The inset shows the same measurements made over a broader range of field strengths. Reproduced with permission from Chem. Commun. 174 (2005). Copyright 2005 Royal Society of Chemistry. (b) MARY spectrum of MP-$(OCH_2CH_2)_3$-C_{60} where M = Zn. Reproduced with permission from Phys. Med. Biol. 54, 1-16 (2009). Copyright 2009 IOP Publishing.

While $^1O_2$ is usually not formed in the wild-type *Rb. sphaeroides* as the triplet excited state of the primary donor (^3P) is rapidly quenched by a nearby carotenoid molecule. In the carnotenoidless mutant, ^3P is long-lived (49 μs),[205] allowing time for the formation of $^1O_2$. They observed ~50% reduction of $^1O_2$ formation at B_{sat} = ~50 mT with $B_{1/2}$ = 4.6 ± 0.3 mT (**Fig. 15a**), which is very similar to $B_{1/2}$ values found for the yield of ^3P (4.2 mT[205] and 5.7 mT[206]). This data is consistent with the spin dynamics of singlet-born RPs. Because of the efficiency of a homoeostatic buffering process, the authors wrote that it is unlikely that physiologically significant changes occur in cellular functions or of long-term mutagenic effects arising from magnetic field-induced variations in free radical concentrations or fluxes.

Mermut et al.[148] took this interesting result to use artificial magneto-optical probes as a photosensitizer in PDT. The idea is similar to emission-based probes in that we can achieve spatial selection of reactive oxygen species by using a magnetic field. They used the metalloporphyrin (MP where M = Cu and Zn) and C_{60} dyads, linked by a flexible triethylene glycol linker (MP-$(OCH_2CH_2)_3$-C_{60} where M = Zn and Cu, **Fig. 15b**). The authors showed the modulation of MP's fluorescence by an external magnetic field. They observed ~8% increase in emission intensity at B_0 = 300 mT for the ZnP-based molecule (**Fig. 15b**). While the details of photo- and spin dynamics like τ_{RP} were not understood in these systems, the positive MFE, combined with

the observation of relatively long-lived emission component (5-10 ns), suggests that the photophysical pathway follows the singlet-born RPs, and the observed MFE likely comes from recombination fluorescence. They also showed that MFEs are sensitive to oxygen concentration, suggesting its application to PDT. Indeed, performing PDT experiments in rat prostate tumor cells, they observed cell survival increased 50% in the presence of a magnetic field, using the CuP-based molecule. These studies show the possibility of using MFEs on PDT, and one can also envision using them to perform spin-selective catalytic reactions.

E.3. Other Applications

Another possible application is a molecular logic gate such as AND gate (not gating operations in quantum computing).[208] In the study of C-P-C_{60}, Moore, Moore, Gust, and co-workers envisioned that the ability to alter charge recombination by magnetic field significantly could be the basis of a magnetically controlled optical or optoelectronic switch,[209] where photo-excitation and magnetic field can act as two inputs. Here, photo-excitation alone does not produce the signal of interest (e.g., triplet excited states absorption) over a suitable threshold, and the application of magnetic field alone does not produce the signal either. In this scenario, the output signal is produced only when we photoexcite the system in the presence of a magnetic field (simultaneous presence of two inputs) as required for an AND gate. In this regard, a room temperature solid state device application of SCRPs as a magnetically controlled optical probe is reported by Elliott and coworkers,[210] where they used an optically clear composite material (polymer-encapsulated reverse micelles) which is a macroscopic solid incorporating fluid domains with the probe molecules. One could also imagine a similar device with three and more inputs (e.g., photon, magnetic field, temperature, pH, and polarity).

IV. CONCLUDING REMARKS

We have reviewed the basic spin chemistry of SCRPs and recent efforts of using them as qubits in the context of quantum sensing. Molecular-based SCRPs can provide a great deal of flexibility in molecular design, and therefore can be a complement and alternative candidate as qubits to other electron-spin-based qubits including solid-state defects and metal-centered molecular systems. We exploit SCRPs' sensitivity to magnetic fields and spin-selective chemical reactions. One of the promising applications is the use of molecular qubits/sensors as magneto-optical probes in optical imaging, magnetometer, and PDT. We paid particular attention to MFEs on molecular emission in this review. At present, the development of such quantum sensors remains a significant challenge. Yet, we can learn from the rich history of spin chemistry in which developments of SCRPs-based quantum sensors are firmly rooted.

We use MARY spectra as a guide to understanding and designing molecular qubits for sensing applications. We have noted a couple of molecular parameters that contribute to MARY spectra. Among them, we paid great attention to exchange couplings 2*J* that can serve as a field-response range and spectral linewidth. We identified some ways to control them synthetically, and they could be areas of further endeavors in designing qubits. Another area deserving of concerted attention in the future is suppressing decoherence sources. Quantum sensors take advantage of exquisite sensitivity to environments. Yet, like many other qubit systems, we need to protect SCRPs' quantum systems from unwanted disturbance so that RPs themselves are long-lived and, at the same time, can exhibit long-lived coherence and undergo spin-selective recombination processes. We, therefore, need to find a middle ground between sensitivity and functionality.

One issue in designing new quantum sensors is that we still lack predicting power. This is because the number of molecular systems investigated is still relatively small. The spin chemistry field has long used a small set of D/A pairs such as Pyr/DMA, and we still have only a handful of rigidly linked D-B-A systems whose spin characteristics were well understood. While synthesizing D-B-A molecular systems is admittedly more costly and time-consuming, we could use the help of computational/theoretical tools to this end. With the development of long-range corrected hybrid functionals,[211] density functional theory (DFT) calculations can now decently predict energy ordering of RPs and local states, and electronic couplings,[212, 213] and are routinely used in many of the studies of D-B-A molecules mentioned in this review. Spin chemistry has also developed sophisticated theoretical frameworks for properly treating the quantum nature of RPs that can provide a reasonable understanding of the existing molecular systems.[74, 214-217] However, purposeful attempts to exploit in practice these developments to design molecular systems with desirable spin properties and dynamics (e.g., 2*J* and a_{eff}) have been very rare. We believe that expanding the chemical space for spin chemistry studies, with the help of computational and theoretical approaches, will eventually equip us with reasonable predicting power.

Another important goal is to make full use of the quantum nature of SCRPs, that is, entanglement. So far, the use of SCRPs in quantum sensing, covered in this review, has also been limited to Type-I and Type-II sensors in Degen et al.'s classification.[1] Clearly, an important goal is to explicitly use them as SQPs, which undoubtedly offer edges over other qubits. Adopting an approach employed in metal-centered molecular qubits, we may be able to integrate SQPs into discrete ordered arrays such as MOF[218, 219] for further scaling.

Developments of quantum sensors based on SCRPs will benefit from efforts in quantum computing and communication and quantum biology that share the working principles. Whether

or not they are functionally important in magnetoreception, further clarifications of SCRPs systems found in nature at the molecular level may reveal their strategies of keeping qubits protected, which in turn may help us design new generations of D-B-A molecular qubits or protein-based qubits through engineering[220, 221] for sensing. Vice versa, molecular quantum sensors, if realized, can provide insight into the environments of qubits, and may help understand material conditions and biological phenomena beyond what is possible with classical sensors to live up to their name.

ACKNOWLEDGEMENT

The author acknowledges funding by JST, PRESTO Grant Number JPMJPR17GA, Japan, the National Science Foundation under Grant No. 2144787, an NSF CAREER Award, and Brookhaven National Laboratory, Program Development Fund (PD 22-014).

DATA AVAILABILITY

The data that support the findings of this study are available from the corresponding author upon reasonable request.

REFERENCE

[1] C. L. Degen, F. Reinhard, and P. Cappellaro, "Quantum sensing," Rev. Mod. Phys. **89**, 035002 (2017).

[2] D. P. DiVincenzo, "The physical implementation of quantum computation," Fortschritte der Phys. **48**, 771-783 (2000).

[3] T. D. Ladd, F. Jelezko, R. Laflamme, Y. Nakamura, C. Monroe, and J. L. O'Brien, "Quantum computers," Nature **464**, 45-53 (2010).

[4] A. Chatterjee, P. Stevenson, S. De Franceschi, A. Morello, N. P. de Leon, and F. Kuemmeth, "Semiconductor qubits in practice," Nature Reviews Physics **3**, 157-177 (2021).

[5] M. W. Doherty, N. B. Manson, P. Delaney, F. Jelezko, J. Wrachtrup, and L. C. L. Hollenberg, "The nitrogen-vacancy colour centre in diamond," Phys. Rep. **528**, 1-45 (2013).

[6] L. Rondin, J. P. Tetienne, T. Hingant, J. F. Roch, P. Maletinsky, and V. Jacques, "Magnetometry with nitrogen-vacancy defects in diamond," Rep. Prog. Phys. **77**, 056503 (2014).

[7] R. Schirhagl, K. Chang, M. Loretz, and C. L. Degen, "Nitrogen-vacancy centers in diamond: Nanoscale sensors for physics and biology," Annu. Rev. Phys. Chem. **65**, 83-105 (2014).

[8] W. F. Koehl, B. B. Buckley, F. J. Heremans, G. Calusine, and D. D. Awschalom, "Room temperature coherent control of defect spin qubits in silicon carbide," Nature **479**, 84-87 (2011).

[9] M. Widmann, S.-Y. Lee, T. Rendler, N. T. Son, H. Fedder, S. Paik, L.-P. Yang, N. Zhao, S. Yang, I. Booker, A. Denisenko, M. Jamali, S. A. Momenzadeh, I. Gerhardt, T. Ohshima, A. Gali, E. Janzén, and J. Wrachtrup, "Coherent control of single spins in silicon carbide at room temperature," Nat. Mater. **14**, 164-168 (2015).

[10] D. J. Christle, A. L. Falk, P. Andrich, P. V. Klimov, J. U. Hassan, Nguyen T. Son, E. Janzén, T. Ohshima, and D. D. Awschalom, "Isolated electron spins in silicon carbide with millisecond coherence times," Nat. Mater. **14**, 160-163 (2015).

[11] R. Sessoli, "Toward the quantum computer: Magnetic molecules back in the race," ACS Cent. Sci. **1**, 473-474 (2015).

[12] J. M. Zadrozny, J. Niklas, O. G. Poluektov, and D. E. Freedman, "Millisecond coherence time in a tunable molecular electronic spin qubit," ACS Cent. Sci. **1**, 488-492 (2015).

[13] S. L. Bayliss, D. W. Laorenza, P. J. Mintun, B. D. Kovos, D. E. Freedman, and D. D. Awschalom, "Optically addressable molecular spins for quantum information processing," Science **370**, 1309-1312 (2020).

[14] M. S. Fataftah, J. M. Zadrozny, S. C. Coste, M. J. Graham, D. M. Rogers, and D. E. Freedman, "Employing forbidden transitions as qubits in a nuclear spin-free chromium complex," J. Am. Chem. Soc. **138**, 1344-1348 (2016).

[15] M. Šimėnas, B. Jee, M. Hartmann, J. r. Banys, and A. Pöppl, "Adsorption and desorption of hd on the metal–organic framework cu2.97zn0.03(btc)2 studied by three-pulse eseem spectroscopy," J. Phys. Chem. C **119**, 28530-28535 (2015).

[16] B. Jee, M. Hartmann, and A. Pöppl, "H, d and hd adsorption upon the metal-organic framework [cuzn(btc)] studied by pulsed endor and hyscore spectroscopy," Mol. Phys. **111**, 2950-2966 (2013).

[17] M. R. Wasielewski, M. D. E. Forbes, N. L. Frank, K. Kowalski, G. D. Scholes, J. Yuen-Zhou, M. A. Baldo, D. E. Freedman, R. H. Goldsmith, T. Goodson, M. L. Kirk, J. K. McCusker, J. P. Ogilvie, D. A. Shultz, S. Stoll, and K. B. Whaley, "Exploiting chemistry and molecular systems for quantum information science," Nat. Rev. Chem. **4**, 490-504 (2020).

[18] M. J. Graham, J. M. Zadrozny, M. S. Fataftah, and D. E. Freedman, "Forging solid-state qubit design principles in a molecular furnace," Chem. Mater. **29**, 1885-1897 (2017).

[19] M. S. Fataftah, and D. E. Freedman, "Progress towards creating optically addressable molecular qubits," Chem. Commun. **54**, 13773-13781 (2018).

[20] C.-J. Yu, S. von Kugelgen, D. W. Laorenza, and D. E. Freedman, "A molecular approach to quantum sensing," ACS Cent. Sci. **7**, 712-723 (2021).

[21] S. M. Harvey, and M. R. Wasielewski, "Photogenerated spin-correlated radical pairs: From photosynthetic energy transduction to quantum information science," J. Am. Chem. Soc. **143**, 15508-15529 (2021).

[22] M. R. Wasielewski, "Energy, charge, and spin transport in molecules and self-assembled nanostructures inspired by photosynthesis," J. Org. Chem. **71**, 5051-5066 (2006).

[23] O. A. Anisimov, V. L. Bizyaev, N. N. Lukzen, V. M. Grigoryants, and Y. N. Molin, "The induction of quantum beats by hyperfine interactions in radical-ion pair recombination," Chem. Phys. Lett. **101**, 131-135 (1983).

[24] V. A. Bagryansky, V. I. Borovkov, Y. N. Molin, M. P. Egorov, and O. M. Nefedov, "Quantum beats in the recombination fluorescence of radical ion pairs caused by the hyperfine coupling in radical anions," Chem. Phys. Lett. **295**, 230-236 (1998).

[25] J. N. Nelson, J. Zhang, J. Zhou, B. K. Rugg, M. D. Krzyaniak, and M. R. Wasielewski, "Effect of electron–nuclear hyperfine interactions on multiple-quantum coherences in photogenerated covalent radical (qubit) pairs," J. Phys. Chem. A **122**, 9392-9402 (2018).

[26] J. N. Nelson, M. D. Krzyaniak, N. E. Horwitz, B. K. Rugg, B. T. Phelan, and M. R. Wasielewski, "Zero quantum coherence in a series of covalent spin-correlated radical pairs," J. Phys. Chem. A **121**, 2241-2252 (2017).

[27] M. E. Flatté, D. Schlom, I. Siddiqi, and T. Taylor, "Opportunities for basic research for next-generation quantum systems pro 2: Enhance creation and control of coherence in quantum systems," Basic Energy Science Roundtable, 13-18 (2017).

[28] J. N. Nelson, J. Zhang, J. Zhou, B. K. Rugg, M. D. Krzyaniak, and M. R. Wasielewski, "Cnot gate operation on a photogenerated molecular electron spin-qubit pair," J. Chem. Phys. **152**, 014503 (2020).

[29] B. K. Rugg, M. D. Krzyaniak, B. T. Phelan, M. A. Ratner, R. M. Young, and M. R. Wasielewski, "Photodriven quantum teleportation of an electron spin state in a covalent donor–acceptor–radical system," Nat. Chem. **11**, 981-986 (2019).

[30] U. E. Steiner, and T. Ulrich, "Magnetic-field effects in chemical-kinetics and related phenomena," Chem. Rev. **89**, 51-147 (1989).

[31] H. Hayashi, *Introduction to dynamic spin chemistry* (World Scientific, Singapore, 2004), Vol. 8, World scientific lecture and notes in chemistry,

[32] R. C. Johnson, R. E. Merrifield, P. Avakian, and R. B. Flippen, "Effects of magnetic fields on the mutual annihilation of triplet excitons in molecular crystals," Phys. Rev. Lett. **19**, 285-287 (1967).

[33] R. C. Johnson, and R. E. Merrifield, "Effects of magnetic fields on the mutual annihilation of triplet excitons in anthracene crystals," Physical Review B **1**, 896-902 (1970).

[34] T. Mani, and S. A. Vinogradov, "Magnetic field effects on triplet-triplet annihilation in solutions: Modulation of visible/nir luminescence," J. Phys. Chem. Lett. **4**, 2799-2804 (2013).

[35] K. Maeda, K. B. Henbest, F. Cintolesi, I. Kuprov, C. T. Rodgers, P. A. Liddell, D. Gust, C. R. Timmel, and P. J. Hore, "Chemical compass model of avian magnetoreception," Nature **453**, 387-390 (2008).

[36] K. Maeda, A. J. Robinson, K. B. Henbest, H. J. Hogben, T. Biskup, M. Ahmad, E. Schleicher, S. Weber, C. R. Timmel, and P. J. Hore, "Magnetically sensitive light-induced reactions in cryptochrome are consistent with its proposed role as a magnetoreceptor," Proc. Natl. Acad. Sci. U.S.A. **109**, 4774-4779 (2012).

[37] J. Xu, L. E. Jarocha, T. Zollitsch, M. Konowalczyk, K. B. Henbest, S. Richert, M. J. Golesworthy, J. Schmidt, V. Déjean, D. J. C. Sowood, M. Bassetto, J. Luo, J. R. Walton, J. Fleming, Y. Wei, T. L. Pitcher, G. Moise, M. Herrmann, H. Yin, H. Wu, R. Bartölke, S. J. Käsehagen, S. Horst, G. Dautaj, P. D. F. Murton, A. S. Gehrckens, Y. Chelliah, J. S. Takahashi, K.-W. Koch, S. Weber, I. A. Solov'yov, C. Xie, S. R. Mackenzie, C. R. Timmel, H. Mouritsen, and P. J. Hore, "Magnetic sensitivity of cryptochrome 4 from a migratory songbird," Nature **594**, 535-540 (2021).

[38] L. M. Antill, J. P. Beardmore, and J. R. Woodward, "Time-resolved optical absorption microspectroscopy of magnetic field sensitive flavin photochemistry," Rev. Sci. Instrum. **89**, 023707 (2018).

[39] J. P. Beardmore, L. M. Antill, and J. R. Woodward, "Optical absorption and magnetic field effect based imaging of transient radicals," Angew. Chem. Int. Edit. **54**, 8494-8497 (2015).

[40] L. M. Antill, and J. R. Woodward, "Flavin adenine dinucleotide photochemistry is magnetic field sensitive at physiological ph," J. Phys. Chem. Lett. **9**, 2691-2696 (2018).

[41] H. Mouritsen, "Long-distance navigation and magnetoreception in migratory animals," Nature **558**, 50-59 (2018).

[42] P. J. Hore, and H. Mouritsen, "The radical-pair mechanism of magnetoreception," Annu. Rev. Biophys. **45**, 299-344 (2016).

[43] C. T. Rodgers, and P. J. Hore, "Chemical magnetoreception in birds: The radical pair mechanism," Proc. Natl. Acad. Sci. U.S.A. **106**, 353-360 (2009).

[44] M. R. Wasielewski, "Photoinduced electron transfer in supramolecular systems for artificial photosynthesis," Chem. Rev. **92**, 435-461 (1992).

[45] D. Gust, T. A. Moore, and A. L. Moore, "Molecular mimicry of photosynthetic energy and electron transfer," Accounts Chem. Res. **26**, 198-205 (1993).

[46] D. Gust, T. A. Moore, and A. L. Moore, "Solar fuels via artificial photosynthesis," Accounts Chem. Res. **42**, 1890-1898 (2009).

[47] N. Lambert, Y.-N. Chen, Y.-C. Cheng, C.-M. Li, G.-Y. Chen, and F. Nori, "Quantum biology," Nature Physics **9**, 10-18 (2013).

[48] Y.-N. Chiu, and M. Gong, "Spin symmetry and interaction mechanisms in free radical reactions," Chem. Phys. **145**, 397-412 (1990).

[49] E. Wigner, and E. E. Witmer, "Über die struktur der zweiatomigen molekelspektren nach der quantenmechanik," Zeitschrift für Physik **51**, 859-886 (1928).

[50] R. T. Carter, and J. R. Huber, "Quantum beat spectroscopy in chemistry," Chem. Soc. Rev. **29**, 305-314 (2000).

[51] V. Bagryansky, A. , V. I. Borovkov, and Y. Molin, N., "Quantum beats in radical pairs," Russ. Chem. Rev. **76**, 493 (2007).

[52] P. Gilch, F. Pöllinger-Dammer, C. Musewald, M. E. Michel-Beyerle, and U. E. Steiner, "Magnetic field effect on picosecond electron transfer," Science **281**, 982-984 (1998).

[53] D. Mims, J. Herpich, N. N. Lukzen, U. E. Steiner, and C. Lambert, "Readout of spin quantum beats in a charge-separated radical pair by pump-push spectroscopy," Science **374**, 1470-1474 (2021).

[54] K. A. McLauchlan, and U. E. Steiner, "The spin-correlated radical pair as a reaction intermediate," Mol. Phys. **73**, 241-263 (1991).

[55] N. J. Turro, V. Ramamurhy, and J. C. Scaiano, *Principles of molecular photochemistry: An introdcution* (University Science Books, 2009),

[56] H. Hayashi, and S. Nagakura, "Theoretical study of relaxation mechanism in magnetic field effects on chemical reactions," Bulletin of the Chemical Society of Japan **57**, 322-328 (1984).

[57] C. D. Buckley, D. A. Hunter, P. J. Hore, and K. A. McLauchlan, "Electron spin resonance of spin-correlated radical pairs," Chem. Phys. Lett. **135**, 307-312 (1987).

[58] G. L. Closs, M. D. E. Forbes, and J. R. Norris, "Spin-polarized electron paramagnetic resonance spectra of radical pairs in micelles: Observation of electron spin-spin interactions," J. Phys. Chem. **91**, 3592-3599 (1987).

[59] J. R. Norris, A. L. Morris, M. C. Thurnauer, and J. Tang, "A general model of electron spin polarization arising from the interactions within radical pairs," J. Chem. Phys. **92**, 4239-4249 (1990).

[60] R. H. Clarke, and R. H. Clarke, in *Triplet state odmr spectroscopy: Techniques and applications to biophysical systems* (John Wiley & Sons, 1982).

[61] W. Lersch, and M. E. Michel-Beyerle, "Magnetic field effects on the recombination of radical ions in reaction centers of photosynthetic bacteria," Chem. Phys. **78**, 115-126 (1983).

[62] A. L. Buchachenko, and V. L. Berdinsky, "Electron spin catalysis," Chem. Rev. **102**, 603-612 (2002).

[63] T. Okada, I. Karaki, E. Matsuzawa, N. Mataga, Y. Sakata, and S. Misumi, "Ultrafast intersystem crossing in some intramolecular heteroexcimers," J. Phys. Chem. **85**, 3957-3960 (1981).

[64] H. vanWilligen, G. Jones, and M. S. Farahat, "Time-resolved epr study of photoexcited triplet-state formation in electron-donor-substituted acridinium ions," J. Phys. Chem. **100**, 3312-3316 (1996).

[65] Z. E. X. Dance, Q. X. Mi, D. W. McCamant, M. J. Ahrens, M. A. Ratner, and M. R. Wasielewski, "Time-resolved epr studies of photogenerated radical ion pairs separated by p-

phenylene oligomers and of triplet states resulting from charge recombination," J. Phys. Chem. B **110**, 25163-25173 (2006).

[66] J. T. Buck, A. M. Boudreau, A. DeCarmine, R. W. Wilson, J. Hampsey, and T. Mani, "Spin-allowed transitions control the formation of triplet excited states in orthogonal donor-acceptor dyads," Chem **5**, 138-155 (2019).

[67] A. Weller, F. Nolting, and H. Staerk, "A quantitative interpretation of the magnetic field effect on hyperfine-coupling-induced triplet fromation from radical ion pairs," Chem. Phys. Lett. **96**, 24-27 (1983).

[68] B. Brocklehurst, "Spin correlation in the geminate recombination of radical ions in hydrocarbons. Part 1.—theory of the magnetic field effect," Journal of the Chemical Society, Faraday Transactions 2: Molecular and Chemical Physics **72**, 1869-1884 (1976).

[69] C. R. Timmel, U. Till, B. Brocklehurst, K. A. McLauchlan, and P. J. Hore, "Effects of weak magnetic fields on free radical recombination reactions," Mol. Phys. **95**, 71-89 (1998).

[70] C. R. Timmel, and K. B. Henbest, "A study of spin chemistry in weak magnetic fields," Philos Transact A Math Phys Eng Sci **362**, 2573-2589 (2004).

[71] T. Miura, "Studies on coherent and incoherent spin dynamics that control the magnetic field effect on photogenerated radical pairs," Mol. Phys. **118**, e1643510 (2020).

[72] O. M. Usov, V. M. Grigoryants, B. M. Tadjikov, and Y. N. Molin, "Determination of a fraction of spin-correlated radical ion pairs in irradiated alkanes by quantum oscillation technique," Radiat. Phys. Chem. **49**, 237-243 (1997).

[73] V. M. Grigoryants, B. M. Tadjikov, O. M. Usov, and Y. N. Molin, "Phase shift of quantum oscillations in the recombination luminescence of spin-correlated radical ion pairs," Chem. Phys. Lett. **246**, 392-398 (1995).

[74] U. E. Steiner, J. Schäfer, N. N. Lukzen, and C. Lambert, "J-resonance line shape of magnetic field-affected reaction yield spectrum from charge recombination in a linked donor–acceptor dyad," J. Phys. Chem. C **122**, 11701-11708 (2018).

[75] B. Brocklehurst, and K. A. McLauchlan, "Free radical mechanism for the effects of environmental electromagnetic fields on biological systems," International Journal of Radiation Biology **69**, 3-24 (1996).

[76] J. H. Klein, D. Schmidt, U. E. Steiner, and C. Lambert, "Complete monitoring of coherent and incoherent spin flip domains in the recombination of charge-separated states of donor-iridium complex-acceptor triads," J. Am. Chem. Soc. **137**, 11011-11021 (2015).

[77] H. Staerk, H. G. Busmann, W. Kuehnle, and R. Treichel, "Temperature study of the magnetic field effect in photogenerated flexibly-linked radical ion pairs: Influence of the stochastically modulated exchange interaction," J. Phys. Chem. **95**, 1906-1917 (1991).

[78] D. R. Kattnig, A. Rosspeintner, and G. Grampp, "Magnetic field effects on exciplex-forming systems: The effect on the locally excited fluorophore and its dependence on free energy," Phys. Chem. Chem. Phys. **13**, 3446-3460 (2011).

[79] L. A. Margulis, I. V. Khudyakov, and V. A. Kuzmin, "Magnetic field effects on radical recombination in a cage and in the bulk of a viscous solvent," Chem. Phys. Lett. **119**, 244-250 (1985).

[80] E. A. Weiss, M. J. Tauber, M. A. Ratner, and M. R. Wasielewski, "Electron spin dynamics as a probe of molecular dynamics: Temperature-dependent magnetic field effects on charge recombination within a covalent radical ion pair," J. Am. Chem. Soc. **127**, 6052-6061 (2005).

[81] J. T. Buck, and T. Mani, "Magnetic control of recombination fluorescence and tunability by modulation of radical pair energies in rigid donor–bridge–acceptor systems," J. Am. Chem. Soc. **142**, 20691-20700 (2020).

[82] P. W. Anderson, "New approach to the theory of superexchange interactions," Phys. Rev. **115**, 2-13 (1959).

[83] Y. Kobori, S. Sekiguchi, K. Akiyama, and S. Tero-Kubota, "Chemically induced dynamic electron polarization study on the mechanism of exchange interaction in radical ion pairs

generated by photoinduced electron transfer reactions," J. Phys. Chem. A **103**, 5416-5424 (1999).

[84] J. W. Verhoeven, "On the role of spin correlation in the formation, decay, and detection of long-lived, intramolecular charge-transfer states," J. Photochem. Photobiol. C **7**, 40-60 (2006).

[85] T. Miura, R. Carmieli, and M. R. Wasielewski, "Time-resolved epr studies of charge recombination and triplet-state formation within donor−bridge−acceptor molecules having wire-like oligofluorene bridges," J. Phys. Chem. A **114**, 5769-5778 (2010).

[86] E. A. Weiss, M. J. Ahrens, L. E. Sinks, M. A. Ratner, and M. R. Wasielewski, "Solvent control of spin-dependent charge recombination mechanisms within donor-conjugated bridge-acceptor molecules," J. Am. Chem. Soc. **126**, 9510-9511 (2004).

[87] M. Wegner, H. Fischer, S. Grosse, H.-M. Vieth, A. M. Oliver, and M. N. Paddon-Row, "Field dependent cidnp from photochemically generated radical ion pairs in rigid bichromophoric systems," Chem. Phys. **264**, 341-353 (2001).

[88] E. A. Weiss, M. J. Ahrens, L. E. Sinks, A. V. Gusev, M. A. Ratner, and M. R. Wasielewski, "Making a molecular wire: Charge and spin transport through para-phenylene oligomers," J. Am. Chem. Soc. **126**, 5577-5584 (2004).

[89] J. Schäfer, M. Holzapfel, A. Schmiedel, U. E. Steiner, and C. Lambert, "Fine tuning of electron transfer and spin chemistry parameters in triarylamine–bridge–naphthalene diimide dyads by bridge substituents," Phys. Chem. Chem. Phys. **20**, 27093-27104 (2018).

[90] A. S. Lukas, P. J. Bushard, E. A. Weiss, and M. R. Wasielewski, "Mapping the influence of molecular structure on rates of electron transfer using direct measurements of the electron spin-spin exchange interaction," J. Am. Chem. Soc. **125**, 3921-3930 (2003).

[91] A. M. Scott, T. Miura, A. B. Ricks, Z. E. X. Dance, E. M. Giacobbe, M. T. Colvin, and M. R. Wasielewski, "Spin-selective charge transport pathways through p-oligophenylene-linked donor−bridge−acceptor molecules," J. Am. Chem. Soc. **131**, 17655-17666 (2009).

[92] A. Weller, H. Staerk, and R. Treichel, "Magnetic-field effects on geminate radical-pair recombination," Farad. Discuss. **78**, 271-278 (1984).

[93] H. Cao, Y. Fujiwara, T. Haino, Y. Fukazawa, C.-H. Tung, and Y. Tanimoto, "Magnetic field effects on intramolecular exciplex fluorescence of chain-linked phenanthrene and n,n-dimethylaniline: Influence of chain length, solvent, and temperature," Bulletin of the Chemical Society of Japan **69**, 2801-2813 (1996).

[94] M. N. Paddon-Row, A. M. Oliver, J. M. Warman, K. J. Smit, M. P. De Haas, H. Oevering, and J. W. Verhoeven, "Factors affecting charge separation and recombination in photoexcited rigid donor-insulator-acceptor compounds," J. Phys. Chem. **92**, 6958-6962 (1988).

[95] J. M. Warman, K. J. Smit, M. P. De Haas, S. A. Jonker, M. N. Paddon-Row, A. M. Oliver, J. Kroon, H. Oevering, and J. W. Verhoeven, "Long-distance charge recombination within rigid molecular assemblies in nondipolar solvents," J. Phys. Chem. **95**, 1979-1987 (1991).

[96] G. L. Closs, in *Advances in magnetic and optical resonance*, edited by J. S. Waugh (Academic Press, 1974), pp. 157-229.

[97] H. R. Ward, and R. G. Lawler, "Nuclear magnetic resonance emission and enhanced absorption in rapid organometallic reactions," J. Am. Chem. Soc. **89**, 5518-5519 (1967).

[98] J. Bargon, H. Fischer, and U. Johnsen, "Kernresonanz-emissionslinien während rascher radikalreaktionen: I. Aufnahmeverfahren und beispiele," Zeitschrift für Naturforschung A **22**, 1551-1555 (1967).

[99] M. N. Paddon-Row, and M. J. Shephard, "A time-dependent density functional study of the singlet−triplet energy gap in charge-separated states of rigid bichromophoric molecules," J. Phys. Chem. A **106**, 2935-2944 (2002).

[100] B. Albinsson, M. P. Eng, K. Pettersson, and M. U. Winters, "Electron and energy transfer in donor-acceptor systems with conjugated molecular bridges," Phys. Chem. Chem. Phys. **9**, 5847-5864 (2007).

[101] H. B. Gray, and J. R. Winkler, "Long-range electron transfer," Proc. Natl. Acad. Sci. U.S.A. **102**, 3534-3539 (2005).

[102] O. S. Wenger, "How donor-bridge-acceptor energetics influence electron tunneling dynamics and their distance dependences," Accounts Chem. Res. **44**, 25-35 (2011).

[103] A. M. Scott, A. Butler Ricks, M. T. Colvin, and M. R. Wasielewski, "Comparing spin-selective charge transport through donor–bridge–acceptor molecules with different oligomeric aromatic bridges," Angew. Chem. Int. Edit. **49**, 2904-2908 (2010).

[104] M. Di Valentin, A. Bisol, G. Agostini, P. A. Liddell, G. Kodis, A. L. Moore, T. A. Moore, D. Gust, and D. Carbonera, "Photoinduced long-lived charge separation in a tetrathiafulvalene−porphyrin−fullerene triad detected by time-resolved electron paramagnetic resonance," J. Phys. Chem. B **109**, 14401-14409 (2005).

[105] D. Carbonera, M. Di Valentin, C. Corvaja, G. Agostini, G. Giacometti, P. A. Liddell, D. Kuciauskas, A. L. Moore, T. A. Moore, and D. Gust, "Epr investigation of photoinduced radical pair formation and decay to a triplet state in a carotene−porphyrin−fullerene triad," J. Am. Chem. Soc. **120**, 4398-4405 (1998).

[106] U. Werner, Y. Sakaguchi, H. Hayashi, G. Nohya, R. Yoneshima, S. Nakajima, and A. Osuka, "Magnetic field effects in the radical ion pair recombination of fixed-distance triads consisting of porphyrins and an electron acceptor," J. Phys. Chem. **99**, 13930-13937 (1995).

[107] H. Staerk, H. G. Busmann, W. Kühnle, and A. Weller, "Solvent effects on the magnetic-field-dependent reaction yields of photogenerated radical ion pairs," Chem. Phys. Lett. **155**, 603-608 (1989).

[108] H. M. Hoang, V. T. B. Pham, G. Grampp, and D. R. Kattnig, "Magnetic field-sensitive radical pair dynamics in polymethylene ether-bridged donor–acceptor systems," ACS Omega **3**, 10296-10305 (2018).

[109] R. H. Goldsmith, L. E. Sinks, R. F. Kelley, L. J. Betzen, W. Liu, E. A. Weiss, M. A. Ratner, and M. R. Wasielewski, "Wire-like charge transport at near constant bridge energy through fluorene oligomers," Proc. Natl. Acad. Sci. U.S.A. **102**, 3540-3545 (2005).

[110] T. Miura, A. M. Scott, and M. R. Wasielewski, "Electron spin dynamics as a controlling factor for spin-selective charge recombination in donor−bridge−acceptor molecules," J. Phys. Chem. C **114**, 20370-20379 (2010).

[111] M. D. Newton, "Quantum chemical probes of electron-transfer kinetics - the nature of donor-acceptor interactions," Chem. Rev. **91**, 767-792 (1991).

[112] M. E. Michel-Beyerle, R. Haberkorn, W. Bube, E. Steffens, H. Schröder, H. J. Neusser, E. W. Schlag, and H. Seidlitz, "Magnetic field modulation of geminate recombination of radical ions in a polar solvent," Chem. Phys. **17**, 139-145 (1976).

[113] K. Schulten, H. Staerk, A. Weller, H. J. Werner, and B. Nickel, "Magnetic field dependence of the geminate recombination of radical ion pairs in polar solvents," Z. Phys. Chem. **101**, 371-390 (1976).

[114] H. J. Werner, H. Staerk, and A. Weller, "Solvent, isotope, and magnetic field effects in the geminate recombination of radical ion pairs," J. Chem. Phys. **68**, 2419-2426 (1978).

[115] M. E. Michel-Beyerle, H. W. Krüger, R. Haberkorn, and H. Seidlitz, "Nanosecond time-resolved magnetic field effect on radical recombination in solution," Chem. Phys. **42**, 441-447 (1979).

[116] H. Staerk, R. Treichel, and A. Weller, "Life uncertainty broadening in photoinduced electron transfer," Chem. Phys. Lett. **96**, 28-30 (1983).

[117] K. Pal, G. Grampp, and D. R. Kattnig, "Solvation dynamics of a radical ion pair in micro-heterogeneous binary solvents: A semi-quantitative study utilizing mary line-broadening experiments," Chemphyschem **14**, 3389 (2013).

[118] E. W. Knapp, and K. Schulten, "Magnetic field effect on the hyperfine-induced electron spin motion in radicals undergoing diamagnetic−paramagnetic exchange," J. Chem. Phys. **71**, 1878-1883 (1979).

[119] K. Schulten, and P. G. Wolynes, "Semiclassical description of electron spin motion in radicals including the effect of electron hopping," J. Chem. Phys. **68**, 3292-3297 (1978).

[120] M. Justinek, G. Grampp, S. Landgraf, P. J. Hore, and N. N. Lukzen, "Electron self-exchange kinetics determined by mary spectroscopy: Theory and experiment," J. Am. Chem. Soc. **126**, 5635-5646 (2004).

[121] G. Grampp, M. Justinek, and S. Landgraf, "Magnetic field effects on the pyrene—dicyanobenzene system: Determination of electron self-exchange rates by mary spectroscopy," Mol. Phys. **100**, 1063-1070 (2002).

[122] G. Grampp, "Intermolecular electron-self exchange kinetics measured by electron paramagnetic resonance-linebroadening effects: Useful rate constants for the application of marcus theory," Spectrochim. Acta A **54**, 2349-2358 (1998).

[123] K. Pal, D. R. Kattnig, G. Grampp, and S. Landgraf, "Experimental observation of preferential solvation on a radical ion pair using mary spectroscopy," Phys. Chem. Chem. Phys. **14**, 3155 (2012).

[124] D. N. Nath, and M. Chowdhury, "Effect of environment on the magnetic field modulation of exciplex luminescence," Chem. Phys. Lett. **109**, 13-17 (1984).

[125] P. Roy, A. K. Jana, G. M.B, and D. N. Nath, "Studies on b1/2 value of pyrene–dimethylaniline radical pair system in single and binary solvents," Chem. Phys. Lett. **554**, 82-85 (2012).

[126] N. K. Petrov, "A fluorescence spectroscopy study of preferential solvation in binary solvents," High Energ. Chem. **40**, 22-34 (2006).

[127] M. V. Basilevsky, A. V. Odinokov, E. A. Nikitina, and N. C. Petrov, "The dielectric continuum solvent model adapted for treating preferential solvation effects," J. Electroanal. Chem. **660**, 339-346 (2011).

[128] S. Richert, A. Rosspeintner, S. Landgraf, G. Grampp, E. Vauthey, and D. R. Kattnig, "Time-resolved magnetic field effects distinguish loose ion pairs from exciplexes," J. Am. Chem. Soc. **135**, 15144-15152 (2013).

[129] H. M. Hoang, T. B. V. Pham, G. Grampp, and D. R. Kattnig, "Exciplexes versus loose ion pairs: How does the driving force impact the initial product ratio of photoinduced charge separation reactions?," J. Phys. Chem. Lett. **5**, 3188 (2014).

[130] R. Bittl, and K. Schulten, "Length dependence of the magnetic field modulated triplet yield of photogenerated biradicals," Chem. Phys. Lett. **146**, 58-62 (1988).

[131] R. Bittl, and K. Schulten, "A static ensemble approximation for stochastically modulated quantum systems," J. Chem. Phys. **90**, 1794-1803 (1989).

[132] R. Bittl, and K. Schulten, "Biradical spin dynamics with distance-dependent exchange interaction and electron transfer efficiency," Chem. Phys. Lett. **173**, 387 (1990).

[133] A. I. Shushin, "The effect of the spin exchange interaction on snp and rydmr spectra of geminate radical pairs," Chem. Phys. Lett. **181**, 274-278 (1991).

[134] K. Maeda, T. Miura, and T. Arai, "A practical simulation and a novel insight to the magnetic field effect on a radical pair in a micelle," Mol. Phys. **104**, 1779-1788 (2006).

[135] T. Suzuki, T. Miura, K. Maeda, and T. Arai, "Spin dynamics of the radical pair in a low magnetic field studied by the transient absorption detected magnetic field effect on the reaction yield and switched external magnetic field," J. Phys. Chem. A **109**, 9911-9918 (2005).

[136] T. Miura, K. Maeda, and T. Arai, "The spin mixing process of a radical pair in low magnetic field observed by transient absorption detected nanosecond pulsed magnetic field effect," J. Phys. Chem. A **110**, 4151-4156 (2006).

[137] M. D. Newton, "Modeling donor/acceptor interactions: Combined roles of theory and computation," Int. J. Quantum Chem. **77**, 255-263 (2000).

[138] Y. A. Berlin, F. C. Grozema, L. D. A. Siebbeles, and M. A. Ratner, "Charge transfer in donor-bridge-acceptor systems: Static disorder, dynamic fluctuations, and complex kinetics," J. Phys. Chem. C **112**, 10988-11000 (2008).

[139] S. Jang, and M. D. Newton, "Theory of torsional non-condon electron transfer: A generalized spin-boson hamiltonian and its nonadiabatic limit solution," J. Chem. Phys. **122**, 024501 (2005).

[140] E. A. Weiss, M. A. Ratner, and M. R. Wasielewski, "Direct measurement of singlet-triplet splitting within rodlike photogenerated radical ion pairs using magnetic field effects: Estimation of the electronic coupling for charge recombination," J. Phys. Chem. A **107**, 3639-3647 (2003).

[141] G. Moise, L. Tejerina, M. Rickhaus, H. L. Anderson, and C. R. Timmel, "Spin delocalization in the radical cations of porphyrin molecular wires: A new perspective on epr approaches," J. Phys. Chem. Lett. **10**, 5708-5712 (2019).

[142] M. D. Peeks, C. E. Tait, P. Neuhaus, G. M. Fischer, M. Hoffmann, R. Haver, A. Cnossen, J. R. Harmer, C. R. Timmel, and H. L. Anderson, "Electronic delocalization in the radical cations of porphyrin oligomer molecular wires," J. Am. Chem. Soc. **139**, 10461-10471 (2017).

[143] J. Rawson, P. J. Angiolillo, and M. J. Therien, "Extreme electron polaron spatial delocalization in π-conjugated materials," Proc. Natl. Acad. Sci. U.S.A. **112**, 13779-13783 (2015).

[144] J. Rawson, P. J. Angiolillo, P. R. Frail, I. Goodenough, and M. J. Therien, "Electron spin relaxation of hole and electron polarons in π-conjugated porphyrin arrays: Spintronic implications," J. Phys. Chem. B **119**, 7681-7689 (2015).

[145] D. Mims, A. Schmiedel, M. Holzapfel, N. N. Lukzen, C. Lambert, and U. E. Steiner, "Magnetic field effects in rigidly linked d-a dyads: Extreme on-resonance quantum coherence effect on charge recombination," J. Chem. Phys. **151**, 244308 (2019).

[146] H. Lee, N. Yang, and A. E. Cohen, "Mapping nanomagnetic fields using a radical pair reaction," Nano Lett **11**, 5367-5372 (2011).

[147] N. Yang, and A. E. Cohen, "Optical imaging through scattering media via magnetically modulated fluorescence," Opt. Express **18**, 25461-25467 (2010).

[148] O. Mermut, K. R. Diamond, J. F. Cormier, P. Gallant, N. Ho, S. Leclair, J. S. Marois, I. Noiseux, J. F. Morin, M. S. Patterson, and M. L. Vernon, "The use of magnetic field effects on photosensitizer luminescence as a novel probe for optical monitoring of oxygen in photodynamic therapy," Phys. Med. Biol. **54**, 1-16 (2009).

[149] G. Balasubramanian, I. Y. Chan, R. Kolesov, M. Al-Hmoud, J. Tisler, C. Shin, C. Kim, A. Wojcik, P. R. Hemmer, A. Krueger, T. Hanke, A. Leitenstorfer, R. Bratschitsch, F. Jelezko, and J. Wrachtrup, "Nanoscale imaging magnetometry with diamond spins under ambient conditions," Nature **455**, 648-651 (2008).

[150] D. Le Sage, K. Arai, D. R. Glenn, S. J. DeVience, L. M. Pham, L. Rahn-Lee, M. D. Lukin, A. Yacoby, A. Komeili, and R. L. Walsworth, "Optical magnetic imaging of living cells," Nature **496**, 486-489 (2013).

[151] L. P. McGuinness, Y. Yan, A. Stacey, D. A. Simpson, L. T. Hall, D. Maclaurin, S. Prawer, P. Mulvaney, J. Wrachtrup, F. Caruso, R. E. Scholten, and L. C. L. Hollenberg, "Quantum measurement and orientation tracking of fluorescent nanodiamonds inside living cells," Nat. Nanotechnol. **6**, 358-363 (2011).

[152] G. Kucsko, P. C. Maurer, N. Y. Yao, M. Kubo, H. J. Noh, P. K. Lo, H. Park, and M. D. Lukin, "Nanometre-scale thermometry in a living cell," Nature **500**, 54-58 (2013).

[153] W. J. Baker, K. Ambal, D. P. Waters, R. Baarda, H. Morishita, K. van Schooten, D. R. McCamey, J. M. Lupton, and C. Boehme, "Robust absolute magnetometry with organic thin-film devices," Nat. Commun. **3**, 898 (2012).

[154] T. Grünbaum, S. Milster, H. Kraus, W. Ratzke, S. Kurrmann, V. Zeller, S. Bange, C. Boehme, and J. M. Lupton, "Oleds as models for bird magnetoception: Detecting electron spin resonance in geomagnetic fields," Faraday Discuss. **221**, 92-109 (2020).

[155] B. Koopmans, W. Wagemans, F. L. Bloom, P. A. Bobbert, M. Kemerink, and M. Wohlgenannt, "Spin in organics: A new route to spintronics," Philosophical Transactions of the Royal Society A: Mathematical, Physical and Engineering Sciences **369**, 3602-3616 (2011).

[156] H. Xu, M. Wang, Z.-G. Yu, K. Wang, and B. Hu, "Magnetic field effects on excited states, charge transport, and electrical polarization in organic semiconductors in spin and orbital regimes," Adv. Phys. **68**, 49-121 (2019).

[157] K. L. Ivanov, A. Wagenpfahl, C. Deibel, and J. Matysik, "Spin-chemistry concepts for spintronics scientists," Beilstein Journal of Nanotechnology **8**, 1427-1445 (2017).

[158] H. Leonhardt, and A. Weller, "Elektronenübertragungsreaktionen des angeregten perylens," Ber. Bunsenges. Phys. Chem. **67**, 791-795 (1963).

[159] S. Murata, and M. Tachiya, "Unified interpretation of exciplex formation and marcus electron transfer on the basis of two-dimensional free energy surfaces," J. Phys. Chem. A **111**, 9240-9248 (2007).

[160] I. R. Gould, R. H. Young, L. J. Mueller, and S. Farid, "Mechanisms of exciplex formation. Roles of superexchange, solvent polarity, and driving force for electron transfer," J. Am. Chem. Soc. **116**, 8176-8187 (1994).

[161] I. R. Gould, R. H. Young, L. J. Mueller, A. C. Albrecht, and S. Farid, "Electronic-structures of exciplexes and excited charge-transfer complexes," J. Am. Chem. Soc. **116**, 8188-8199 (1994).

[162] I. R. Gould, and S. Farid, "Dynamics of bimolecular photoinduced electron-transfer reactions," Accounts Chem. Res. **29**, 522-528 (1996).

[163] A. Katsuki, Y. Kobori, S. Tero-Kubota, S. Milikisyants, H. Paul, and U. E. Steiner, "Magnetic field and spin effects from sequential p-type and d-type triplet mechanisms," Mol. Phys. **100**, 1245-1259 (2002).

[164] D. R. Kattnig, A. Rosspeintner, and G. Grampp, "Fully reversible interconversion between locally excited fluorophore, exciplex, and radical ion pair demonstrated by a new magnetic field effect," Angew. Chem. Int. Edit. **47**, 960-962 (2008).

[165] Y. Marcus, and G. Hefter, "Ion pairing," Chem. Rev. **106**, 4585-4621 (2006).

[166] N. K. Petrov, E. Y. Fedotova, and E. L. Frankevich, "Magnetic modulation of exciplex fluorescence in a polar-solvent," High Energ. Chem. **14**, 257-261 (1980).

[167] N. K. Petrov, A. I. Shushin, and E. L. Frankevich, "Solvent effect on magnetic field modulation of excbplex fluorescence in polar solutions," Chem. Phys. Lett. **82**, 339-343 (1981).

[168] N. Mataga, H. Chosrowjan, and S. Taniguchi, "Ultrafast charge transfer in excited electronic states and investigations into fundamental problems of exciplex chemistry: Our early studies and recent developments," J. Photochem. Photobiol. C **6**, 37-79 (2005).

[169] R. Treichel, H. Staerk, and A. Weller, "Magnetic field effect measurements by time-selective absorption sampling," Appl. Phys. B **31**, 15-17 (1983).

[170] L. R. Faulkner, and A. J. Bard, "Magnetic field effects on anthracene triplet-triplet annihilation in fluid solutions," J. Am. Chem. Soc. **91**, 6495-6947 (1969).

[171] B. Brocklehurst, "Magnetic fields and radical reactions: Recent developments and their role in nature," Chem. Soc. Rev. **31**, 301-311 (2002).

[172] L. R. Faulkner, and A. J. Bard, "Electrogenerated chemiluminescence. Iv. Magnetic field effects on the electrogenerated chemiluminescence of some anthracenes," J. Am. Chem. Soc. **91**, 209-210 (1969).

[173] V. T. B. Pham, H. M. Hoang, G. Grampp, and D. R. Kattnig, "Effects of preferential solvation revealed by time-resolved magnetic field effects," J. Phys. Chem. B **121**, 2677 (2017).

[174] H. Staerk, W. Kühnle, R. Treichel, and A. Weller, "Magnetic field dependence of intramolecular exciplex formation in polymethyelene-linked a-d systems," Chem. Phys. Lett. **118**, 19 (1985).

[175] Y. Tanimoto, N. Okada, M. Itoh, K. Iwai, K. Sugioka, F. Takemura, R. Nakagaki, and S. Nagakura, "Magnetic field effects on the fluorescence of intramolecular electron-donor-acceptor systems," Chem. Phys. Lett. **136**, 42 (1987).

[176] H. Cao, K. Miyata, T. Tamura, Y. Fujiwara, A. Katsuki, C.-H. Tung, and Y. Tanimoto, "Effects of high magnetic field on the intramolecular exciplex fluorescence of chain-linked phenanthrene and dimethylaniline," J. Phys. Chem. A **101**, 407-411 (1997).

[177] H. Oevering, J. W. Verhoeven, M. N. Paddon-Row, and J. M. Warman, "Charge-transfer absorption and emission resulting from long-range through-bond interaction; exploring the relation between electronic coupling andelectron-transfer in bridged donor-acceptor systems," Tetrahedron **45**, 4751-4766 (1989).

[178] H. Oevering, M. N. Paddon-Row, M. Heppener, A. M. Oliver, E. Cotsaris, J. W. Verhoeven, and N. S. Hush, "Long-range photoinduced through-bond electron transfer and radiative recombination via rigid nonconjugated bridges: Distance and solvent dependence," J. Am. Chem. Soc. **109**, 3258-3269 (1987).

[179] J. T. Buck, R. W. Wilson, and T. Mani, "Intramolecular long-range charge-transfer emission in donor–bridge–acceptor systems," J. Phys. Chem. Lett. **10**, 3080-3086 (2019).

[180] M. Bixon, J. Jortner, and J. W. Verhoeven, "Lifetimes for radiative charge recombination in donor-acceptor molecules," J. Am. Chem. Soc. **116**, 7349-7355 (1994).

[181] D. Kim, Y. J. Lee, D.-H. Ahn, J.-W. Song, J. Seo, and H. Lee, "Peptoid-conjugated magnetic field-sensitive exciplex system at high and low solvent polarities," J. Phys. Chem. Lett. **11**, 4668-4677 (2020).

[182] W. Liptay, "Electrochromism and solvatochromism," Angew. Chem. Int. Edit. **8**, 177-188 (1969).

[183] L. Takiff, and S. G. Boxer, "Phosphorescence from the primary electron-donor in rhodobacter-sphaeroides and rhodopseudomonas-viridis reaction centers," Biochimica Et Biophysica Acta **932**, 325-334 (1988).

[184] A. J. Hoff, "Magnetic interactions between photosynthetic reactants," Photochem. Photobiol. **43**, 727-745 (1986).

[185] R. A. Goldstein, and S. G. Boxer, "The effect of very high magnetic fields on the delayed fluorescence from oriented bacterial reaction centers," Biochim. Biophys. Acta Bioenerg. **977**, 70-77 (1989).

[186] R. A. Goldstein, and S. G. Boxer, "The effect of very high magnetic fields on the reaction dynamics in bacterial reaction centers: Implications for the reaction mechanism," Biochim. Biophys. Acta Bioenerg. **977**, 78-86 (1989).

[187] T. Mani, M. Tanabe, S. Yamauchi, N. V. Tkachenko, and S. A. Vinogradov, "Modulation of visible room temperature phosphorescence by weak magnetic fields," J. Phys. Chem. Lett. **3**, 3115-3119 (2012).

[188] T. Kobayashi, K. D. Straub, and P. M. Rentzepis, "Energy relaxation mechanism in ni(ii), pd(ii), pt(ii) and zn(ii) porphyrins," Photochem. Photobiol. **29**, 925-931 (1979).

[189] Y. Tanimoto, A. Kita, M. Itoh, M. Okazaki, R. Nakagaki, and S. Nagakura, "Effects of trivalent lanthanide complexes on the lifetimes of methylene-chain-linked biradicals in magnetic fields," Chem. Phys. Lett. **165**, 184-188 (1990).

[190] M. Igarashi, Y. Sakaguchi, and H. Hayashi, "Effects of large magnetic fields on the dynamic behavior of radical ion pairs in a non-viscous solution at room temperature," Chem. Phys. Lett. **243**, 545-551 (1995).

[191] M. Murakami, K. Maeda, and T. Arai, "Dynamics of intramolecular electron transfer reaction of fad studied by magnetic field effects on transient absorption spectra," J. Phys. Chem. A **109**, 5793-5800 (2005).

[192] R. Carmieli, A. L. Smeigh, S. M. Mickley Conron, A. K. Thazhathveetil, M. Fuki, Y. Kobori, F. D. Lewis, and M. R. Wasielewski, "Structure and dynamics of photogenerated triplet radical ion pairs in DNA hairpin conjugates with anthraquinone end caps," J. Am. Chem. Soc. **134**, 11251-11260 (2012).

[193] T. Mani, *Magnetic field effects on molecular emissivity in solutions* (University of Pennsylvania, 2013).

[194] H. Lee, D. Brinks, and A. E. Cohen, "Two-photon imaging of a magneto-fluorescent indicator for 3d optical magnetometry," Opt. Express **23**, 28022-28030 (2015).

[195] D. Kim, M. Jung, H. Kim, W.-j. Chung, and H. Lee, "Quantitative imaging of magnetic field distribution using a pyrene-based magnetosensing exciplex fluorophore," Photochem. Photobiol. Sci. **18**, 2688-2695 (2019).

[196] N. Ikeya, and J. R. Woodward, "Cellular autofluorescence is magnetic field sensitive," Proc. Natl. Acad. Sci. U.S.A. **118**, e2018043118 (2021).

[197] C. Bialas, L. E. Jarocha, K. B. Henbest, T. M. Zollitsch, G. Kodali, C. R. Timmel, S. R. Mackenzie, P. L. Dutton, C. C. Moser, and P. J. Hore, "Engineering an artificial flavoprotein magnetosensor," J. Am. Chem. Soc. **138**, 16584-16587 (2016).

[198] T. M. Zollitsch, L. E. Jarocha, C. Bialas, K. B. Henbest, G. Kodali, P. L. Dutton, C. C. Moser, C. R. Timmel, P. J. Hore, and S. R. Mackenzie, "Magnetically sensitive radical photochemistry of non-natural flavoproteins," J. Am. Chem. Soc. **140**, 8705-8713 (2018).

[199] R. L. Koder, J. L. R. Anderson, L. A. Solomon, K. S. Reddy, C. C. Moser, and P. L. Dutton, "Design and engineering of an o2 transport protein," Nature **458**, 305-309 (2009).

[200] C. C. Moser, M. M. Sheehan, N. M. Ennist, G. Kodali, C. Bialas, M. T. Englander, B. M. Discher, and P. L. Dutton, in *Methods in enzymology*, edited by V. L. Pecoraro (Academic Press, 2016), pp. 365-388.

[201] K. Schulten, "Magnetic-field effects in chemistry and biology," Festkor-Adv Solid St **22**, 61-83 (1982).

[202] M. Weiger, D. Schmidig, S. Denoth, C. Massin, F. Vincent, M. Schenkel, and M. Fey, "Nmr microscopy with isotropic resolution of 3.0 μm using dedicated hardware and optimized methods," Concepts in Magnetic Resonance Part B: Magnetic Resonance Engineering **33B**, 84-93 (2008).

[203] J. J. Flint, C. H. Lee, B. Hansen, M. Fey, D. Schmidig, J. D. Bui, M. A. King, P. Vestergaard-Poulsen, and S. J. Blackband, "Magnetic resonance microscopy of mammalian neurons," NeuroImage **46**, 1037-1040 (2009).

[204] R. P. Briñas, T. Troxler, R. M. Hochstrasser, and S. A. Vinogradov, "Phosphorescent oxygen sensor with dendritic protection and two-photon absorbing antenna," J. Am. Chem. Soc. **127**, 11851-11862 (2005).

[205] C. E. D. Chidsey, L. Takiff, R. A. Goldstein, and S. G. Boxer, "Effect of magnetic-fields on the triplet-state lifetime in photosynthetic reaction centers - evidence for thermal repopulation of the initial radical pair," Proc. Natl. Acad. Sci. U.S.A. **82**, 6850-6854 (1985).

[206] M. H. Vidal, P. Setif, and P. Mathis, "Influence of magnetic fields on the p-870 triplet state in rps.Sphaeroides reaction centers," Photosynth. Res. **10**, 347-354 (1986).

[207] Y. Liu, R. Edge, K. Henbest, C. R. Timmel, P. J. Hore, and P. Gast, "Magnetic field effect on singlet oxygen production in a biochemical system," Chem. Commun., 174-176 (2005).

[208] S. Erbas-Cakmak, S. Kolemen, A. C. Sedgwick, T. Gunnlaugsson, T. D. James, J. Yoon, and E. U. Akkaya, "Molecular logic gates: The past, present and future," Chem. Soc. Rev. **47**, 2228-2248 (2018).

[209] D. Kuciauskas, P. A. Liddell, A. L. Moore, T. A. Moore, and D. Gust, "Magnetic switching of charge separation lifetimes in artificial photosynthetic reaction centers," J. Am. Chem. Soc. **120**, 10880-10886 (1998).

[210] C. M. Elliott, U. E. Steiner, J. J. Kremer, and K. A. Hötzer, "Polymer-encapsulated reverse micelles: A composite material design for the optical detection of weak magnetic fields," Chem. Mater. **17**, 941-943 (2005).

[211] T. Tsuneda, and K. Hirao, "Long-range correction for density functional theory," WIREs Computational Molecular Science **4**, 375-390 (2014).

[212] B. S. Veldkamp, X. Liu, M. R. Wasielewski, J. E. Subotnik, and M. A. Ratner, "Molecular excited states: Accurate calculation of relative energies and electronic coupling between charge transfer and non-charge transfer states," J. Phys. Chem. A **119**, 253-262 (2015).

[213] Z.-Q. You, Y.-C. Hung, and C.-P. Hsu, "Calculating electron-transfer coupling with density functional theory: The long-range-corrected density functionals," J. Phys. Chem. B **119**, 7480-7490 (2015).

[214] R. Haberkorn, "Density matrix description of spin-selective radical pair reactions," Mol. Phys. **32**, 1491-1493 (1976).

[215] K. L. Ivanov, M. V. Petrova, N. N. Lukzen, and K. Maeda, "Consistent treatment of spin-selective recombination of a radical pair confirms the haberkorn approach," J. Phys. Chem. A **114**, 9447-9455 (2010).

[216] T. P. Fay, A. M. Lewis, and D. E. Manolopoulos, "Spin-dependent charge recombination along para-phenylene molecular wires," J. Chem. Phys. **147**, 064107 (2017).

[217] T. P. Fay, and D. E. Manolopoulos, "Radical pair intersystem crossing: Quantum dynamics or incoherent kinetics?," J. Chem. Phys. **150**, 151102 (2019).

[218] T. Yamabayashi, M. Atzori, L. Tesi, G. Cosquer, F. Santanni, M.-E. Boulon, E. Morra, S. Benci, R. Torre, M. Chiesa, L. Sorace, R. Sessoli, and M. Yamashita, "Scaling up electronic spin qubits into a three-dimensional metal–organic framework," J. Am. Chem. Soc. **140**, 12090-12101 (2018).

[219] C.-J. Yu, M. D. Krzyaniak, M. S. Fataftah, M. R. Wasielewski, and D. E. Freedman, "A concentrated array of copper porphyrin candidate qubits," Chem. Sci. **10**, 1702-1708 (2019).

[220] S. Lutz, "Beyond directed evolution—semi-rational protein engineering and design," Curr. Opin. Biotechnol. **21**, 734-743 (2010).

[221] E. C. Alley, G. Khimulya, S. Biswas, M. AlQuraishi, and G. M. Church, "Unified rational protein engineering with sequence-based deep representation learning," Nat. Methods **16**, 1315-1322 (2019).

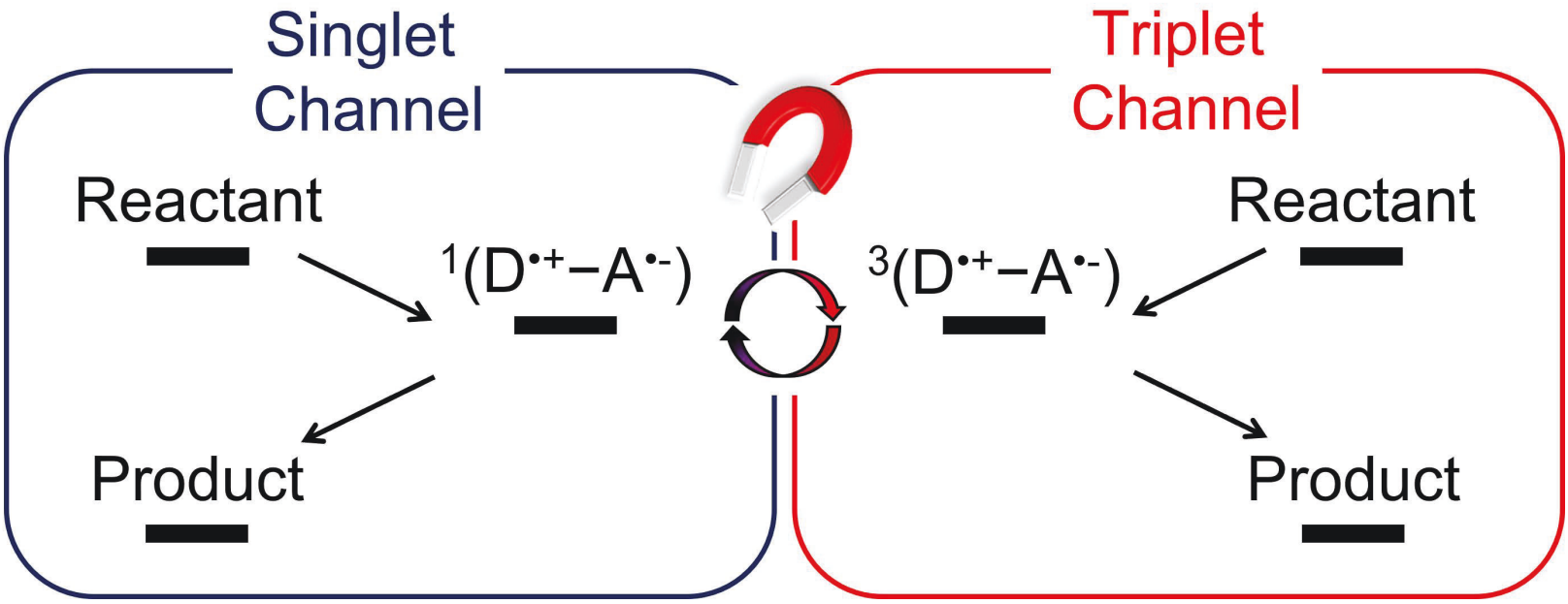

Response/Readout

Absorption
Fluorescence
Exciplex/CT emission

Absorption
Phosphorescence
Singlet oxygen generation
Catalytic activities

Resolution-enhanced Imaging
Magnetometer
Photodynamic Therapy
Magnetic Switch for Logic Gates, and more

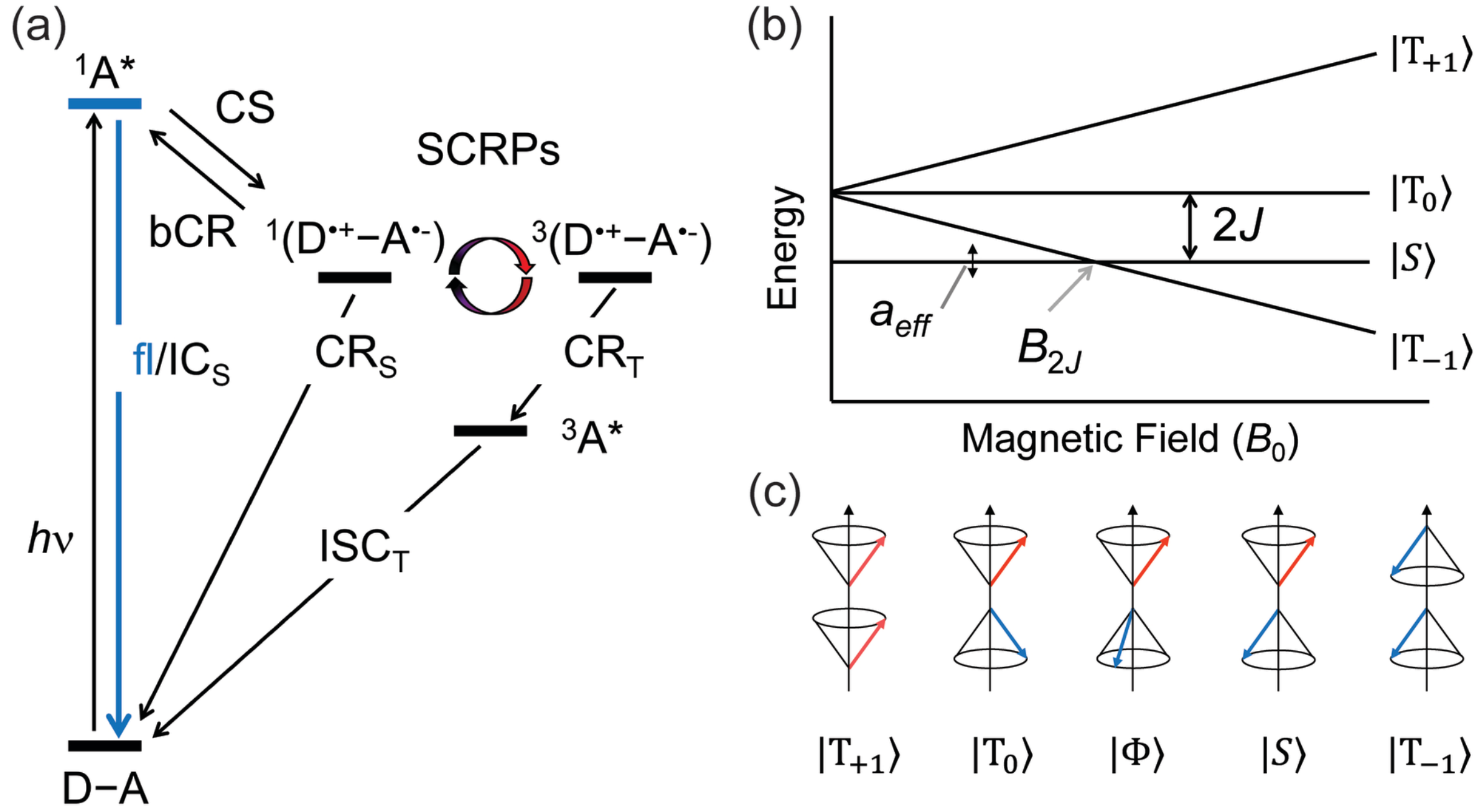
(a)
^{1}A*
CS
SCRPs
bCR
^{1}(D$^{\bullet+}$–A$^{\bullet-}$)
^{3}(D$^{\bullet+}$–A$^{\bullet-}$)
fl/IC$_S$
CR$_S$
CR$_T$
^{3}A*
$h\nu$
ISC$_T$
D–A
(b)
Energy
$|T_{+1}\rangle$
$|T_0\rangle$
$2J$
$|S\rangle$
$|T_{-1}\rangle$
a_{eff}
B_{2J}
Magnetic Field (B_0)
(c)
$|T_{+1}\rangle$
$|T_0\rangle$
$|\Phi\rangle$
$|S\rangle$
$|T_{-1}\rangle$

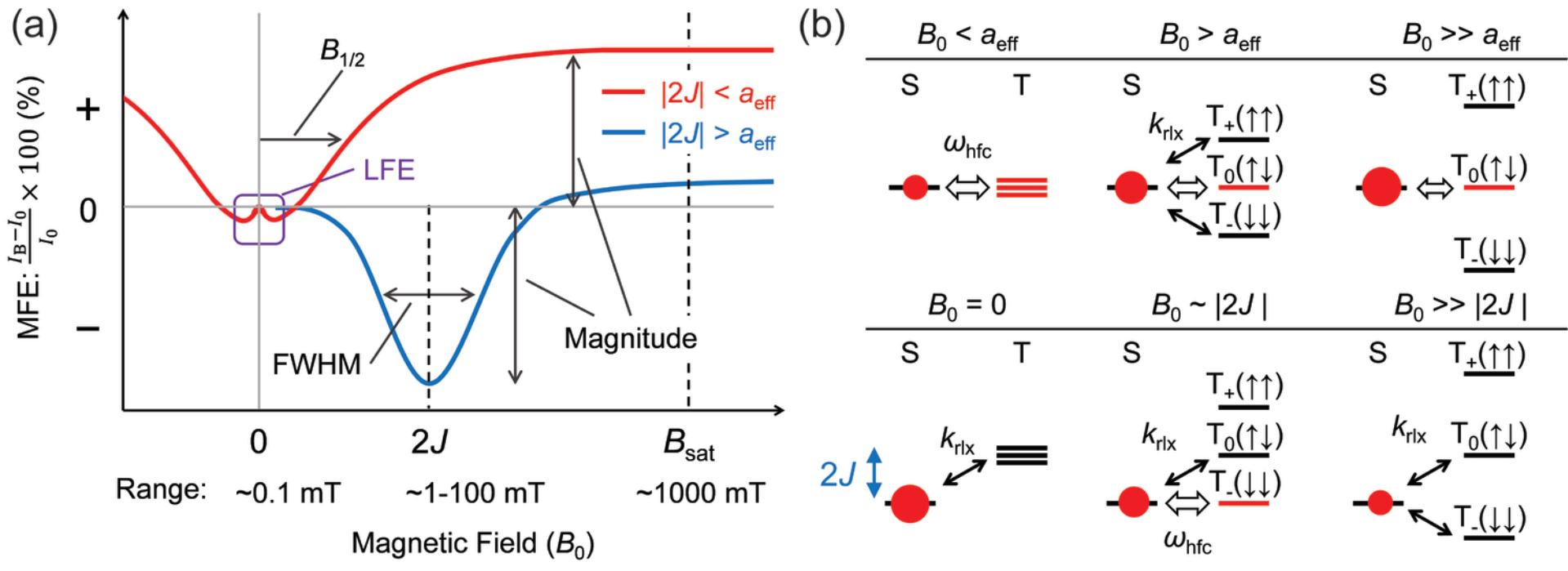
(a)
MFE: $\frac{I_B - I_0}{I_0} \times 100$ (%)
+
0
−
$B_{1/2}$
LFE
FWHM
Magnitude
$|2J| < a_{eff}$
$|2J| > a_{eff}$
0
$2J$
B_{sat}
Range:
~0.1 mT
~1-100 mT
~1000 mT
Magnetic Field (B_0)
(b)
$B_0 < a_{eff}$
$B_0 > a_{eff}$
$B_0 >> a_{eff}$
S
T
ω_{hfc}
k_{rlx}
$T_+(\uparrow\uparrow)$
$T_0(\uparrow\downarrow)$
$T_-(\downarrow\downarrow)$
$B_0 = 0$
$B_0 \sim |2J|$
$B_0 >> |2J|$
$2J$

Flexible Linkers

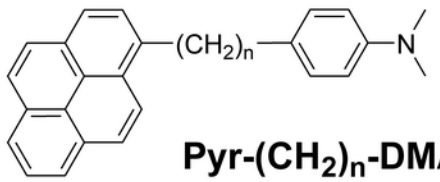

Pyr-$(CH_2)_n$-DMA

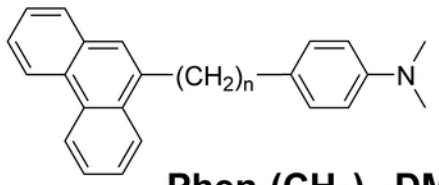

Phen-$(CH_2)_n$-DMA

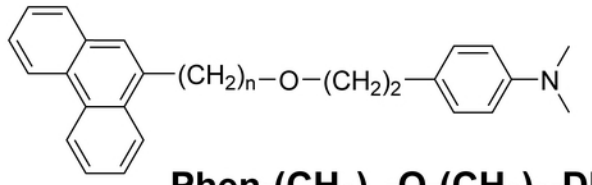

Phen-$(CH_2)_n$-O-$(CH_2)_2$-DMA

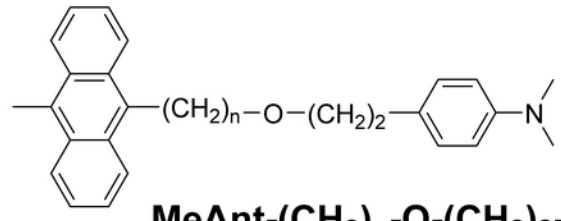

MeAnt-$(CH_2)_n$-O-$(CH_2)_2$-DMA

Rigdly Linked

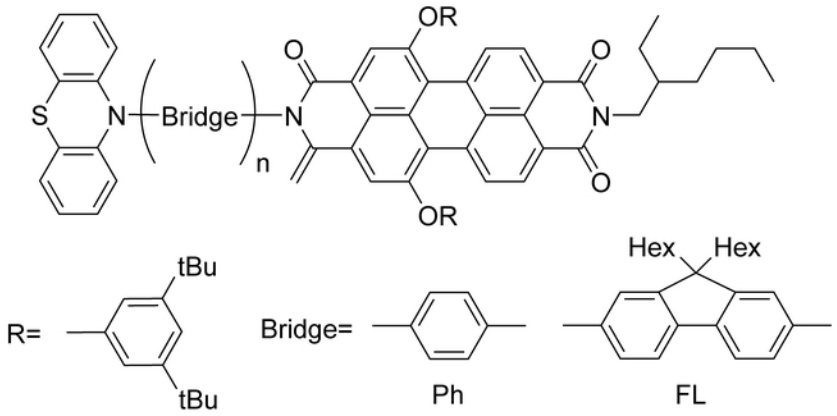

PTZ-Bridge-PDI

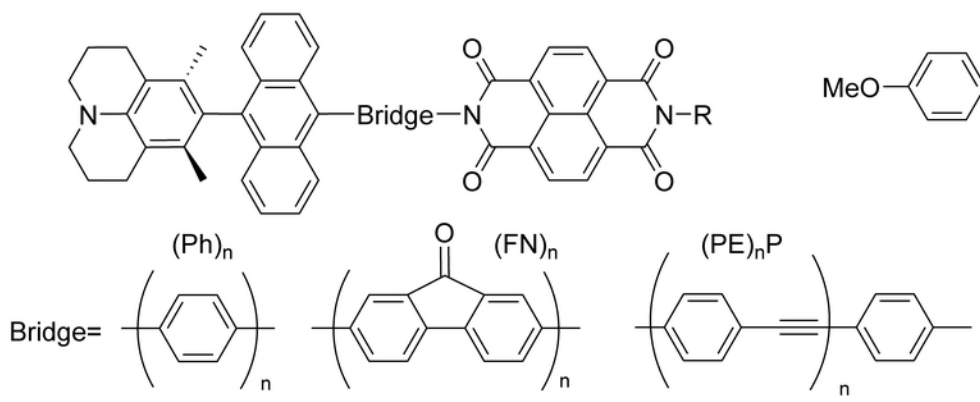

DMJAn-Bridge-NI

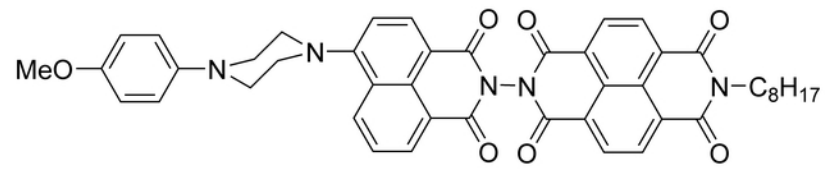

MeOAn-6ANI-NI

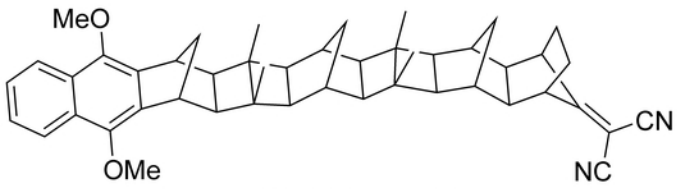

DMN[12]DCV

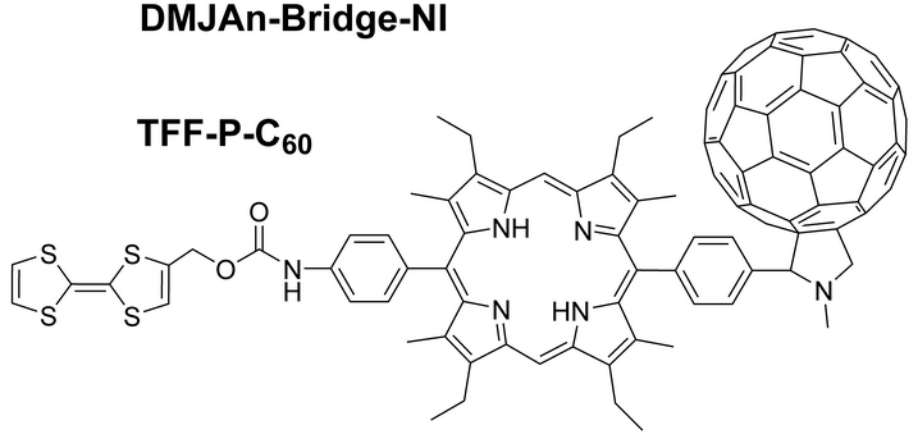

TFF-P-C_{60}

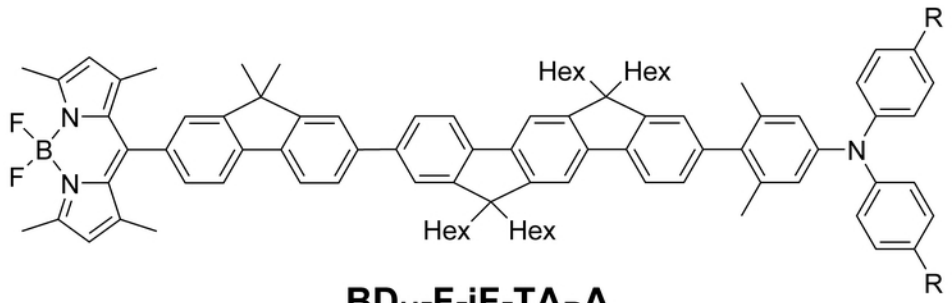

BD_H-F-iF-TA_RA
R= OMe, Me, H

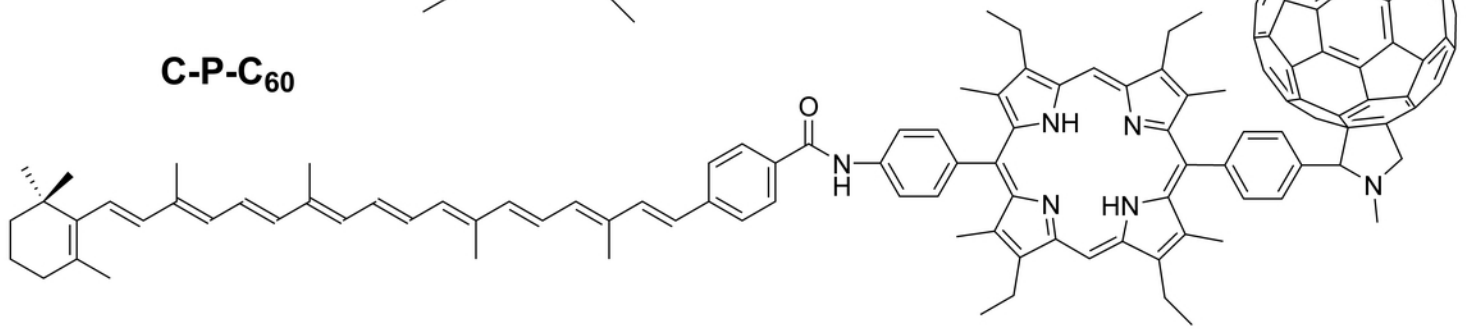

C-P-C_{60}

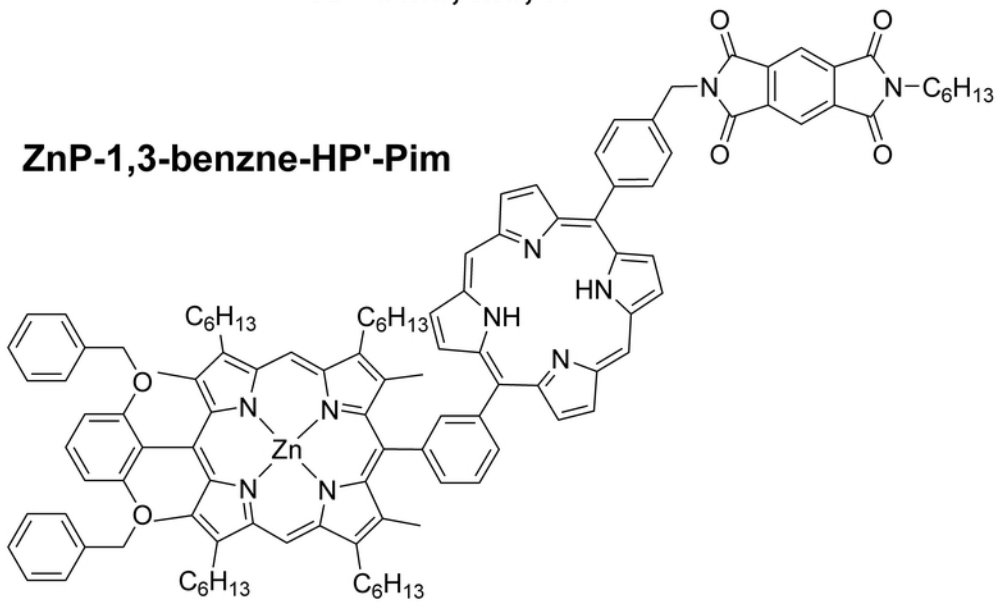

ZnP-1,3-benzne-HP'-Pim

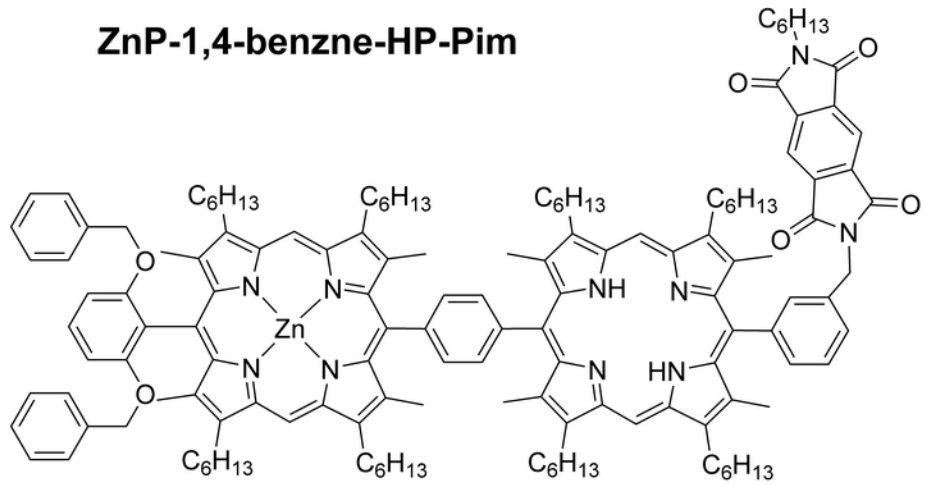

ZnP-1,4-benzne-HP-Pim

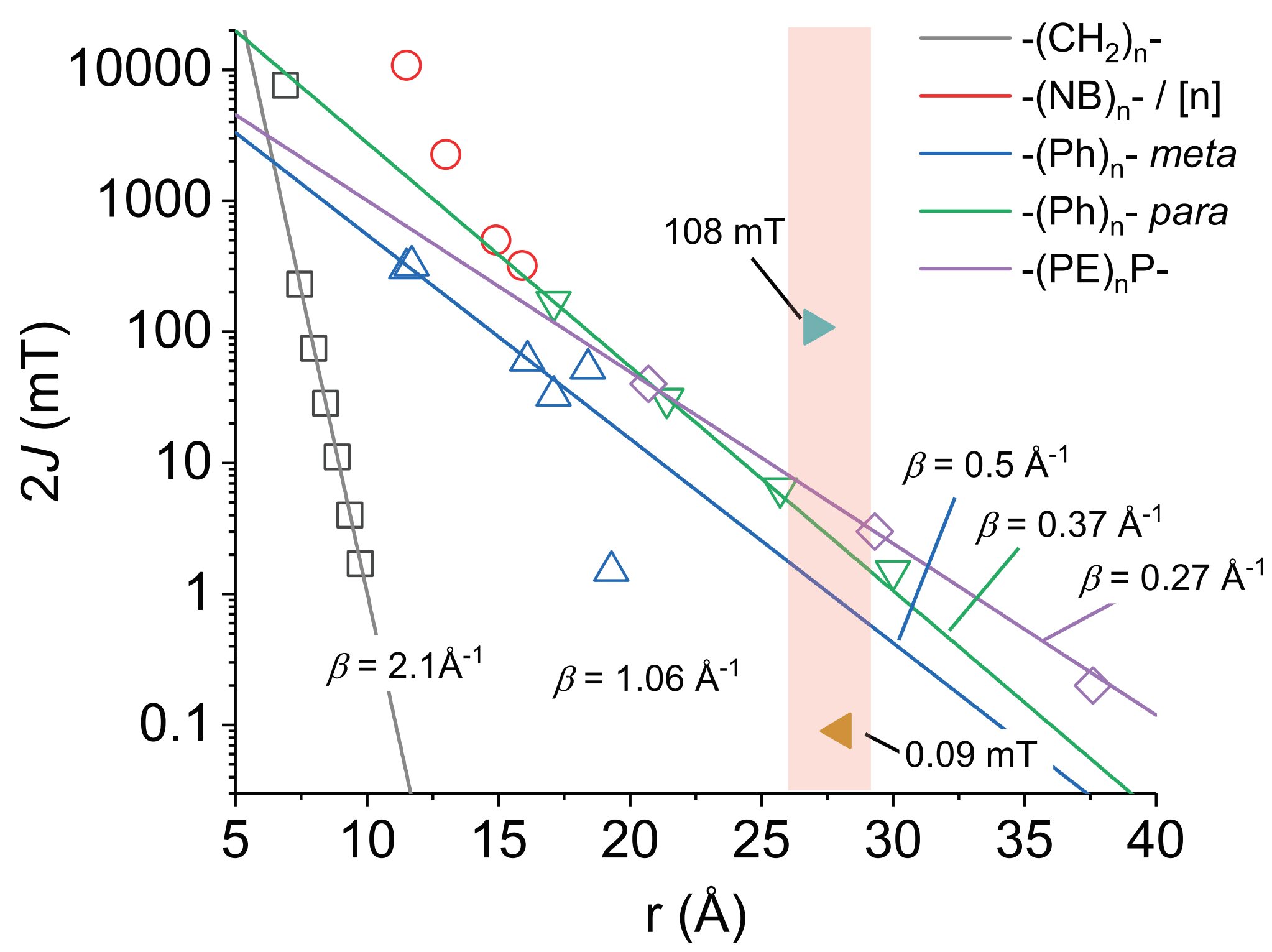
-(CH2)n-
-(NB)n- / [n]
-(Ph)n- meta
-(Ph)n- para
-(PE)nP-
108 mT
β = 0.5 Å-1
β = 0.37 Å-1
β = 0.27 Å-1
β = 2.1Å-1
β = 1.06 Å-1
0.09 mT
2J (mT)
r (Å)
10000
1000
100
10
1
0.1
5
10
15
20
25
30
35
40

(a)

	Primary Factor	Examples	Ref.
V	Distance (r_{DA})	Chain motion in flexible D/A	92
		Bridge length in rigidly-linked D-B-A	89
	Conformation change at fixed r_{DA}	Torsional motion of bridge	110
		Chair/boat interconversion	80
	Bridge effects	Bridge coupling/energy levels	89
Δ*E*	RP energy	Reduction potential	81
		Solvent polarity	81

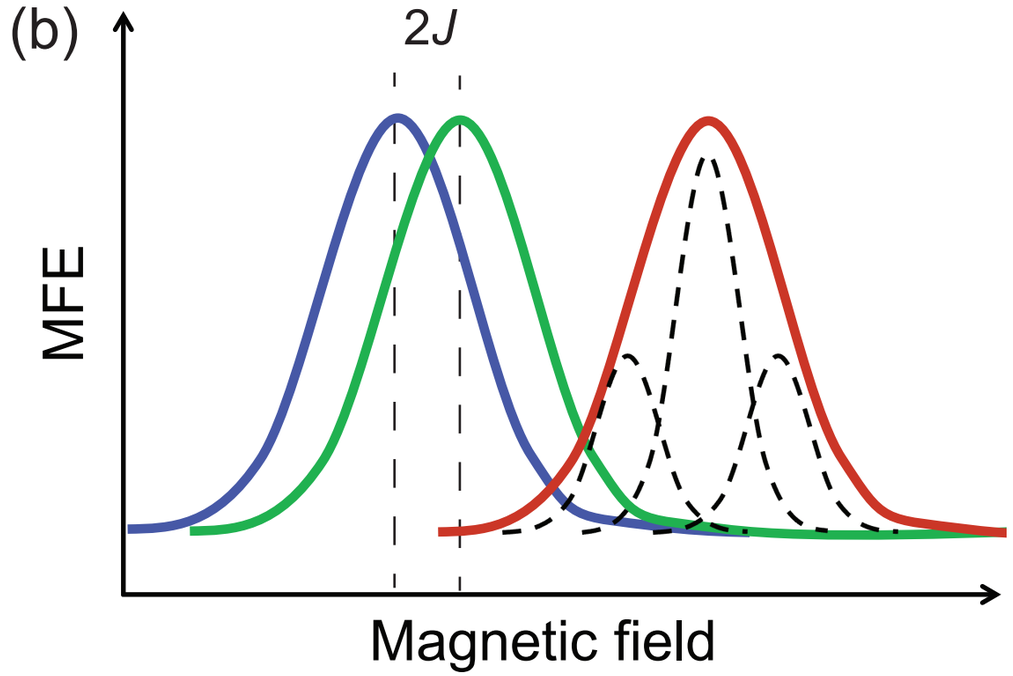

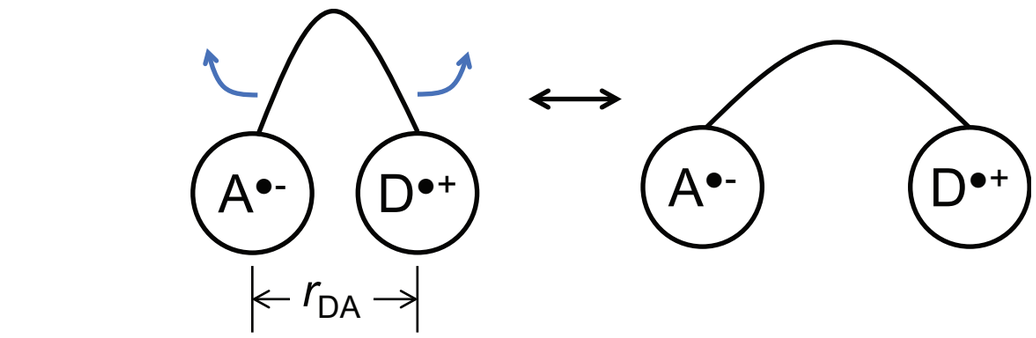

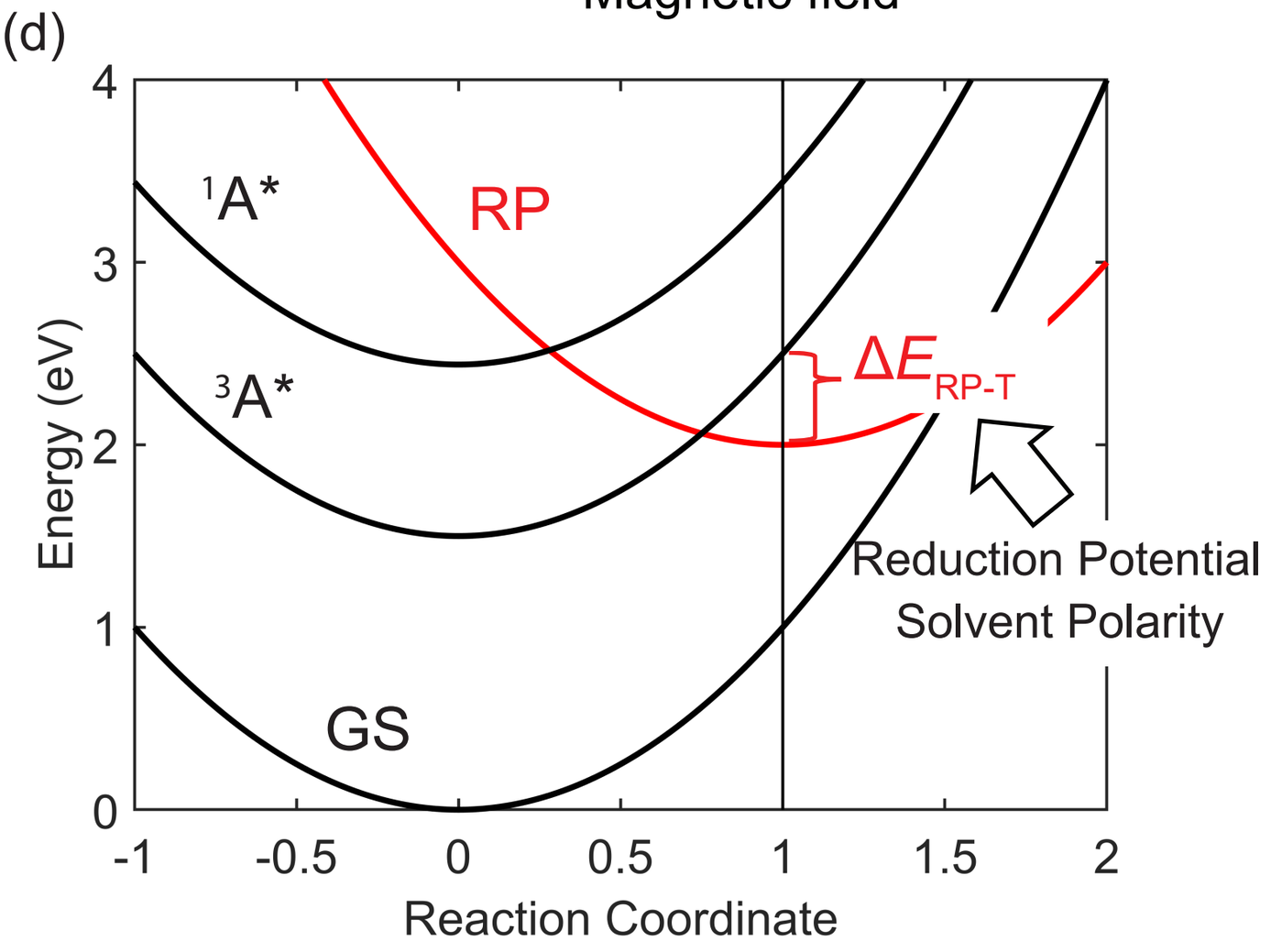

(a)

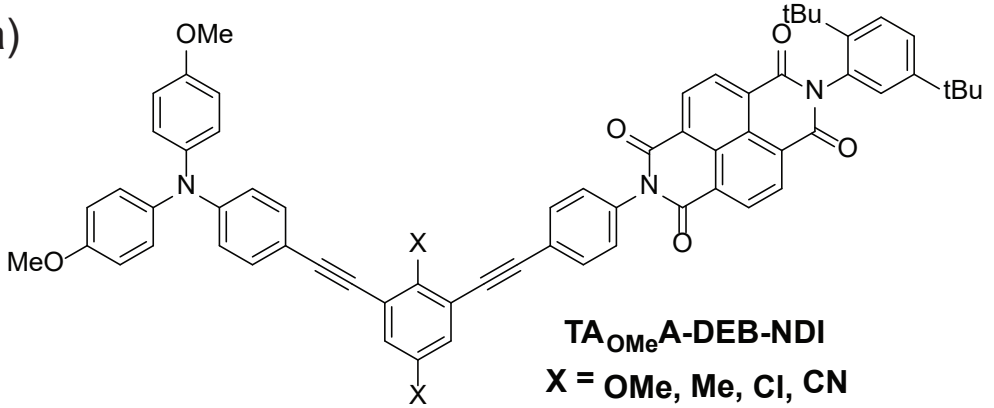

$TA_{OMe}A$-DEB-NDI

X = OMe, Me, Cl, CN

(b)

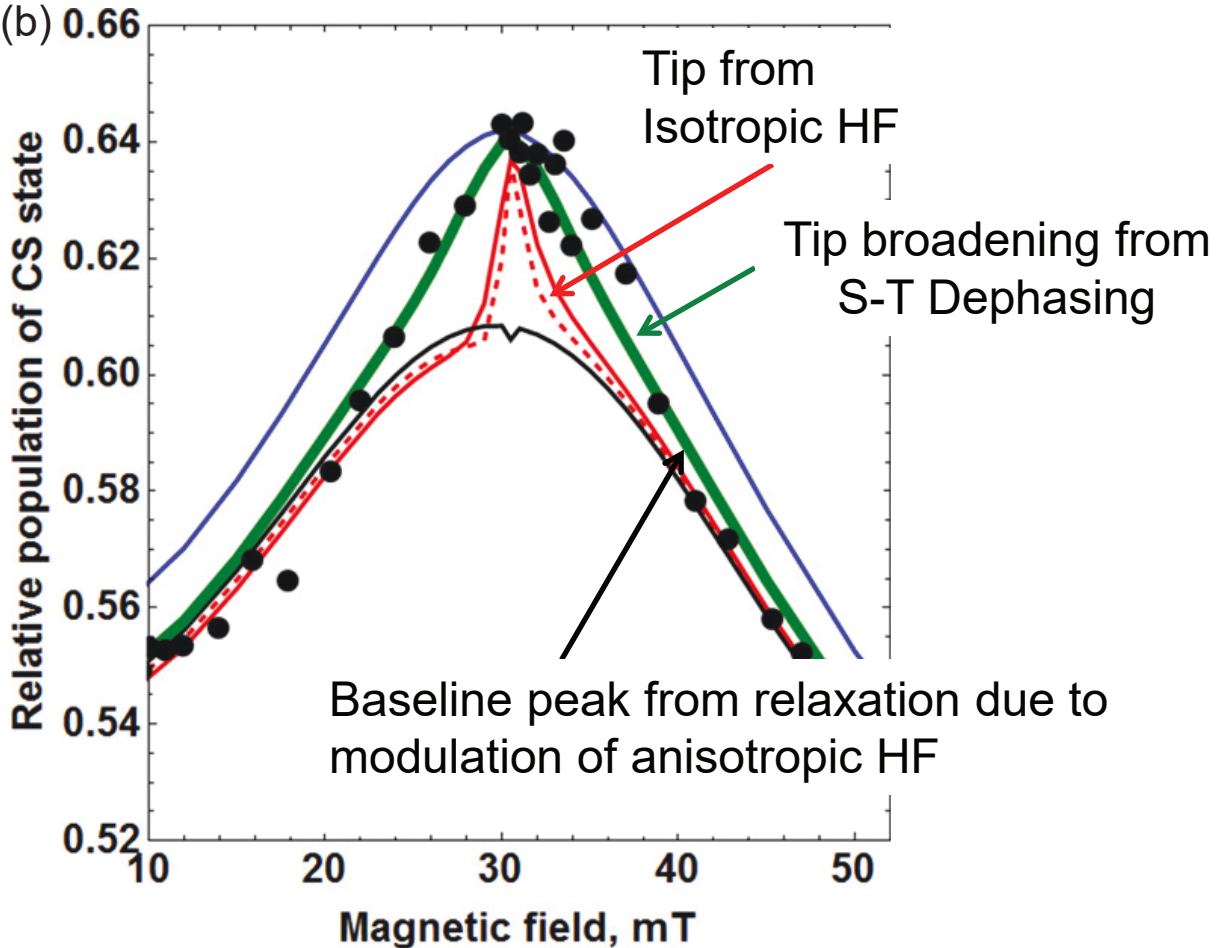

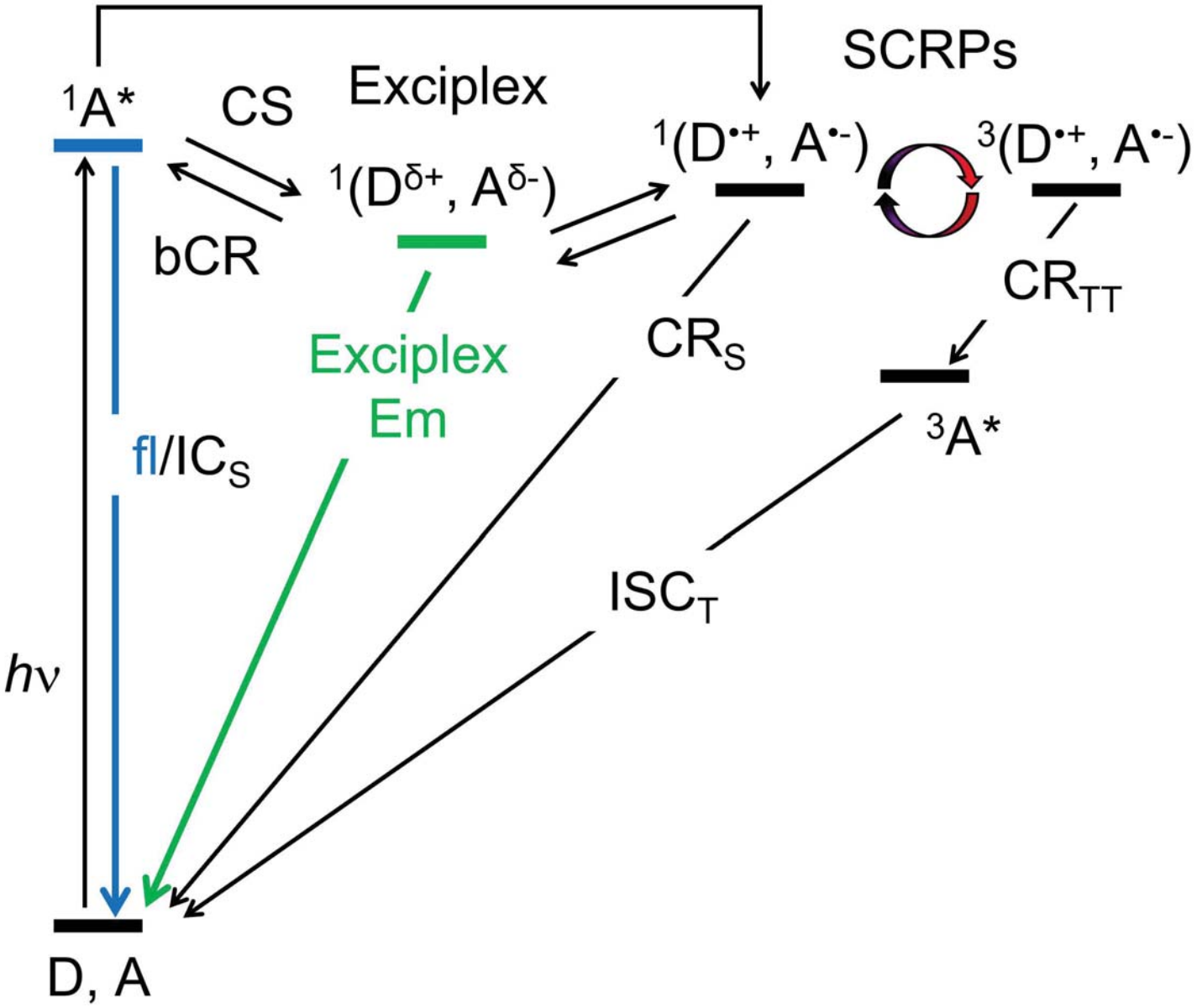
SCRPs
$^1A^*$
CS
Exciplex
$^1(D^{\delta+}, A^{\delta-})$
$^1(D^{\bullet+}, A^{\bullet-})$
$^3(D^{\bullet+}, A^{\bullet-})$
bCR
CR_{TT}
Exciplex
Em
CR_S
$^3A^*$
fl/IC_S
ISC_T
$h\nu$
D, A

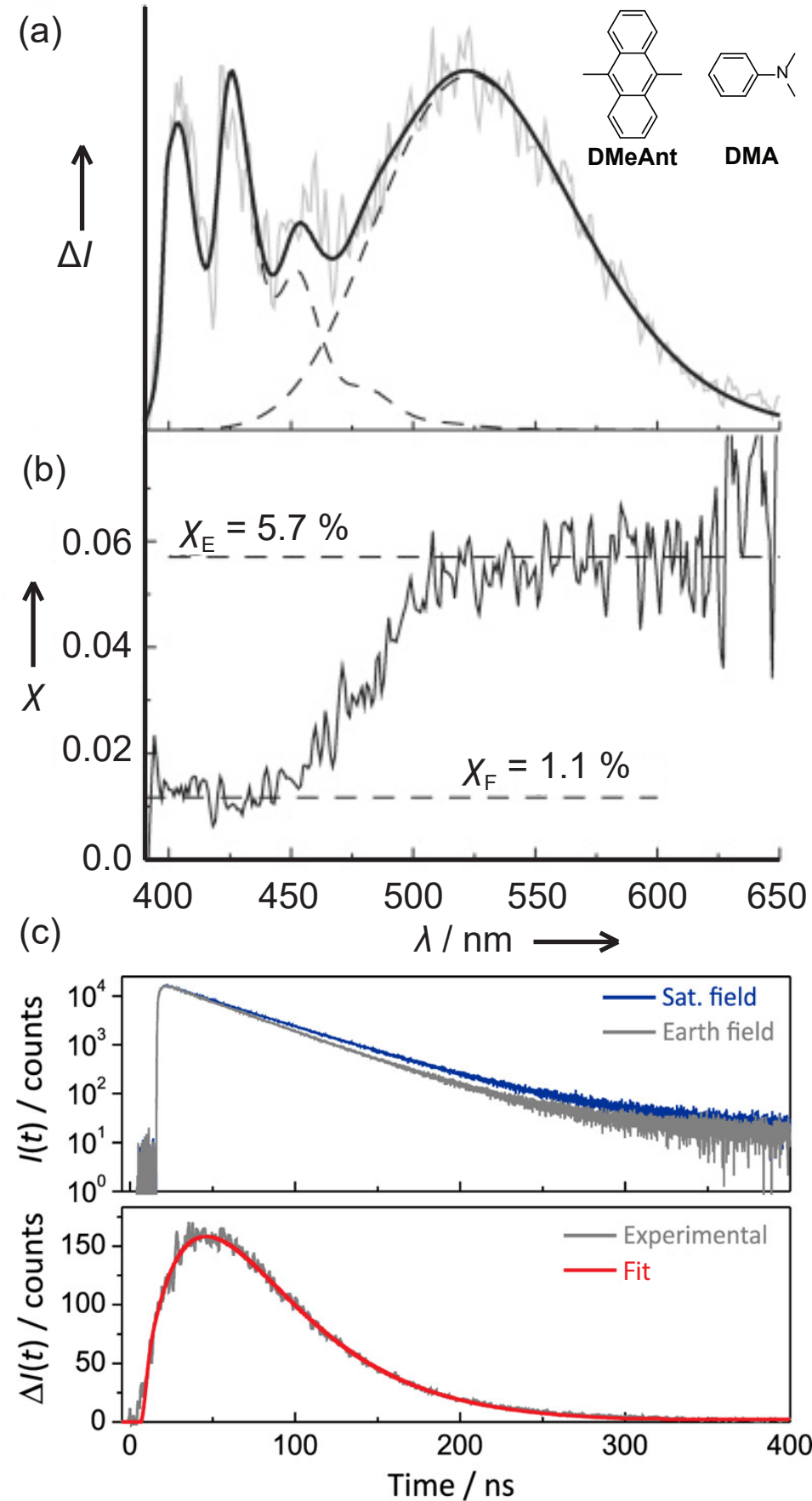
(a)
ΔI
DMeAnt
DMA
(b)
X
0.06
0.04
0.02
0.0
X_E = 5.7 %
X_F = 1.1 %
400
450
500
550
600
650
λ / nm
(c)
I(t) / counts
10^4
10^3
10^2
10^1
10^0
Sat. field
Earth field
ΔI(t) / counts
150
100
50
0
Experimental
Fit
0
100
200
300
400
Time / ns

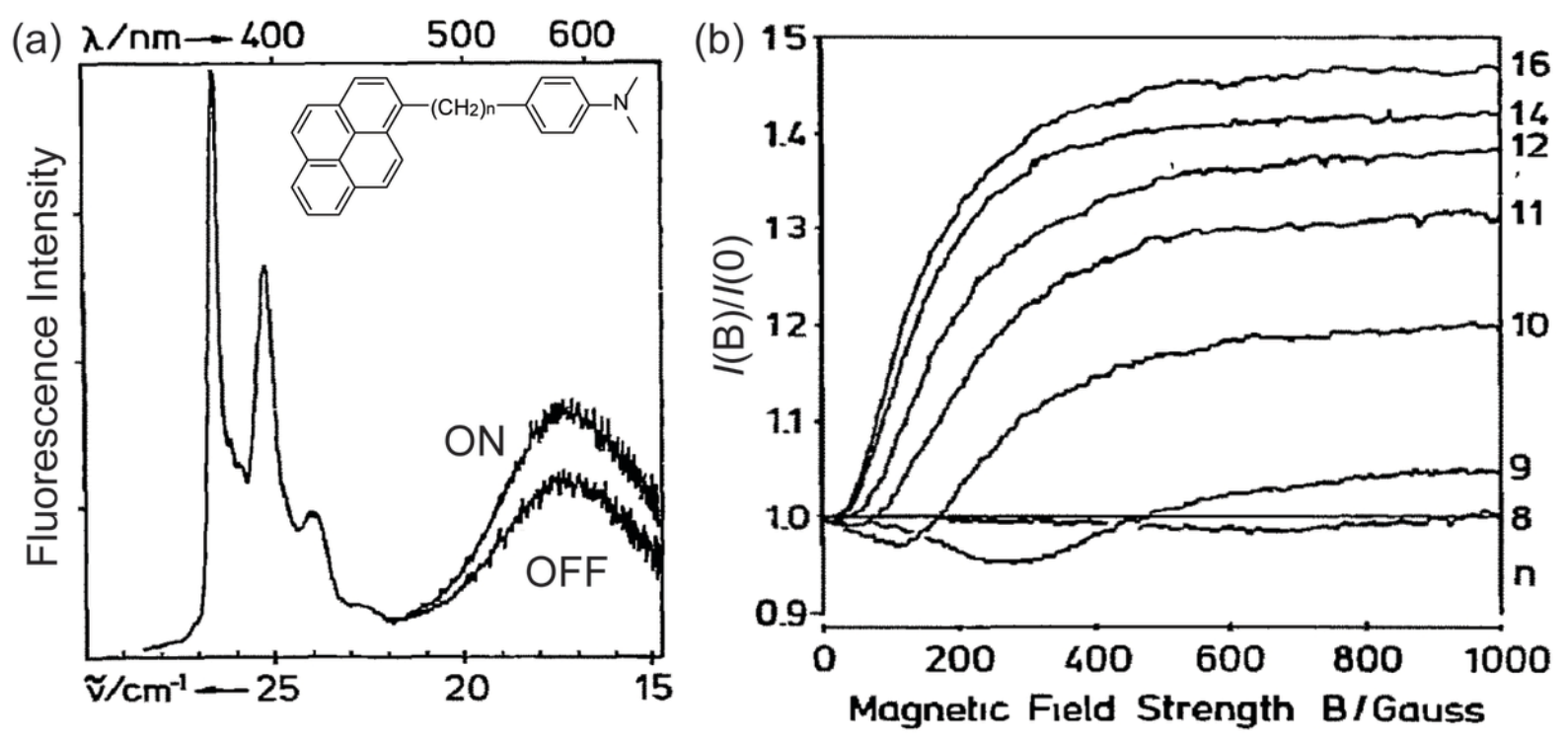
(a)
λ/nm
400
500
600
Fluorescence Intensity
(CH2)n
N
ON
OFF
ν̃/cm-1
25
20
15
(b)
I(B)/I(0)
15
1.4
1.3
1.2
1.1
1.0
0.9
16
14
12
11
10
9
8
n
0
200
400
600
800
1000
Magnetic Field Strength B/Gauss

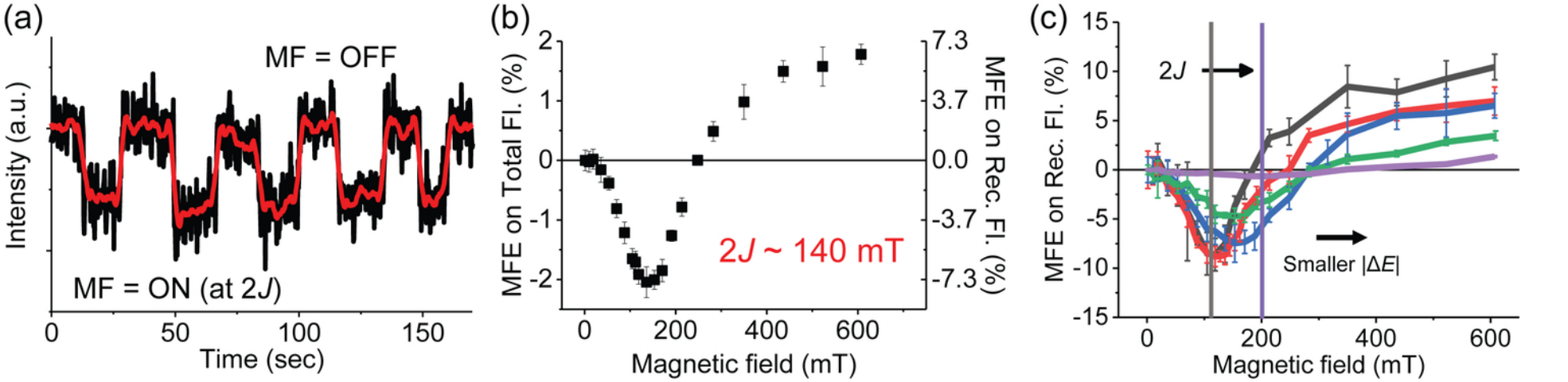
(a)
MF = OFF
MF = ON (at 2J)
Intensity (a.u.)
0
50
100
150
Time (sec)
(b)
MFE on Total Fl. (%)
MFE on Rec. Fl. (%)
2
1
0
-1
-2
7.3
3.7
0.0
-3.7
-7.3
2J ~ 140 mT
0
200
400
600
Magnetic field (mT)
(c)
MFE on Rec. Fl. (%)
15
10
5
0
-5
-10
-15
2J
Smaller |ΔE|
0
200
400
600
Magnetic field (mT)

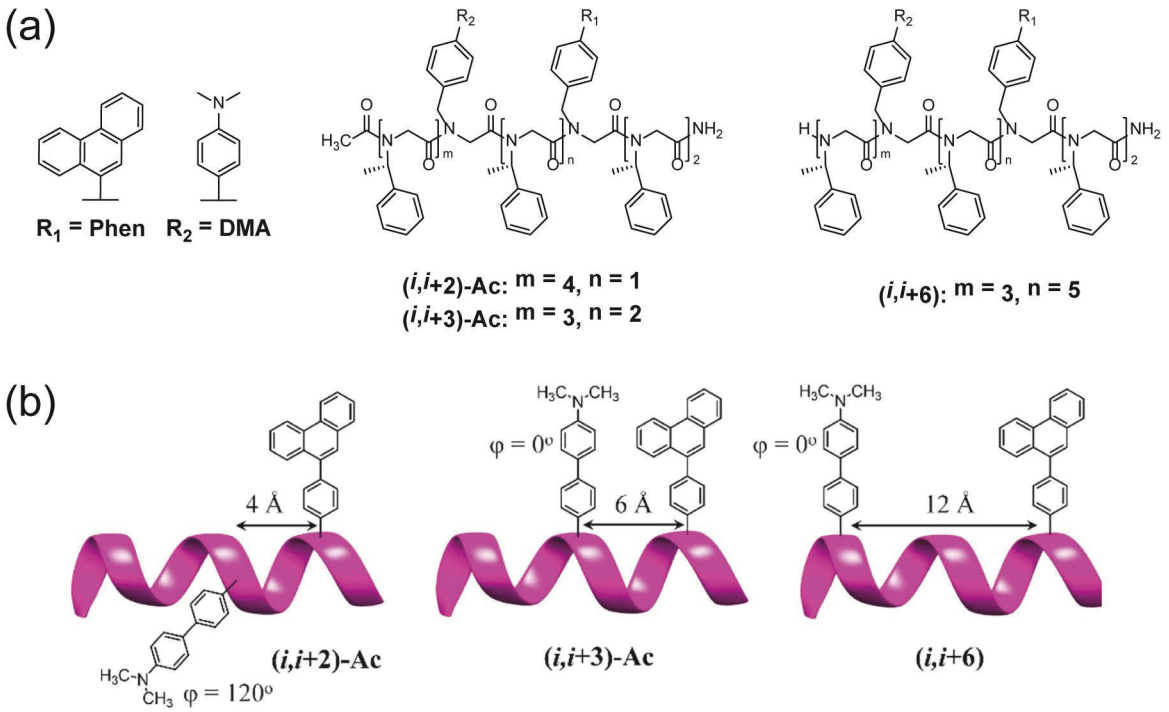
(a)
R1 = Phen R2 = DMA
(i,i+2)-Ac: m = 4, n = 1
(i,i+3)-Ac: m = 3, n = 2
(i,i+6): m = 3, n = 5
(b)
4 Å
6 Å
12 Å
φ = 0°
φ = 120°
(i,i+2)-Ac
(i,i+3)-Ac
(i,i+6)

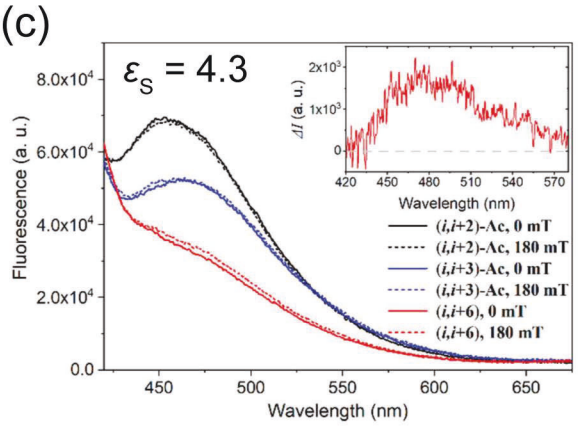
(c)
εS = 4.3
Fluorescence (a. u.)
Wavelength (nm)
ΔI (a. u.)
(i,i+2)-Ac, 0 mT
(i,i+2)-Ac, 180 mT
(i,i+3)-Ac, 0 mT
(i,i+3)-Ac, 180 mT
(i,i+6), 0 mT
(i,i+6), 180 mT

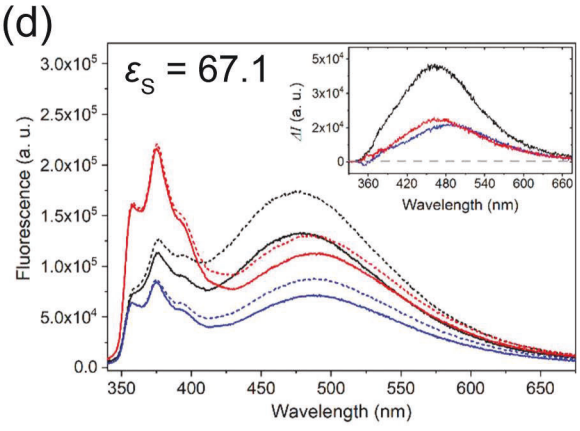
(d)
εS = 67.1
Fluorescence (a. u.)
Wavelength (nm)
ΔI (a. u.)

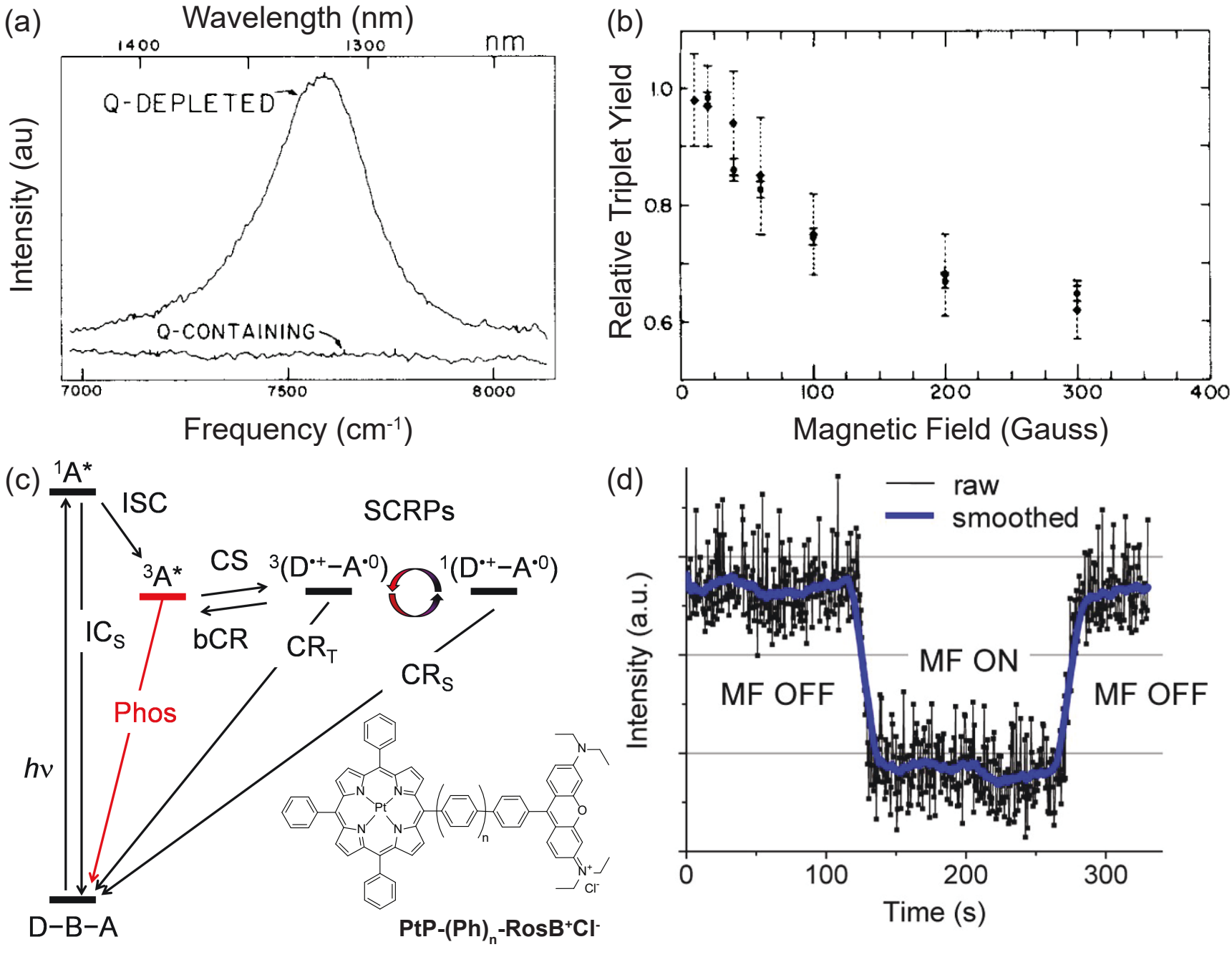
(a)
Wavelength (nm)
1400
1300
nm
Q-DEPLETED
Q-CONTAINING
Intensity (au)
7000
7500
8000
Frequency (cm-1)
(b)
Relative Triplet Yield
1.0
0.8
0.6
0
100
200
300
400
Magnetic Field (Gauss)
(c)
1A*
ISC
3A*
CS
3(D•+–A•0)
1(D•+–A•0)
SCRPs
ICS
bCR
CRT
CRS
Phos
hν
D–B–A
PtP-(Ph)n-RosB+Cl-
(d)
raw
smoothed
Intensity (a.u.)
MF OFF
MF ON
MF OFF
0
100
200
300
Time (s)

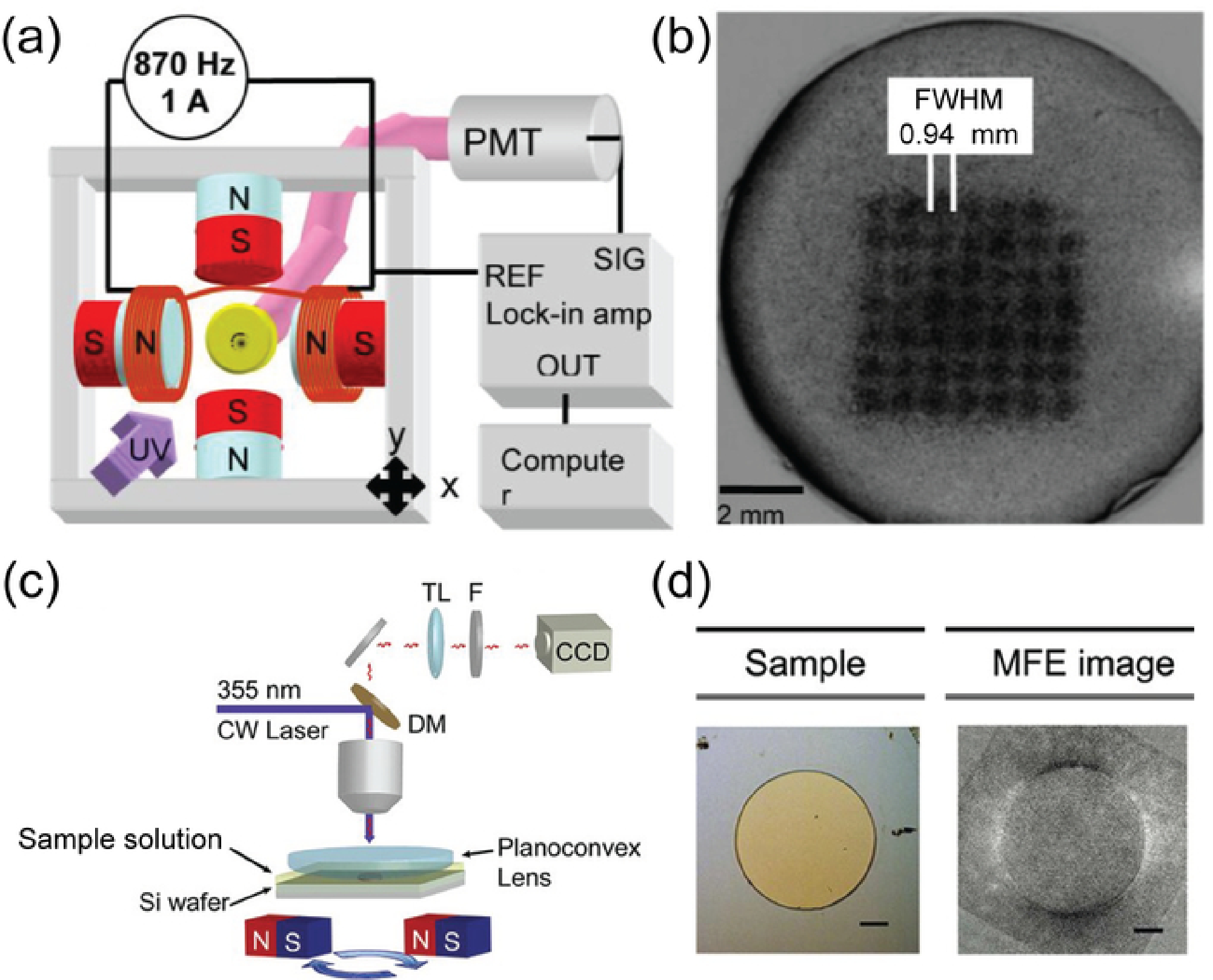
(a)
870 Hz
1 A
PMT
N
S
REF
SIG
Lock-in amp
OUT
S
N
N
S
S
N
UV
y
x
Compute
r
(b)
FWHM
0.94 mm
2 mm
(c)
TL
F
CCD
355 nm
CW Laser
DM
Sample solution
Planoconvex
Lens
Si wafer
N
S
N
S
(d)
Sample
MFE image

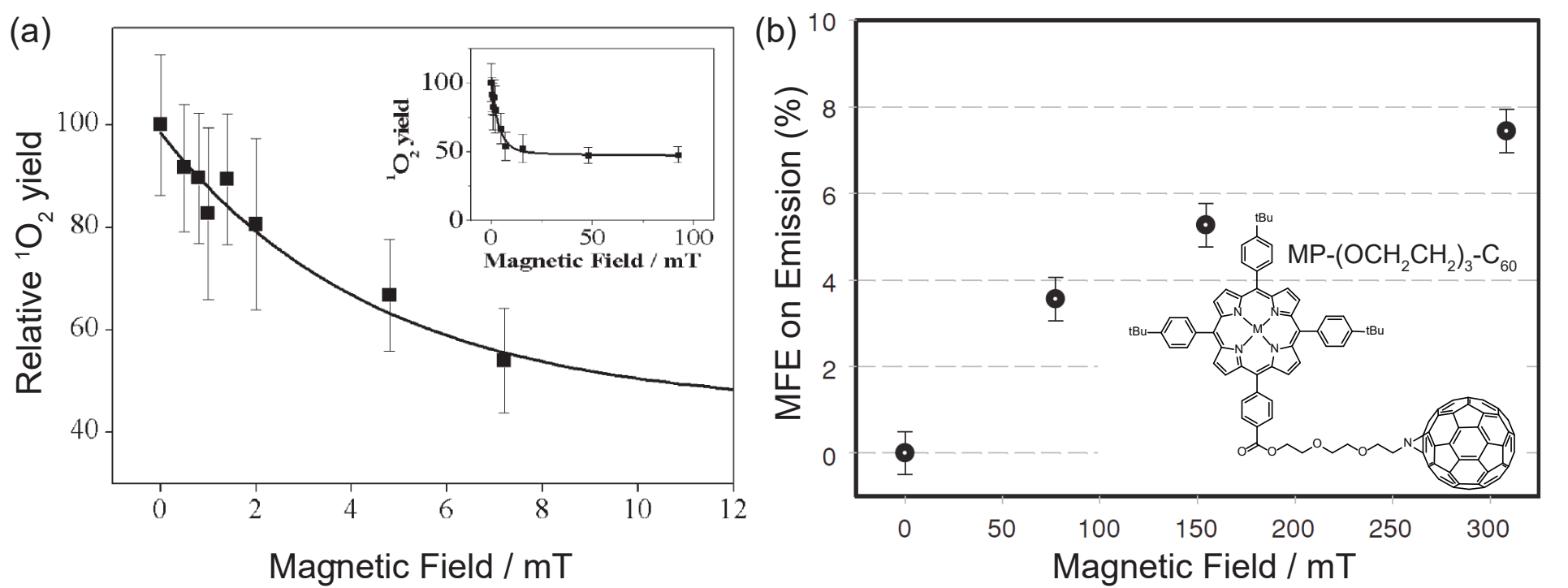
(a)
Relative $^1O_2$ yield
100
80
60
40
0
2
4
6
8
10
12
Magnetic Field / mT
$^1O_2$ yield
100
50
0
0
50
100
Magnetic Field / mT
(b)
MFE on Emission (%)
10
8
6
4
2
0
0
50
100
150
200
250
300
Magnetic Field / mT
MP-(OCH2CH2)3-C60
tBu
tBu
tBu
M
N
O
O
O
O
N